

*APPLICATION OF SOFT COMPUTING
FOR COMPUTED TOMOGRAPHY*

**A Thesis Submitted for the Award of the
Degree of**

DOCTOR OF PHILOSOPHY

in

Electrical Engineering

By

Nimit D. Shah



**ELECTRICAL ENGINEERING DEPARTMENT
FACULTY OF TECHNOLOGY & ENGINEERING
THE MAHARAJA SAYAJIRAO UNIVERSITY OF BARODA
VADODARA – 390 001
GUJARAT, INDIA**

May 2014.

Certificate

This is to certify that the thesis entitled, '**Application of Soft Computing for Computed Tomography**' submitted by **Nimit D. Shah** in fulfillment of the degree of **DOCTOR OF PHILOSOPHY** in Electrical Engineering Department, Faculty of Technology & Engineering, the M. S. University of Baroda, Vadodara is a bonafide record of investigations carried out by his in the Department of Electrical Engineering, Faculty of Technology & Engineering, M. S. University of Baroda, Vadodara under my guidance and supervision. In my opinion the standards fulfilling the requirements of the Ph.D. Degree as prescribed in the regulations of the University has been attained.

May 2014

Prof. Satish K. Shah

Department of Electrical
Engineering,
Faculty of Technology & Engineering,
The Maharaja Sayajirao University of
Baroda, Vadodara-390001

Head

Department of Electrical Engineering,
Faculty of Technology & Engineering,
The Maharaja Sayajirao University of
Baroda, Vadodara - 390001

Dean

Faculty of Technology & Engineering,
The Maharaja Sayajirao University of
Baroda, Vadodara - 390001

Declaration

I, **Nimit D. Shah** hereby declare that the work reported in this thesis entitled '**Application of Soft Computing for Computed Tomography**' submitted for the award of the degree of **DOCTOR OF PHILOSOPHY** in Electrical Engineering Department, Faculty of Technology & Engineering, The M. S. University of Baroda, Vadodara is original and has been carried out in the Department of Electrical Engineering, Faculty of Technology & Engineering, M. S. University of Baroda, Vadodara. I further declare that this thesis is not substantially the same as one, which has already been submitted in part or in full for the award of any degree or academic qualification of this University or any other Institution or examining body in India or abroad.

May 2014

Nimit D. Shah

Dedicated
To
My Beloved Mother
Smt. Daxa Deepak Shah

Acknowledgement

This journey has been an incredible one for me personally for various reasons. I feel a deep sense of gratitude as I am reaching the final destination of completing my doctoral thesis.

First and foremost, I would like to thank my guide, **Prof. S. K. Shah** for sharing his experience and expertise in my research work. I have no words to thank him for his invaluable support. He has been my mentor, my guide and my philosopher. He shared some of his valuable experiences that helped me to shape my research. With that, he provided me much needed support when I had almost given up. This wouldn't have been possible without him and I will be in debt to him for my entire life. I am also thankful to **Dr. S. K. Joshi**, Head of Electrical Engineering Department, Faculty of Technology & Engineering for his inspiration and support.

I am deeply indebted to the entire CCET Family, Management, Principal, and Dr. H. J. Jani Vice-Chancellor of C. U. Shah University and all my colleagues especially to Mr. Manoj Shah who have supported me in research work. I heartily thank to Robert Ciernaiks for providing reference material.

I would also like to thank my family for providing their undying love and support to make this happen. I would like to thank my parents for being my inspiration, my wife **Nauka** for being patient while handling my educational tantrums and giving me space, and my daughter **Kavni** to make me happy when I would think to give up. I would also like to thank my sister and brother-in-law for supporting me and proof reading my work from time to time.

Finally, I thank all those who helped me directly or indirectly and whose names would have been inadvertently missed above.

Nimit Shah

Abstract

Constant efforts are being done to improve the health care of the human race by developing non invasive diagnostic techniques. One of the modality, which has over the time proved its importance, is Computer Tomography Scanner. Researchers across the globe constantly work on improving the quality of the reconstructed image. One of the possible ways to achieve this task is by developing an efficient reconstruction algorithm which can be universally applied to all types of existing scanners. So, a novel algorithm is being developed to solve the problem of reconstruction is discussed in this thesis.

A new algorithm is developed by reformulating the problem of reconstruction, which is popularly known as inverse reconstruction problem. This algorithm is developed for the two beam profiles namely Parallel Beam and Fan Beam profile, so that the algorithm can be implemented universally keeping in mind its practical implantation.

In recent years, soft computing techniques are used to solve the complex problem of engineering where conventional approaches have failed. Extending the application of the soft computing techniques to medical image processing domain, the problem of reconstruction is solved employing soft computing techniques for the solution of the novel developed algorithm.

The novel algorithm developed for the parallel beam and fan beam profile is tested by the multi density phantom. The image reconstructed by the novel approach is compared to the images reconstructed by the exiting analytical and algebraic reconstruction method. This validates the developed algorithm's computational efficiency and its diagnostic value addition.

Contents

<i>Dedication</i>	<i>i</i>
<i>Acknowledgement</i>	<i>ii</i>
<i>Abstract</i>	<i>iii</i>
<i>List of Figures</i>	<i>vii</i>
<i>List of Tables</i>	<i>x</i>
1. Introduction	
1.1 <i>Computed Tomography</i>	2
1.2 <i>Aim of Research</i>	3
1.3 <i>Organization of Thesis</i>	5
2. Technical Aspects of Computed Tomography	
2.1 <i>Energy Sources</i>	7
2.1.1 <i>Physics of X-ray Sources</i>	7
2.1.2 <i>X-ray Tubes</i>	7
2.2 <i>X-ray Detectors</i>	9
2.2.1 <i>Scintillation Detectors</i>	9
2.2.2 <i>Xenon Detectors</i>	9
2.2.3 <i>Detector Parameters</i>	11
2.3 <i>Data Accusation</i>	11
2.4 <i>Scanner Generation</i>	14
2.4.1 <i>First Generation Scanner</i>	15
2.4.2 <i>Second Generation Scanner</i>	15
2.4.3 <i>Third Generation Scanner</i>	16
2.4.4 <i>Fourth Generation Scanner</i>	16
2.4.5 <i>Fifth Generation Scanner</i>	17
2.5 <i>Artefacts</i>	18
2.6 <i>Evaluation Parameters</i>	19
2.7 <i>Concluding Remarks</i>	23
3. Reconstruction Techniques	
3.1 <i>Image Reconstruction Techniques</i>	24
3.2 <i>Reconstruction Methods</i>	29
3.2.1 <i>Algebraic Reconstruction Technique</i>	29
3.2.2 <i>Analytical Reconstruction Techniques</i>	32
3.3 <i>Display of Image</i>	37
3.4 <i>Concluding Remarks</i>	39

4. Soft Computing Techniques Design and Development Tools	
4.1 Introduction.....	40
4.2 Artificial Neural Network.....	40
4.2.1 Model of Neuron.....	41
4.2.2 Neural Network Architecture.....	43
4.2.3 Neural Network Learning.....	44
4.3.4 Hopfield Network.....	45
4.3 Genetic Algorithm.....	48
4.4 MATLAB® Platform.....	51
4.4.1 Neural Network Toolbox.....	52
4.4.2 Global Optimization Toolbox.....	53
4.5 Concluding Remarks.....	54
5. Problem Formulation	
5.1 Problem Formulation for Parallel Beam Scanner.....	55
5.1.1 Geometry of Parallel Beam Scanner.....	55
5.1.2 Convolution and Back projection Method.....	57
5.1.3 Filtration and Back projection Method.....	59
5.2 Problem Formulation for Fan Beam Scanner.....	61
5.2.1 Geometry of Fan Beam Scanner.....	61
5.2.2 Rebinning Reconstruction Method.....	63
5.2.3 Direct Fan Beam Reconstruction Method.....	65
5.3 Implementation.....	66
5.4 Concluding Remarks.....	69
6. Artificial Neural Network Implementation	
6.1 Approach.....	70
6.2 Parallel Beam Projection System.....	71
6.2.1 Mathematical Remodeling.....	71
6.2.2 Implementation.....	76
6.3 Fan Beam Projection System.....	80
6.3.1 Mathematical Remodeling.....	80
6.3.2 Implementation.....	84
6.4 Concluding Remarks.....	88
7. Advance Neural Network Implementation	
7.1 User Defined Phantom.....	89
7.2 Advance Neural Network.....	93
7.3 Concluding Remarks.....	96

8. User Interface Development	
<i>8.1. Graphical User Interface Environment</i>	97
8.1.1 Working of Graphical User Interface.....	97
8.1.2 Graphical User Interface Components.....	99
<i>8.2 Designing of User Interface</i>	102
<i>8.3 Concluding Remarks</i>	106
9. Conclusions and Future Scopes	
<i>9.1 Research Contribution</i>	107
9.1.1 Problem Formulation.....	107
9.1.2 Problem Reformulation.....	108
9.1.3 Implementation of Problem.....	108
9.1.4 Overall Conclusion.....	109
<i>9.2 Future Scope</i>	112
10. Bibliography	114
11. Appendix	
<i>Appendix A</i>	125
<i>Appendix B</i>	144

List of Figures

2.1: Basic Construction of X-ray tube.....	8
2.2: Basic Construction of Scintillation Detectors.....	9
2.3: Basic Construction of Xenon Detectors.....	10
2.4: Object with Uniform Density.....	14
2.5: First Generation Scanner Gantry.....	15
2.6: Second Generation Scanner Gantry.....	16
2.7: Third Generation Scanner Gantry.....	16
2.8: Fourth Generation Scanner Gantry.....	17
2.9: Fifth Generation Scanner Gantry.....	18
2.10: Design of ATS Phantom.....	20
2.11: Design of Mostrom's Phantom.....	20
2.12: Design of Low Contrast Phantom.....	21
2.13: Design of Spatial Resolution Phantom.....	21
2.14: Design of CT Linearity Phantom.....	22
2.15: Design of Slice Thickness Phantom.....	22
3.1: Simple Projection Systems.....	25
3.2: Basic Geometry of Scanner.....	26
3.3: Detail of Trigonometric Relationship.....	27
3.4: Projection Geometry for Algebraic Reconstruction Technique.....	29
3.5: Determination of the Image Block.....	31
3.6: Image Projection and Back projection Operation.....	33
3.7: a) Sequence of Projection	
b) Distorted image after Back projection.....	35
3.7: Sampling and Quantisation of Analogue Images.....	38
4.1: Basic Artificial Neuron.....	41
4.2: Basic Thresholding Function.....	42
4.3: Basic Sigmoid Function.....	42
4.4: Basic Feed Forward Neural Network.....	43
4.5: Basic Feedback Neural Network.....	44
4.6: Basic structure of Hopfield Network.....	46
4.7: Flow Chart showing Implementation of Genetic Algorithm.....	49
4.8: Screen shot of typical MATLAB® Desktop Window.....	51
4.9: Screen Shot of Neural Network Toolbox.....	53
4.9: Screen Shot of Genetic Algorithm Solver.....	54

5.1: Basic Geometry of Parallel Beam Scanner.....	55
5.2: Scanner Geometry in X-Y Plane.....	56
5.3: Projection at various Angle.....	58
5.4: Flow chart for Convolution Back projection Method.....	59
5.5: Flow chart for Filtration Back projection Method.....	60
5.6: Basic shape of Fan Beam Profile.....	61
5.7: Basic Geometrical Relationship for Fan Beam.....	62
5.8: Flow chart for Implementation of Rebinning Method.....	64
5.9: Flow chart for implementation of Direct Fan Beam Method.....	66
5.10: User defined Phantom.....	67
5.11: Reconstructed User defined Phantom using Back projection.....	67
5.12: Reconstructed User defined Phantom using Convolution and Back projection.....	68
5.13: Reconstructed User defined Phantom using Filtration and Back projection.....	68
6.1: Structure of Developed Neural Network.....	74
6.2: Cross Section of the Developed Neural Network.....	76
6.3: Flow chart for Reconstructing Image for Parallel Beam Scanner.....	77
6.4: User defined Phantom with Resolution of 256X256.....	77
6.5: Reconstructed Image by Back projection Operation.....	78
6.6: Reconstructed Image by Hopfield Network after 100 iteration for Parallel Beam.....	80
6.7: Reconstructed Image by Hopfield Network after 1000 iteration for Parallel Beam.....	80
6.8: Reconstructed Image by Hopfield Network after 10000 iteration for Parallel Beam.....	80
6.8: Geometric Relationship between Variables for Fan Beam.....	81
6.9: Cross Section of Neural Network for solving the Problem for Fan Beam.....	84
6.10: Flow chart for Reconstructing Image for Fan Beam Scanner.....	86
6.11: Reconstructed Image by Hopfield Network after 100 iteration for Fan Beam profile.....	86
6.12: Reconstructed Image by Hopfield Network after 1000 iteration for Fan Beam Profile.....	87
6.13: Reconstructed Image by Hopfield Network after 10000 iteration for Fan Beam Profile.....	87

7.1: Topology of User defined Phantom.....	90
7.2: Cross Section of User defined Phantom.....	92
7.3: Flow chart for Implementing Advance Neural Network using Genetic Algorithm.....	94
7.4: Reconstructed user defined phantom by using GA.....	95
8.1: Layout of Guide in MATLAB®.....	99
8.2: Main Window of the Developed Interface.....	102
8.3: Window showing sub menus in Existing Techniques.....	103
8.4: Window showing Implementation of Existing Techniques.....	103
8.5: Window showing Implementation of Convolution Method.....	104
8.6: Window showing sub menus in Developed Techniques.....	104
8.7: Window showing selection of Beam Profile.....	105
8.8: Window showing solving Parallel Beam Profile.....	105
9.1: Cross Section of User defined Phantom.....	109
9.2: Cross Section of User defined Phantom reconstructed by Back Projection	109
9.3: Cross Section of User defined Phantom reconstructed by	
a) Convolution and Back projection	
b) Filtration and Back projection.....	110
9.4: Cross Section of User defined Phantom reconstructed by	
a)Neural Network with 100 iterations	
b) Neural Network with 10000 iterations.....	110
9.5: Main Window of the Developed Interface.....	111
9.6: Window showing sub menus in Developed Techniques.....	112
A-1: Example of Projections.....	126
A-2: Geometrical Relationship for Radon Transform.....	127
A-3: Image with single pixel.....	129
A-4: Sinogram of the Image with single pixel.....	130
A-5: Image of Sheep Logan Phantom.....	130
A-6: Sinogram of the Sheep Logan Phantom.....	130

List of Tables

5.1: Table listing the MATLAB® Function Files Developed for Implementation of Conventional Approach.....	69
6.1: Parameters for the Developed Neural Network	75
6.2: List of the MATLAB® Function Files Developed for the Implementation of Developed Approach using Neural Network.....	88
7.1: Parameters used to Simulate the User Defined Phantom.....	92
7.2: List of the MATLAB® Function Files developed for the Implementation using Genetic Algorithm.....	95
9.1: Values obtained for Evaluation Parameters.....	111

Chapter: 1

Introduction

This chapter provides overview and reminder context of thesis. It also provides the aim of the research work and scope of improvement in the existing techniques.

It took more than three billion years of evolution for the animals and plants that now inhabit the earth, to come into existence. Humankind, the modern form of Homo sapiens, first appeared about 100,000 years ago. Humankind over the centuries has endeavoured for survival, development and up-liftman. During last two centuries, efforts have been made to improve the safety, life span, comfort and many other dimensions of the humankind. Major work has been carried out in the medicinal field so that the human beings living in the world can live a better and long life. In the earlier stages, the emphasis was on the development of the medicines to cure the patients. However, this was based on the external symptoms of the human beings. Over the decades, it was felt that the doctors should be in a position to see the developments occurring inside the human body. This requirement resulted in the development of various non invasive radiographic techniques using electromagnetic radiations like X-rays and gamma rays.

The examination of the person's anatomy, as preliminary to performing the various diagnostic procedures, is a technique that has been used for centuries. Over the centuries, the development of empirical investigation of the body and the observation of variations in the structure of tissues permitted the drawing of conclusions about the normal and abnormal functioning of the human organism. This, in turn, led to evolution of the field of medicine which is known today as pathophysiology.

Certain accidental discovery of X-rays by Conrad Rontgen in 19th Century has made it possible to look at internal of human organism without violating the outer surface of his body. The use of X-ray apparatus to diagnose many serious illnesses and complex post-traumatic complications quickly became standard clinical practice.

1.1 Computed Tomography

With time, one of the more important applications of this radiation turned out to be Computed Tomography (CT). In the case of computed tomography, this has meant the application of not only X-rays but also of the mathematical algorithms that allow the reconstructing of image of any given cross-section of a person's body. By suitably arranging a set of these cross-sections, it is possible to visualise, in three dimensions, the anatomical structure of any part of a human body [1, 2, 3]. A spatial image such as this is of enormous help in medical diagnosis. Tomography examination is currently one the basic techniques of medical diagnosis.

Two people who can be credited for the development of Computer Tomography are MacLeod Cormack and Godfrey Newbold Hounsfield who were also awarded Nobel Prize in 1979 for the same. Cormack was the first person to work on the problem of image reconstruction of X-ray projection and solved the problem theoretically as he was theoretical physicist [4]. Later based on the work of Cormack, Hounsfield designed first prototype scanner and developed EMI Mark I based on gamma radiation. The first scan was performed on 1st October 1971[5].

In typical Computer tomography scanner, the tissues are being illuminated by X-rays and the initial intensity and attenuated intensity are being recorded. This process is commonly known as projection for a particular angle. This process is repeated by illuminating tissues at various angles and thus creating projection data for entire 180°. Once the projection data is obtained, then by application of reconstruction algorithm, the information obtained is converted into volumetric data which results into density information of the tissue.

The key problem arising in computerized tomography is image reconstruction from projections obtained from the X-ray scanner given geometry. There are several reconstruction methods to solve this problem, for example the most popular reconstruction algorithms using convolution and back-projection[6,7] and the algebraic reconstruction technique (ART)[8,9].

In recent years, soft computing techniques have been widely used for solving various complex scientific and engineering problems. Soft Computing techniques like Artificial Neural Network (ANN) and Genetic Algorithm (GA) are widely used to solve the Stochastic Problems where the conventional approaches have not performed well. Artificial Neural networks (ANN) are the approaches which are used for optimization of performance. ANN has proved to be very powerful tool for optimizing the nonlinear systems where input output mapping is not possible from the data [10].

Genetic Algorithm is members of collection of methodologies known as evolutionary computation (EC). These techniques are based on the selection and evolution processes that are met in nature and imitate these principles in many scientific domains. Goldberg, [11] has studied several aspects of the implementation of genetic algorithm and examined their potential in the context of optimization and learning for large scale complex systems.

1.2 Aim of Research

A novel approach is required to overcome the present drawbacks of the existing system by using the conventional optimization problem formulation and solving it with soft computing techniques.

Due to relative advantages as compared to conventional approaches, Neural Network (ANN) is being utilized to solve reconstruction problem. This approach can be classified in two broad categories Algebraic Neural Network Algorithm and Transform Neural Network Algorithm. In Algebraic Neural Network, during the reconstruction, large numbers of variables are being used which lead to large computational complexity which results into large and complicated neural net which cannot be practically implemented for medical imaging [12, 13, 14].

Transform Neural Network approaches utilizes supervised learning algorithm but it does not lead to good performance due to its limitation with respected to number of input output data for learning [15,16,17].In such approach, problem of Tomography reconstruction is reformulated as problem of Optimization for maximum entropy

criterion which is popular method to find out direction and rate of change of algorithm. This has resulted into new novel approach to solve the conventional problem of reconstruction.

Thus, aim of this research is to develop a new reconstruction algorithm which is more efficient and easily implementable. The features and work of research carried out in the thesis include:

- Problem Formulation for Computed Tomography Reconstruction.
- Mathematical derivations for Back Projection, Filter Back Projection reconstruction techniques for topographic reconstruction [18, 19].
- Design and development of algorithms and their modifications, for back Projection, Filter Back Projection reconstruction techniques for tomography reconstruction [20].
- Reformulating Problem of Reconstruction as an Optimization Problem.
- Designing and simulating newly formulated Problem using MATLAB®
- Employing ANN for Designing and Simulating Reconstruction Problem[21,22]
- Application of GA for tuning weights of Unsupervised Neural Network.[23]
- Performance evaluation of newly developed approach with exiting techniques and approaches.
- Development of testing volume Sheep-Logan phantom for prototype testing of simulation[23]
- Implementation of new developed approaches for standard testing volume Sheep-Logan phantom and evaluating relative performance characteristics with existing techniques[24].

1.3 Organization of Thesis

The Thesis is organized in ten chapters as follows:

Chapter: 1: Introduction

This chapter gives an overview and narrates the context for the entire thesis and also provides objectives of research work and scope of improvement in the existing approaches.

Chapter: 2: Computer Tomography: Technical Aspects

This chapter discusses the various technical aspects of X-ray tomography which include energy sources, detectors, data actuation, beam profiles, artefacts, evaluation parameters and testing phantoms for existing CT scanners.

Chapter: 3: Current State of Art: Reconstruction Techniques

This chapter provides details of Literature survey carried out regarding the existing approaches to solve the problem of reconstruction. It provides information regarding the various basic techniques, modification suggested by researches and limitations of present approaches. It also addresses the basic reconstruction problem and provides brief philosophy of displaying reconstructed image.

Chapter: 4: Design& Development Tools for Soft Computing Techniques

This chapter discusses the mathematical background for Soft Computing Techniques such as Artificial Neural Network (ANN) and Genetic Algorithm (GA). It also covers the implementation of these approaches on MATLAB® platform and its associated toolboxes which are widely used by Researchers across the globe. MATLAB® platform and its toolboxes are used in this research work to design, simulate and test the proposed techniques.

Chapter: 5: Mathematical Modelling: Problem Formulation

This chapter provides details regarding the mathematical framework and the techniques used to solve this problem. It also includes the implementation of the existing techniques and testing.

Chapter: 6: ANN Implementation: Reformulated Optimization Problem

This chapter discusses the reformulation of problem of reconstruction to problem of optimization for parallel beam and fan beam profile. It also discusses the strategy used to solve this problem of optimisation by Neural Network and its implementation on MATLAB® platform. It also states the results obtained by developed reconstructed techniques using user defined phantom.

Chapter: 7: Employing Advance Neural Network

This chapter discusses the mathematical modelling of user defined phantom which is used to test the various reconstruction techniques used in the present research work. It also addresses the modification of the technique developed in previous chapter by employing combination of Neural Network and Genetic Algorithm.

Chapter: 8: User Interface Designing

This chapter gives the overview about the working and building Graphical User Interface in the MATLAB®. It also discusses the User Interface developed for the presented research work and its usage.

Chapter 9: Conclusion & Future Scope

This chapter analyzes the results and summarizes the contribution of research work carried out. It also discusses the limitations and assumptions made for the research. In this chapter suggestions are given for the future research work that can be carried out.

Chapter 10: Bibliography

Thesis ends with bibliography which includes the list of references used in each chapter.

Chapter: 2

Technical Aspects

This Chapter discusses the various technical aspects of X-ray tomography which include energy sources, detectors, data actuation, scanner generations, and artefacts in images of existing CT scanners.

2.1 Energy Source

X-rays are the main source of energy, which are used to illuminate subject of interest. X-rays are produced in the X-ray tube which makes this tube fundamental component of any CT scanner. Operation of X-ray tube is based on the complex physical principles involved in the generation of X-rays.

2.1.1 Physics of X-ray Sources

X-rays are generated by physical processes that take place within matter at the atomic level. The wavelength of these radiations is 10^{-12} to 10^{-8} meters and for medical use; its range is 6×10^{-12} to 1.2×10^{-10} meters [1]. These radiations produced are due to two processes; the transition of electrons between the inner shells of an atom and the deceleration of charged particles caused by electromagnetic fields within the matter. Thus, each translation of an electron from a shell with a higher energy level to a shell with a lower level is accompanied by the emission of quantum of radiation with energy equal to density difference between the shells.

2.1.2 X-ray Tube

X-rays tube uses two voltage sources, one to supply current to heat cathode and second high voltage source to produce the cathode rays. Basic construction of this tube is shown in the figure 2.1[2, 3]. The electrodes are generally sealed in a vacuum, which allow independent control of the number and speed of the accelerated electrons striking the tungsten anode. The presence of gas can result in variation in the number of electrons and reduced speed. The cathode is composed of two elements, the filament, made of tungsten, and a metallic cup for focusing the electrons emitted by the filament. The filament is a helical coil of tungsten wire of about 0.2 millimetres in diameter and one centimetre in length.

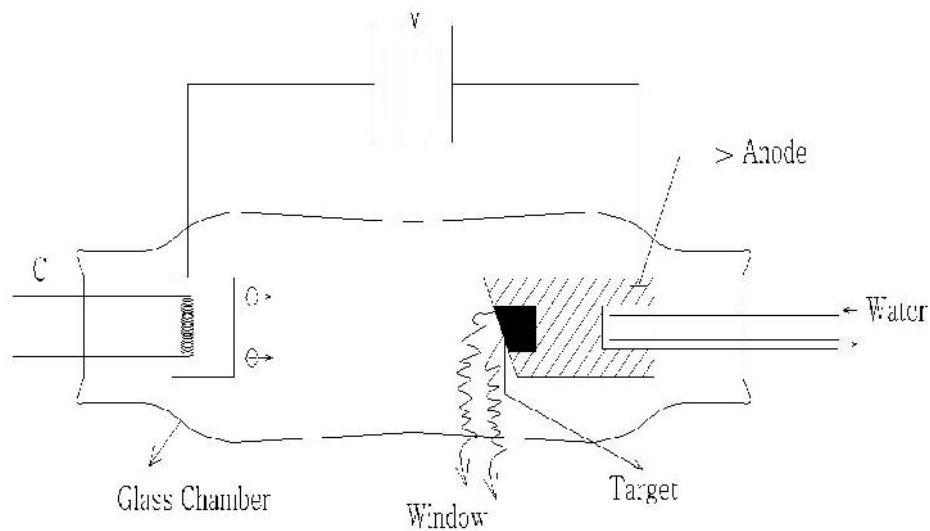


Figure 2.1: Basic Construction of X-ray tube.

When the current is fed through the wire, it becomes heated. The heat is absorbed by the electrons in the wire. When the temperature reaches a certain level, the electrons absorb enough energy to overcome the surface barrier and to escape from the metal. These electrons escape from a cloud, formed around the filament, and are called space charge. They prevent the electrons within the wire from escaping the filament. The effect of the space charge, on limiting the emission of more electrons from the filament, is called space charge effect. The electrons stay around the filament because the loss of electrons causes the filament to become positively charged. These escaped electrons can be accelerated towards the anode by applying a high voltage potential.

Most of the energy carried by the electrons, bombarding the tungsten target on the anode, is converted into heat. Therefore, a large focal spot is preferred because it allows accumulation of a larger amount of heat. However, a small focal spot is needed to generate better images. The typical rating of X-ray tube includes Target Material, Tube Voltage, Tube Current and Filament Current.

2.2 X-ray Detectors

X-ray detectors play very significant role in the quality of image produced from CT scanner. As opposite to conventional x-ray scanners, which use photographic film, CT scanner uses mainly two types of detectors namely Scintillation detectors and Xenon detectors [4].

2.2.1 Scintillation Detectors

Scintillation detectors are based on photoelectric effect. Scintillation detectors are made from materials such as sodium iodide (NaI) doped with thallium (TI) and they are having the thickness of 1 to 2 centimetres. Whenever X-rays strike this detector, three physical phenomena take place namely Photoelectric Effect, Compton Effect and Pair Production. These detectors have very high resolution, due to primary reason that the material from which they are made are having large atomic number. They absorb radiation strongly and this affects their detection efficiency[5,6].

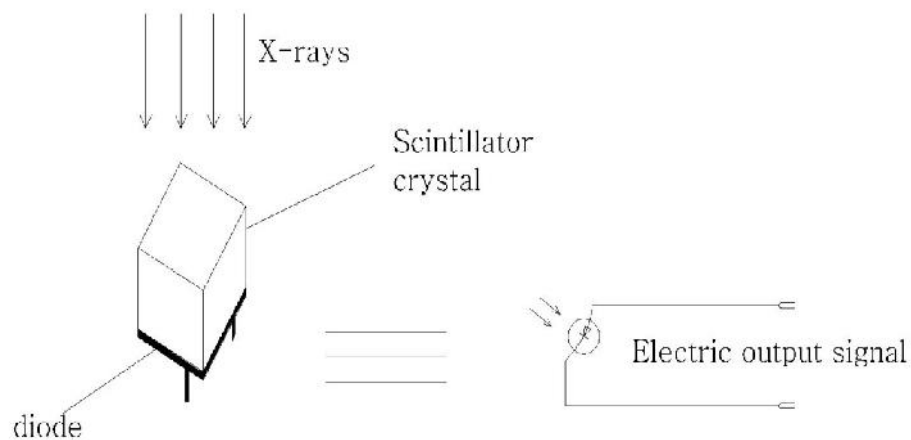


Figure 2.2: Basic Construction Scintillation Detector

2.2.2 Xenon Detectors

In Xenon detectors, popularly known as xenon proportional chambers, the electrical output signal is proportional to the intensity of the radiation that ionizes the gas atoms inside the microgap gas chambers (MCG). The gas, in the ionization chambers of xenon detectors, is at high pressure which is about 10 atmospheres. The electrodes used are made of tantalum and in-collection electrode of copper

with dimension of 6 centimetres length and with the width of 1 millimeter. The typical efficiency of these detectors is about 60% which is their main advantage. A design is shown in the figure 2.3 [7,8,9].

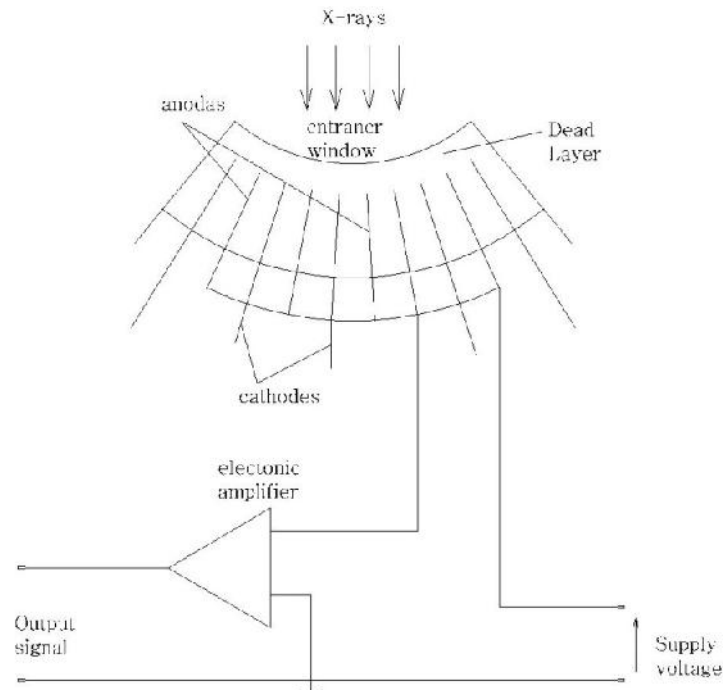


Figure 2.3: Basic Construction of Xenon Detectors

In this detector, a high voltage of about 140 KV is applied across the electrodes. The voltage must not be too large; otherwise it can result into so called gas amplification. If an X-ray photon penetrates the detector's window inside, there is high probability of it ionizing the xenon inside. The probability of this happening is proportional to the length of the chamber and pressure inside. The current that flows between the electrodes and through the gas is ionized by the X-rays and is proportional to the intensity of X-rays. These detectors work in such a way that no heating takes place after the occurrence of ionization, and thus it takes very short time to return to the state of readiness.

2.2.3 Detector parameters

The typical parameters, by which the quality of measurement is achieved, are quantum efficiency, energy resolution, stability over time, inertia, spatial resolution, resistance to irradiation damage and internal detector noise[9,10].

Quantum efficiency is defined as the ratio between the number of quanta registered by the detectors and the total number of quanta striking the detector. Quantum efficiency has an effect on the minimum radiation dose that must be applied in order to obtain an image with a specific contrast and signal to noise ratio. Energy resolution is described as the full width at half maximum of the detector's transfer characteristic as function of the incident X-ray photon energy.

Stability over time of measurements obtained using different types of X-rays detectors is determining above all by the radiation intensity. Xenon proportional chambers meet highest specifications in terms of their insensitivity to radiation overload.

After the X-rays have interacted with the sensor in the matrix, degradation of the output signal takes place. The two parameters which are responsible for degradation are primary speed and afterglow. The primary speed can be understood, as on the impulse response parameter of the detector, which is obtained after the input of a pulse of X-rays. Afterglow occurs due to sudden change in intensity of X-rays which causes defects in the structure of the crystal.

2.3 Data Accusation

One of the fundamental quantities associated with radiation is its intensity I , which is defined as the amount of photon energy passing through unit area in unit time.

$$I = \frac{\text{number of photons} \cdot h\nu}{S \cdot t} \left[\frac{1}{\text{cm}^2 \cdot \text{s}} \right] \quad (2.1)$$

where h is Planck's constant; ν is the frequency of the photon of radiation emitted, S is area and t is the time. When an X-ray beam of intensity $I(0)$ is directed at an

object, the attenuation of the radiation takes place, which includes the photoelectric effect (absorption) and coherent and incoherent scattering.

In photoelectric effect, the X-ray photon interacts with the electron shells of the atoms in the irradiated samples. Some of the incident photon energy is used to overcome the binding energy of the electrons that are ejected; the rest of the energy is transferred to the photoelectrons in the form of kinetic energy. It is mathematically expressed as:

$$E_i = E_b + E_k \quad (2.2)$$

where E_b is the electron binding energy; E_k is the kinetic energy transferred to the photoelectrons and E_i is energy of the incident photon.

The vacancies in lower electrons shells cause the other electrons, from higher shells, to move into them. The energy difference, between the electron that was removed and the electron brought from the higher shell, is emitted as quantum of secondary X-ray energy. In each element, only certain transition between the shells is permitted.

Another effect that influences the attenuation of the radiation is scattering of both types, which are coherent and incoherent. In coherent scattering, X-ray photon loses energy without losing change in direction; while in incoherent scattering, it loses energy as well as changes the direction. Hence the quantum of energy can be expressed as:

$$E_n = \frac{h\nu}{1 + \zeta(1 - \cos\xi)} \quad (2.3)$$

where ζ is the ratio of the incident quantum energy to the rest energy of the target electron, with which the quantum interacts, ξ is the angle of scattering. Thus it can be concluded that all these three factors influence the attenuation of X-rays, which is also known as linear attenuation coefficient. Mathematically, it can be expressed as:

$$\mu = \mu_a + \mu_c + \mu_n \quad (2.4)$$

where μ_a is absorption coefficient which is caused by photoelectrical effect; μ_c is the scattering coefficient caused by coherent scattering and μ_n is the scattering coefficient caused by incoherent scattering.

In view to establish the mathematical relationship between the passages of X-rays through the matter, uniform object with cross sectional area of 1m^2 as shown in the figure 2.4 is considered and is illuminated with X-ray radiation with intensity $I(0)$.

X-ray intensity gets attenuated after travelling the distance u and the value of the intensity is $I(u)$. The total reduction of X-ray intensity $dI(u)$ in this layer is proportional to the number of incident photons per unit time and to the number of centres of interactions in the layer:

$$dI(u) = -\sigma \cdot I(u) \cdot Ndu \quad (2.5)$$

where $\sigma[\text{m}^2]$ is constant of proportionality known as total cross section. Dividing both sides of equation by $I(u)$ and integrating both sides over the thickness of the sample U , we obtain:

$$\int_0^U \frac{dI(u)}{I(u)} = -\sigma N \int_0^U du \quad (2.6)$$

This integration results into:

$$I(U) = I(0) \cdot e^{-\mu_{const}U} \quad (2.7)$$

For the heterogeneous materials like human body, the attenuation coefficient in the equation must be replaced with the integral of the attenuation coefficient over the path though which the radiation passes. Hence, it can be expressed as under:

$$I(U) = I(0) \cdot e^{-\int_0^U \mu(u) \cdot du} \quad (2.8)$$

where $\mu(u)$ is the function defining the attenuation coefficient distribution along the path of radiation[11].

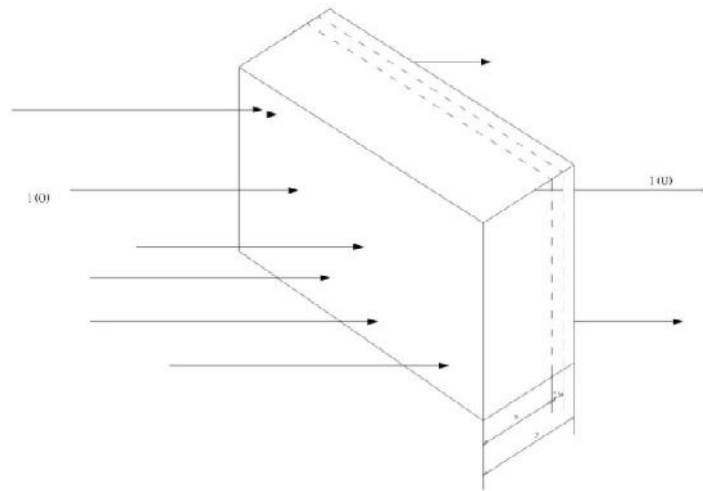


Figure 2.4 Object with Uniform Density.

The determination of $\mu(x, y)$ defines the spatial structure of human body in terms of the ability of its individual layers to attenuate radiation, This will allow to distinguish the body tissues in tomography image, characterised as they are distinct properties of their constituent elements and compounds. For better diagnosis, Hounsfield scale has been introduced to define degree of attenuation of radiation by various substances.

2.4 Scanner Generation

The first commercial scanner was developed in April 1972. Since then, there has been significant development in the CT scanner and quality of image which is obtained. Based on the type of source and detectors, the development of CT scanners can be classified as follow [12, 13]:

1. First Generation Scanner
2. Second Generation Scanner
3. Third Generation Scanner
4. Fourth Generation Scanner
5. Fifth Generation Scanner

2.4.1 First Generation Scanner

First Generation Scanners are popularly known as pencil beam scanners as these devices were simple and were having only one source and one detector as shown in the figure 2.5. Hence, at a time only a single projection was carried in such systems. Here, the source and detectors were moving only in single movement lateral direction only. As there is only a single source and single detector the time required to perform the task was significantly large and patient were exposed to high dose of radiation.

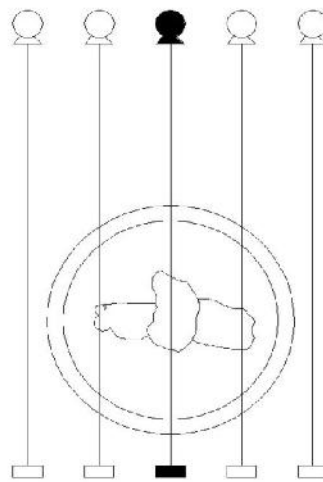


Figure 2.5: First Generation Scanner Gantry

2.4.2 Second Generation Scanner

Significant improvement was made in instrumentation of CT scanner and instead of single detector, array of detectors were used. These second-generation scanners, is also popularly known as partial fan-beam or translation/rotation multiple detector scanner, had between 3 and 52 detectors in the array. The use of the fan shaped radiation beam enabled the projection to cover a larger area of patient's body at any one time and resulted in the reduction of number of projections needed to reconstruct an image of satisfactory quality. The construction of Second Generation scanner is shown in the figure 2.6.

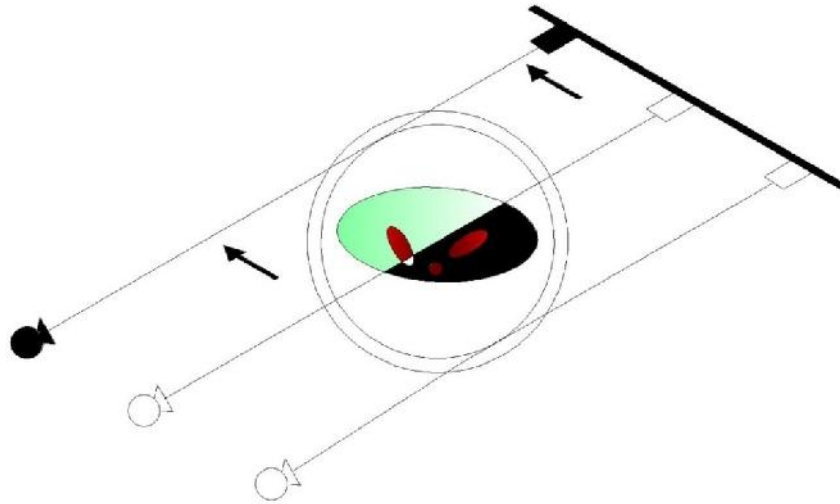


Figure 2.6: Second Generation Scanners Gantry

2.4.3. Third Generation Scanner

In third generation scanner lateral movement of tube detector system was replaced by rotation movement. These generation scanner are popularly known as fan beam or continuous rotation scanner. As shown in figure 2.7, due to fan beam projection system with a beam of radiation in the shape of a fan with an angular spread of between 40 and 55 degree which encompass the whole of the test object as shown in figure. In this scanner after one projection has been made the table is move and the whole process is repeated.

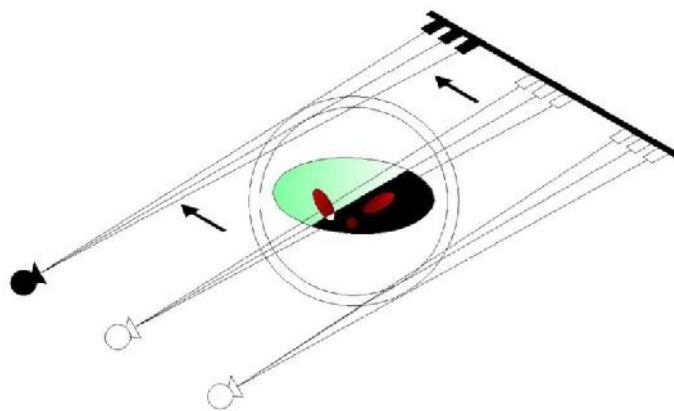


Figure 2.7: Third Generation Scanner Gantry

2.4.4. Fourth Generation Scanner

In fourth generation scanner rotation movement of tube detector was replaced stationary ring of detectors and tube has only rotation motion. It also known as rotate-fixed scanner; the word rotate in the name refers to the movement of the tube and the word fixed to the array of detector. In order to maintain an adequate resolution of the radiation intensity measurement, the number of detectors in the array was increased in the range of 600 to 5000 detectors as shown in figure 2.8.

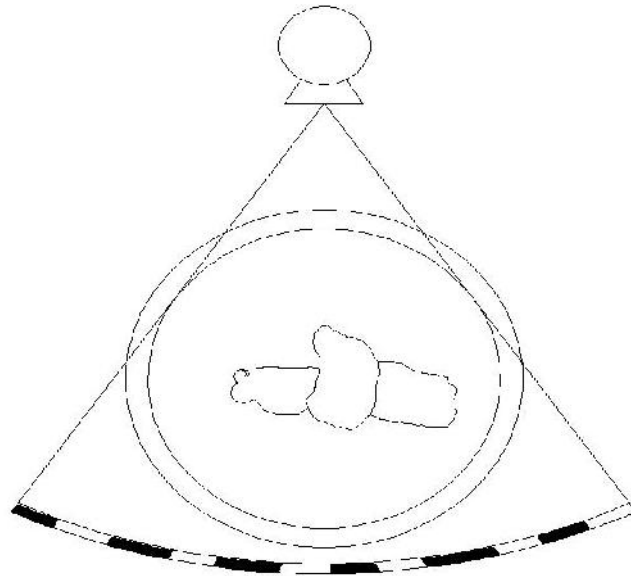


Figure 2.8: Fourth Generation Scanner Gantry

2.4.5 Fifth Generation Scanner

Fifth generation scanner is popularly known as Spiral Scanner which uses either parallel beams of radiation or fan beams. In this scanner there is no movement along the axis of the patient during each of the projection. This scanner uses the cone shaped radiation beam which has made possible to increase the width of the electrode. The biggest advantage of this arrangement as compared to previous designs is the significant rise scanning speed, which results into decrease in radiation dose to the patient.

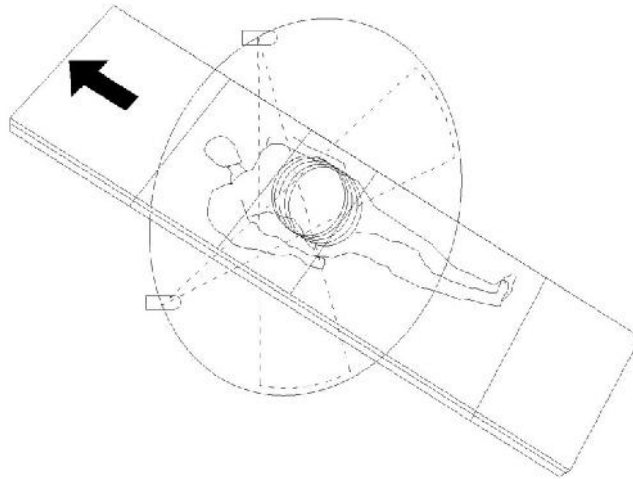


Figure 2.9: Fifth Generation Scanner Gantry

2.5. Artefacts

The two main factors contributing to the artefacts in the reconstructed image are due to simplification made in the reconstruction algorithm and other due to physical condition in the projection. The physical factors effecting the quality of images includes the polychromatic nature of X-ray beams, non-zero thickness of the beam, shortcoming in the collimators, presence of metal elements in the patient's body and measurement noise[14,15,].

2.6 Evaluation Parameter

Assessment of physical and technique capabilities of CT scanner plays very vital role in establishment of standardised, quantitative, comparative criteria. The technical parameters use to evaluate CT Scanners are as below:

Cycle Time: It is time taken to scan and reconstruct image, shorter cycle time will lead to lesser probability of artefacts.

Spatial resolution: It can be defined as the minimum area in the image in which changes can be detected.

Low-contrast resolution: It ability to detect small differences of attenuation coefficient in tissues, in other word it is the ratio between the smallest detectable differences of attenuation coefficient and the average value within an object of a given size, for a specific radiation dose.

Uniformity: It a measure of homogeneity of the image which can be calculated from the average attenuation coefficient measure at the selected area of a uniform standard water phantom.

Linearity: It is the relationship between the attenuation coefficient measures at the average energy of the scanner and value assigned to them on the Hounsfield scale.

Pitch: It is the ration between the displacement of the table with patient on it and the thickness of the scanner layer in one revolution.

In order to control and evaluate the parameters of scanner physical phantoms are used some of the standard phantom includes[16,17]:

- **ATS Phantom**
- **Mostroms's Phantom**
- **Low Contrast Resolution Phantom**
- **Spatial Resolution Phantom**
- **CT Linearity Phantom**
- **Slice Thickness Phantom**

ATS Phantom

This phantom is the most commonly used phantom to CT scanner. It is designed to test low contrast resolution. The figure 2.10 shows the design of the ATS phantom. During the measurement of low contrast resolution, the phantom is subjected to radiation of constant intensity.

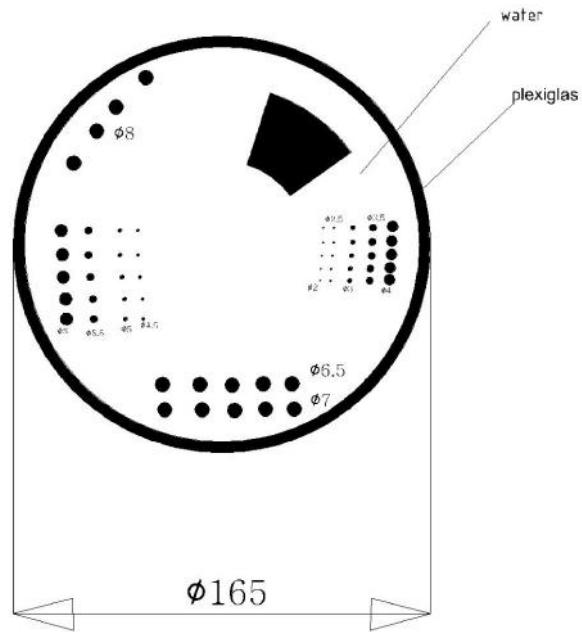


Figure 2.10: Design of ATS Phantom

Mostrom’s Phantom

Homogeneity is very critical parameter to assesses the quality of the image[14]. The example of Mostrom phantom is shown in figure 2.11, as seen from the figure there are five homogenous water column placed at different places of the phantom to ensure accurate homogeneity of scanner.

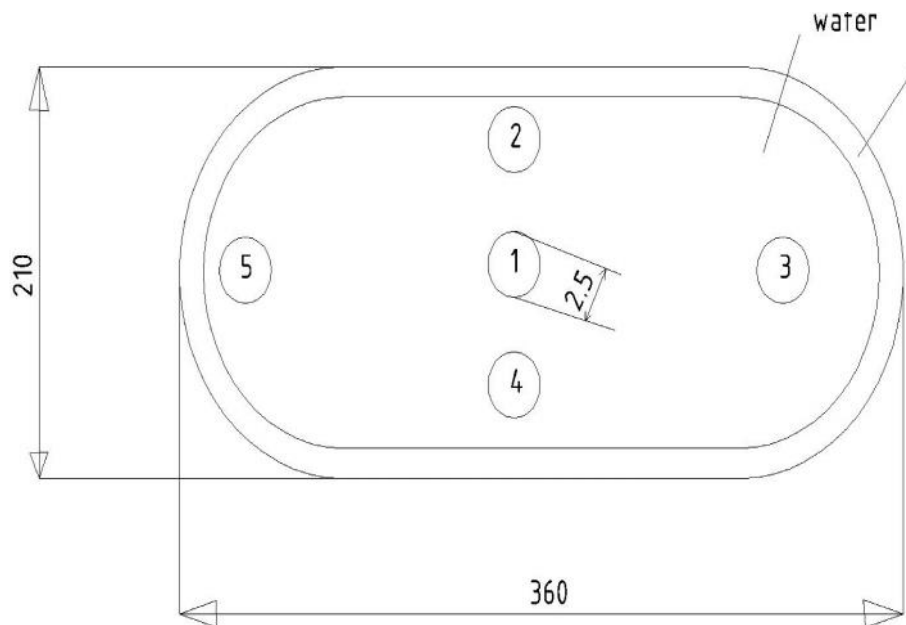


Figure 2.11: Design of Mostrom’s Phantom

Low Contrast Resolution Phantom

The design of this phantom is shown in the figure 2.12. As seen from the figure the metal rods with different diameters are immersed in to the water at decreasing distance.

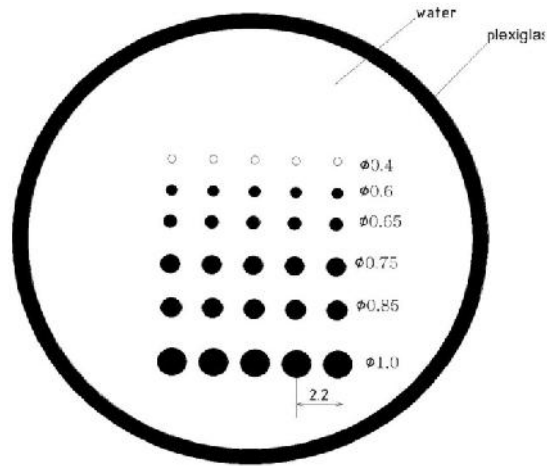


Figure 2.12: Design of Low Contrast Phantom

Spatial Resolution Phantom

Spatial resolution is the most important parameter for the CT scanners, it is nothing but the ability of scanner to distinguish two points in the image higher the spatial resolution better the quality of image. Measurement of this parameter is done with phantom shown in the figure 2.13 as seen from the figure it contains a metal wire of very small diameter.

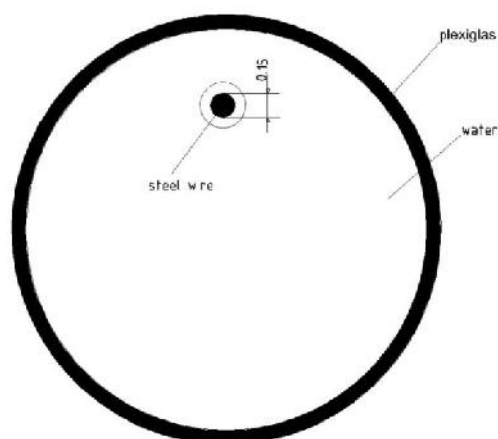


Figure 2.13: Design of Spatial Resolution Phantom.

CT Linearity Phantom

As the name suggest this phantom is used to find out the linearity function of the CT scanner. The design of this phantom is shown is the figure 2.14. It is made up of five materials with different CT number ensuring that the maximum range of CT number is covered.

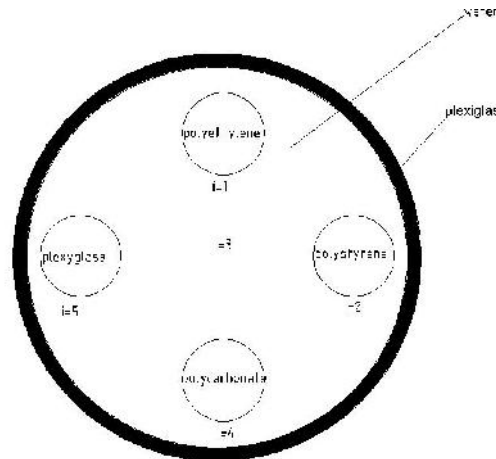


Figure 2.14: Design of CT Linearity Phantom

Slice Thickness Phantom

Slice thickness plays vital role in diagnosis from the reconstructed image especially in calculating the grown of the tumours. In order to measure this parameter the phantom shown in the figure 2.14 is used.

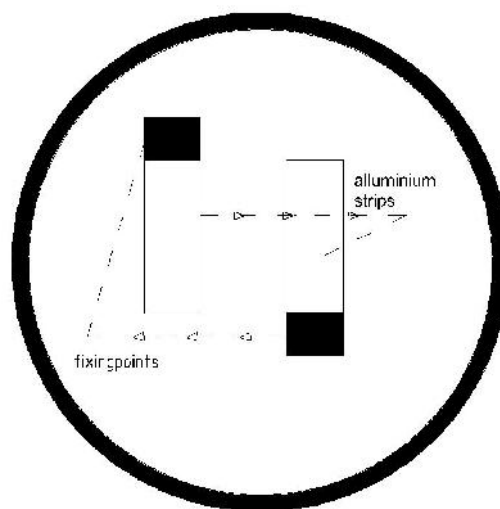


Figure 2.15: Design of Slice Thickness Phantom

2.7 Concluding Remarks

This chapter provides the necessary details regarding the technical aspects of CT scanner and the various evaluation parameters of the scanner and method to evaluate these parameters.

Chapter: 3

Reconstruction Techniques

This chapter addresses the basic reconstruction problem, it also discusses the necessary mathematical framework required to solve the problem of reconstruction by algebraic and analytical approaches.

3.1 Image Reconstruction Problem

As mentioned in Chapter 2, the key problem arising in computerized tomography is image reconstruction from projections obtained from the X-ray scanner given geometry. The human beings are heterogeneous in nature hence the mathematical equation for the attenuation can be expressed as [1-4]:

$$I(U) = I(0) \cdot e^{-\int_0^U \mu(x,y) \cdot du} \quad (3.1)$$

where $I(0)$ is the initial X-ray intensity; $I(U)$ is the X-ray intensity after passing through the distance U ; $\mu(x, y)$ is the function defining the spatial distribution of the attenuation coefficient in the sample.

$\mu(x, y)$ provides the information regarding the spatial distribution of the attenuation coefficient, which in turn provides information regarding the arrangement of various organs inside the body. Applying logarithm to both sides of the equation 3.1 results into:

$$p \triangleq \ln \left(\frac{I(0)}{I(U)} \right) = \int_0^U \mu(x, y) \cdot du \quad (3.2)$$

where p is the quantity ratio of X-ray intensity directed at a given point in body to the radiation intensity after passing through the body. In conventional X-ray films, less darkening of the film signifies more attenuation of the X-ray radiation.

“Projection” is to create image of the internal body organ. Hence, it is necessary to form beam of X-rays, which will form the image on the screen after X-rays pass through the object. In order to obtain image of cross-section of object in the plane of the projection, the parameter of quantity p must be obtained as shown in the figure 3.1:

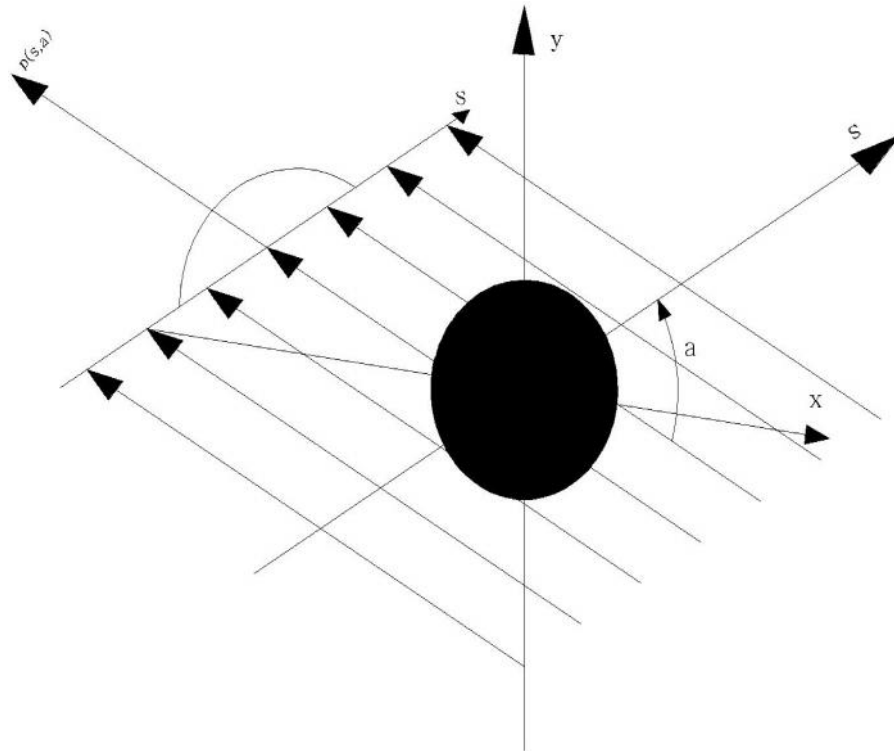


Figure 3.1: Simple Projection Systems

The first parameter is the variable s which is describing the axis perpendicular to the direction of X-ray, the value of $s = 0$ defines the principal axis of projection. The second parameter is the α , at which, at given movement, the projection is made. This relation can be mathematically expressed as:

$$p(s, \alpha) = \int_U \mu(x, y) du \quad (3.3)$$

where the parameter ranges from $-\infty < s < \infty, 0 \leq \alpha < \pi$.

The above equation is also called Radon transform [1-4]. Mathematically, it can be expressed as:

$$R: \mu(x, y) \in \mathbb{H}\mathbb{U} \xrightarrow{R} p(s, \alpha) \in \mathbb{R} \quad (3.4)$$

In Computed tomography, Radon transform is performed physically by the attenuation of the X-rays as they pass through the object. The sensors in the gantry record the change intensity of X-rays after passing through the object.

As shown in the figure 3.2, X-ray intensity at point on the screen corresponds to a single value of $p(s, \alpha)$. Only the material lying in the path of the ray arriving at that point is responsible for the attenuation of the radiation as the radiation is in the form of a parallel beam. It follows the equation that attenuation takes place along the straight line defined by the parameter u , where the total path length is U .

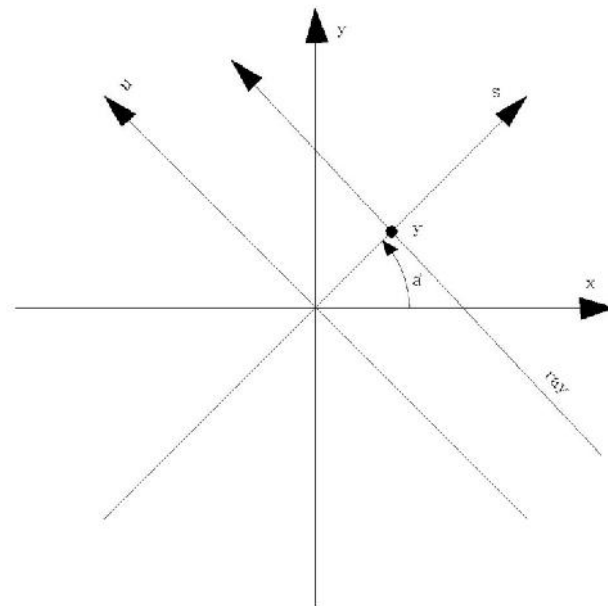


Figure 3.2: Basic Geometry of Scanner

One of the major issues with this relationship is its dependence of the attenuation function on the spatial variable (x, y) . The integration of variable takes place along the line at a distance s from projection axis. So, the fixed coordinate system (x, y)

must be converted in to moving coordinate system (s, u) that is rotated by an angle α with respect to the (x, y) sytem. This relationship can be derived as under:

The trigonometric relationship between the moving coordinate system and fixed coordinate systems can be expressed as under:

From the figure 3.3 it can be interpreted that

$$s = s' + s'' \quad (3.5)$$

The x -relationship in the fixed coordinate system (x, y) can be written as:

$$\frac{s'}{x} = \cos \alpha \quad (3.6)$$

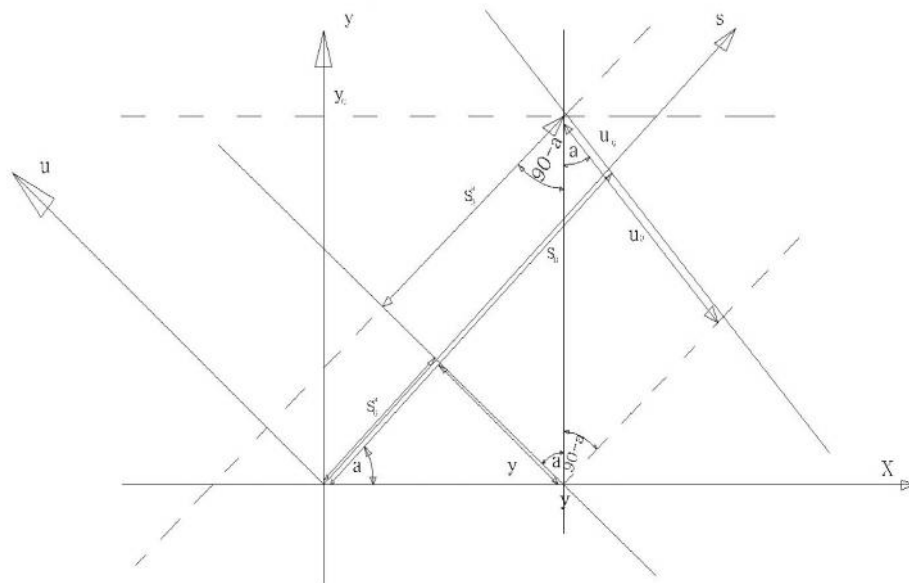


Figure 3.3: Detail of Trigonometric Relationship

Similarly y -relationship in the fixed coordinate system (x, y) can be written as:

$$\frac{s''}{y} = \cos \left(\frac{\pi}{2} - \alpha \right) = \sin \alpha \quad (3.7)$$

Hence,

$$s = x\cos\alpha + y\sin\alpha \quad (3.8)$$

Similarly,

$$u = u' + u'' \quad (3.9)$$

So, y-relationship in the fixed coordinate system (x, y) can be written as:

$$\frac{u'}{x} = \cos\alpha \quad (3.10)$$

For the x-relationship in the fixed coordinate system (x, y) can be written as:

$$\frac{u''}{x} = -\sin\alpha \quad (3.11)$$

Hence,

$$u = -x\sin\alpha + y\cos\alpha \quad (3.12)$$

Applying the above relationships to the basic reconstruction equation 3.1, following equation can be obtained:

$$p(s, \alpha) = \int_{-\infty}^{\infty} \int_{-\infty}^{\infty} \mu(x, y) \delta(x\cos\alpha + y\sin\alpha - s) dx dy \quad (3.13)$$

So, it is evident that to determine the projection function for a particular point s on the screen for particular angle of rotation α of the scanner, the sum of values of attenuation coefficients of the object along the path of the ray is needed.

3.2. Reconstruction Methods

There are two methods to find the solution for reconstruction problem. These methods are analytical and iterative. The basic analytical technique includes back projection method and iterative method includes Algebraic Reconstruction Technique (ART) [5-6].

3.2.1 Algebraic Reconstruction Techniques

Algebraic Reconstruction Techniques use the finite series expansion [6-10]. In this method, the solution is characterized by assumption that reconstructed images consist of a finite number of elements. In this method, discretisation takes place before the introduction of discrete form of algorithm. The area of interest is divided into blocks of identical size. These blocks are defined as having a uniform radiation attenuation coefficient. The geometrical centre of each block will be considered as corresponding to one pixel of the reconstructed digital image. The topology of the reconstructed image is as shown in the figure 3.4:

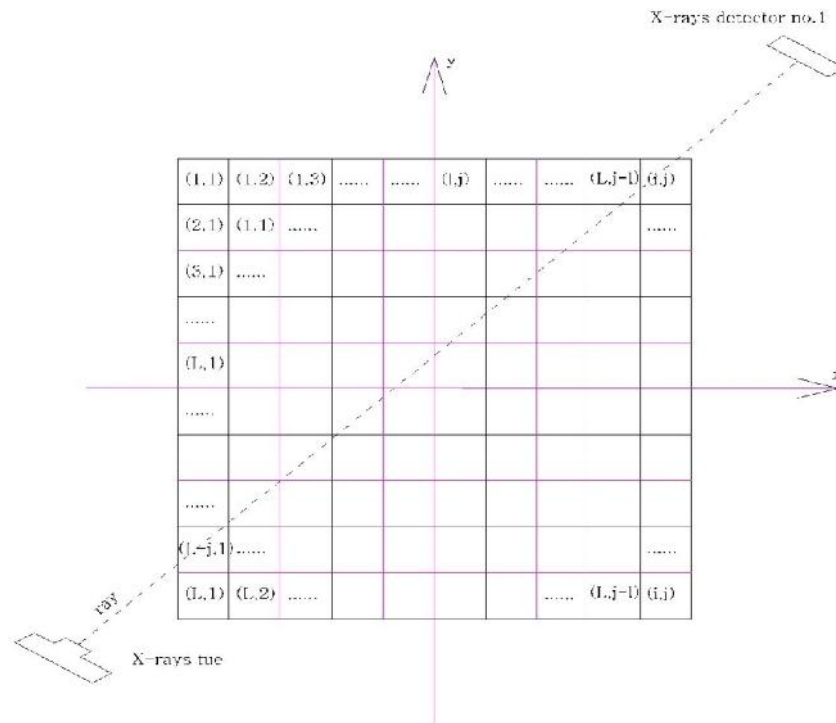


Figure 3.4: Projection Geometry for Algebraic Reconstruction Technique

From the figure, each block in the image is identified horizontally by the coordinates $i = 1, \dots, I$ and $j = 1, \dots, J$. Hence, the uniform attenuation coefficient can be represented by μ_{ij} , This makes it independent of the geometry of projection system. Here, each projection value is obtained at an angle α_{ψ}^p and measured at a point on the screen at a distance s_i away from the axis of the projection which is represented by the discrete form of the projection function:

$$\widehat{P}^p = (l, \psi) \equiv P^p(l\Delta_s^p, \psi\Delta_s^p) \quad (3.14)$$

where l is the detector number, in the matrix; ψ is the projection number, Δ_s^p is the distance between the individual detectors on the screen, Δ_s^p is the angle, through which the lamp-screen arrangement is rotated after each projection. The radon transform in the discrete form can be represented as:

$$\widehat{P}^p(l, \psi) = R(\mu(x, y)) \quad (3.15)$$

The algebraic approach, in addition to this, assumes that attenuation coefficient distribution $\mu(x, y)$ can be represented approximately as a finite linear combination of basis function and constant coefficient which can be written as:

$$\mu(x, y) \cong \hat{\mu}(i, j) = \sum_{i=1}^I \sum_{j=1}^J \mu_{ij} \varrho_{ij}(x, y) \quad (3.16)$$

where $\varrho_{ij}(x, y)$ is elements of set of basic function; μ_{ij} is a constant coefficient with the block (i, j) . Considering the equation 3.16, equation 3.15 can be reformulated as under:

$$\widehat{P}^p(l, \psi) \cong R(\mu(x, y)) = R \left[\sum_{i=1}^I \sum_{j=1}^J \mu_{ij} \varrho_{ij}(x, y) \right] \quad (3.17)$$

$$\widehat{P}^p(l, \psi) \cong \sum_{i=1}^I \sum_{j=1}^J \mu_{ij} R(\varrho_{ij}(x, y)) \quad (3.18)$$

For algebraic method, this equation can be written as:

$$\hat{P}^p(l, \psi) \cong \sum_{i=1}^I \sum_{j=1}^J \mu_{ij} \chi_{ij}(l, \psi) \quad (3.19)$$

where $\chi_{ij}(l, \psi)$ can be interpreted physically as the contribution of a given image block with parameters (i, j) to formulation of the projection value identified by the pair (l, ψ) , measured at the screen.

As shown in the figure 3.5, as the ray passes through the test object, all the squares through which part of the ray passes are taken into consideration. The next step is to consider the contribution made by each image block to the way in which ray (l, ψ) passes through in the course of making a series of projections. The value of each contribution $\chi_{ij}(l, \psi)$ varies between 0 and 1 which can be interpreted as when the ray passes through the block is 1 otherwise 0. Hence, values $\chi_{ij}(l, \psi)$ for all projection angles obtained by using equation 3.19 can formulate a system of linear equations.

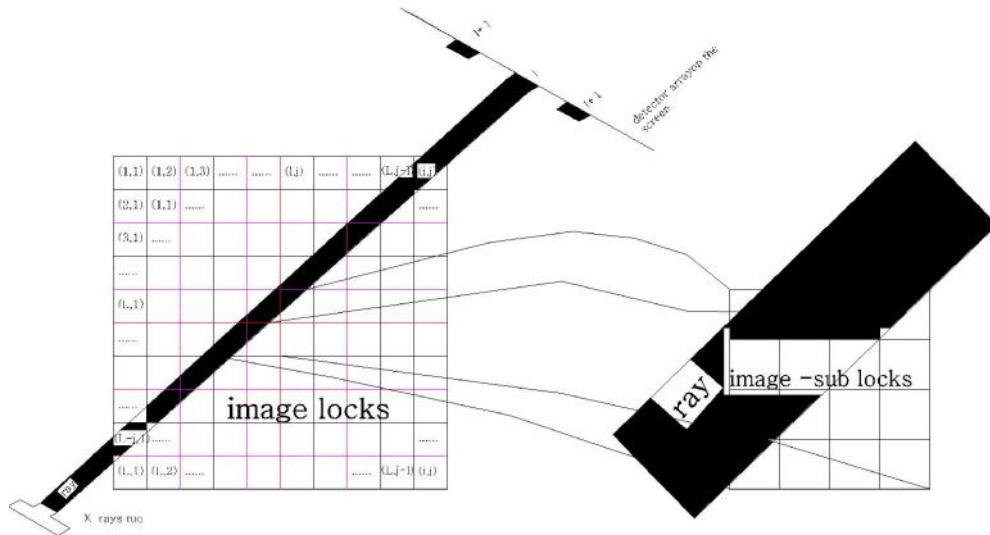


Figure 3.5: Determination of the Image Block.

Thus, the problem of reconstruction can be solved by algebraic method. From implementation point of view, dimensionality ($I \times J$) of the array of μ_{ij} cannot be implemented as one needs to transform this matrix into vector μ with dimension $I \cdot J$. One approach to this is by placing successively of the column $J = 1, \dots, J$ of the array μ_{ij} into the vector μ . This can be mathematically represented as:

$$P = \chi\mu \quad (3.20)$$

where P the projection is vector with dimensions $L \cdot \Psi$; χ is the matrix of values $\chi_{ij}(l, \psi)$ with dimensions $L \cdot \Psi \times I \cdot J$. Hence, the problem is reduced to estimating the value of matrix μ based on the value of matrix P . The biggest disadvantage of this method is the complexity of the calculations caused by enormous size of the matrix χ . For a typical image with dimension of 256×256 , the number of calculation will be 51200×65536 .

3.2.2 Analytical Method

Analytical Method is popularly known as Back-projection method [11-14] and is mathematically expressed as:

$$B(x, y) = \int_0^\pi P^p(x \cos \alpha^p + y \sin \alpha^p, \alpha^p) d\alpha^p \quad (3.21)$$

This equation assigns each point in space (x, y) , as a sum of all projection function values, which correspond to rays going through each point in the course of obtaining projections. Hence, equation 3.21 contains information about attenuation coefficient at that point. But, one of the limitations of this model would produce an indistinct image because back-projection is not same as inverse Radon transform. The image defined by function $\hat{\mu}(x, y) = B(x, y)$, obtained in this way, would be distorted so much that it will make medical interpretation impossible. The process of obtaining the image $\mu(x, y)$ by projection and back projection is shown in the figure 3.5:

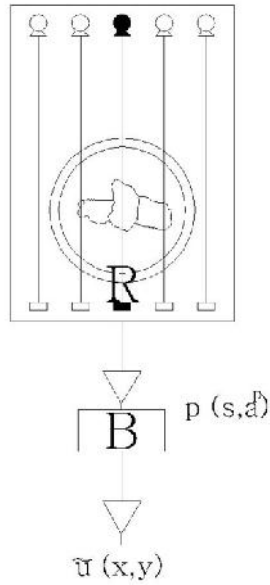


Figure 3.6: Image Projection and Back projection Operation

The relationship between the attenuation function $\mu(x, y)$, obtained by projection and the attenuation coefficient function $\mu(x, y)$ of the cross section of the object can be mathematically analysed as follow:

$$\tilde{\mu}(x, y) = B(x, y) \quad (3.22)$$

$$\tilde{\mu}(x, y) = \int_0^\pi P^p(x \cos \alpha^p + y \sin \alpha^p, \alpha^p) d\alpha^p \quad (3.23)$$

Substituting the value from equation 3.13 in equation 3.23, a new equation is obtained as under:

$$\tilde{\mu}(x, y) = \int_0^\pi \left(\int_{-\infty}^\infty \int_{-\infty}^\infty \mu(\hat{x}, \hat{y}) \delta(\hat{x} \cos \alpha + \hat{y} \sin \alpha - s) d\hat{x} d\hat{y} \right) d\alpha^p \quad (3.24)$$

Coordinates (\hat{x}, \hat{y}) refer to all the points in the reconstructed image, variable s only to those points which for a particular projection, lie on the same straight line as the reconstructed image point specified by coordinates (x, y) . Substituting the formula for the distance s of the reconstructed image point, following equation is obtained:

$$\tilde{\mu}(x, y) = \int_0^\pi \left(\int_{-\infty}^\infty \int_{-\infty}^\infty \mu(\dot{x}, \dot{y}) \delta(\dot{x} \cos \alpha + \dot{y} \sin \alpha - x \cos \alpha^p - y \sin \alpha^p) d\dot{x} d\dot{y} \right) d\alpha^p \quad (3.25)$$

Further simplifying,

$$\tilde{\mu}(x, y) = \int_0^\pi \left(\int_{-\infty}^\infty \int_{-\infty}^\infty \mu(\dot{x}, \dot{y}) \delta(x - \dot{x}) \cos \alpha^p + (y - \dot{y}) \sin \alpha^p \right) d\dot{x} d\dot{y} d\alpha^p \quad (3.26)$$

Changing the order of integration,

$$\tilde{\mu}(x, y) = \int_{-\infty}^\infty \int_{-\infty}^\infty \mu(\dot{x}, \dot{y}) \left(\int_0^\pi \delta(x - \dot{x}) \cos \alpha^p + (y - \dot{y}) \sin \alpha^p \right) d\alpha^p d\dot{x} d\dot{y} \quad (3.27)$$

Using the substitution, following equation is obtained:

$$\tilde{\mu}(x, y) = \int_{-\infty}^\infty \int_{-\infty}^\infty \mu(\dot{x}, \dot{y}) \frac{1}{\sqrt{(x - \dot{x})^2 + (y - \dot{y})^2}} d\dot{x} d\dot{y} \quad (3.28)$$

Hence, the final equation turns out to be:

$$\tilde{\mu}(x, y) = \mu(x, y) * (x^2 + y^2)^{-\frac{1}{2}} \quad (3.29)$$

From the above equation, it is clear that the image that is obtained through back projection lacks information about the actual form of the attenuation function, but is distorted by geometric factor $(x^2 + y^2)^{-\frac{1}{2}}$. This distortion appears to be artefact in the reconstructed image. If a system is shown by only two projections that are performed and it contains artefacts, it takes form of a line lying along the path of the rays as seen in the figure 3.6.

When data processing is done continuously, it is assumed that the object consists of one non-zero point at centre as follows:

$$\mu(x, y) = \delta(x - x_0, y - y_0) \quad (3.30)$$

where $(x - x_0, y - y_0)$ are the coordinates of the centre of object's cross section. In frequency domain, the distortion can be represented by:

$$FUN(f_1, f_2) = (f_1^2 + f_2^2)^{-\frac{1}{2}} \quad (3.31)$$

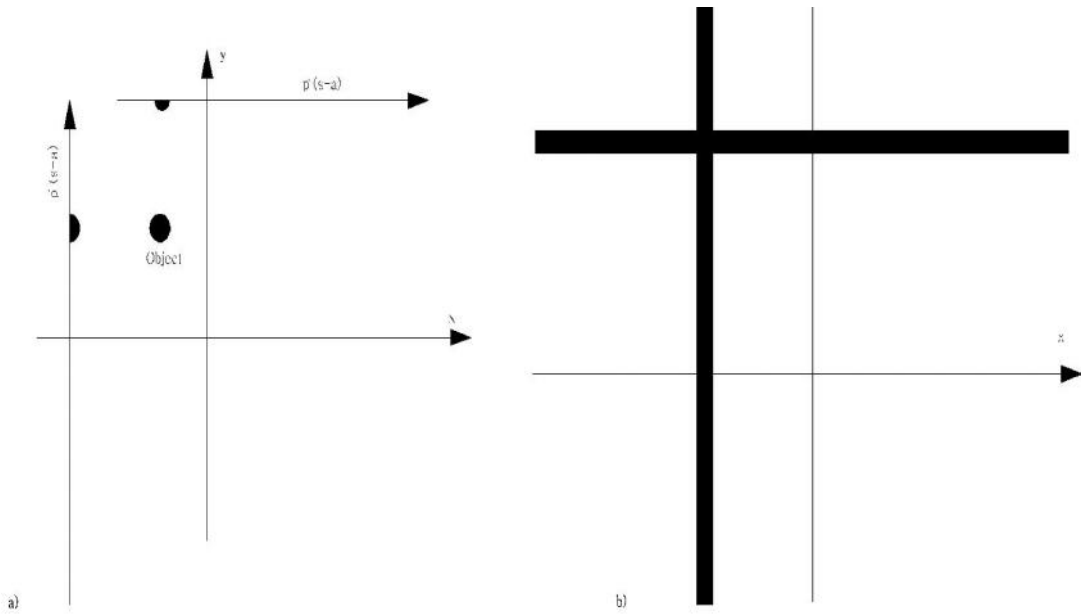


Figure 3.7: a) Sequence of Projection b) Distorted image after Back projection

Considering the moving coordinate system, equation 3.29 can be re written as:

$$\tilde{\mu}(r, \phi) = \mu(r, \phi) * \frac{1}{|r|} \quad (3.32)$$

Following the definition of Fourier Transformation, equation (3.32) can be written as:

$$P(f, \alpha^p) = \int_{-\infty}^{\infty} P^p(s, \alpha^p) e^{-j2\pi f s} ds \quad (3.33)$$

The projection for one particular s is the integral over all the points lying in one straight line and using the equation 3.13, following equation can be obtained:

$$P(f, \alpha^p) = \int_{-\infty}^{\infty} \int_{-\infty}^{\infty} \mu(x, y) \delta(x \cos \alpha + y \sin \alpha - s) e^{-j2\pi f s} ds du \quad (3.34)$$

Modifying the above equation results into:

$$P(f, \alpha^p) = \int_{-\infty}^{\infty} \int_{-\infty}^{\infty} \mu(s \cos \alpha^p - u \sin \alpha^p, s \sin \alpha^p + u \cos \alpha^p) e^{-j2\pi f s} ds du \quad (3.35)$$

Converting into (x, y) coordinate system gives:

$$P(f, \alpha^p) = \int_{-\infty}^{\infty} \int_{-\infty}^{\infty} \mu(x, y) e^{-j2\pi f (x \cos \alpha^p + y \sin \alpha^p)} dx dy \quad (3.36)$$

Applying the definition of two dimensional 'Fourier transformation' to equation 3.36 the final form obtained is:

$$P(f, \alpha^p) = M(f \cos \alpha^p, f \sin \alpha^p) \quad (3.37)$$

From the above equation 3.37, it follow that the frequency spectrum projection carried out at an angle α^p is equal to a section of the two dimensional spectrum of original image. Hence, instead of filtering the whole image in two dimensions, it is enough to filter all projections in one dimension, using the familiar filter form. Also, instead of filtering the image in two dimensions after back projection, each image is filtered separately and followed by back projection. This can be achieved by inverse Radon transform $R^{-1}\{p(s, \alpha^p)\}$. Mathematically it can be expressed as:

$$\mu(x, y) = R^{-1}\{R(\mu(x, y))\} \quad (3.38)$$

This can be further modified as follow [9]

$$\mu(x, y) = R^{-1}p(s, \alpha^p) = \int_0^{\pi} \bar{p}^p(x \cos \alpha^p + y \sin \alpha^p, \alpha^p) d\alpha^p \quad (3.38)$$

Equation 3.38 defines inverse radon transform. The main process in analytical method is to obtain filtered back projection before applying back projection operator to obtain the reconstruction image.

3.3 Display of Images

After applying the appropriate reconstruction algorithm to the project data, the next logical step is display of the image. The projection data obtained depends on the density of the object. In case of human organism, if the tissues are diseased, the attenuation of the X-ray will be different as compared to the healthy tissues. Mathematically, the value of attenuation can be expressed as:

$$\mu: (x, y) \in \mathbb{R}^2 \xrightarrow{\mu} \mu(x, y) \in [\mu_{min}, \mu_{max}] \quad (3.39)$$

The discrete representation of equation (5.33) is:

$$\hat{\mu}: [1, \dots, I] \times [1, \dots, J] \in \mathbb{R}^2 \xrightarrow{\mu} \mu(x, y) \in [\mu_{min}, \mu_{max}] \quad (3.40)$$

One of the important factors which effects the display of image is luminance and defined by the equation [16] as:

$$lum(x, y) \triangleq \int_0^{\infty} \Lambda(\lambda) I_{light}(x, y, \lambda) d\lambda \quad (3.41)$$

where λ is wavelength of the light and $I_{light}(x, y, \lambda)$ is the distribution of the light emitted by the object and $\Lambda(\lambda)$ is the function of efficiency of the visual system.

The analogue luminance of images need to converted to discrete format before displaying it on the computer screen[15]. For converting the image to discrete form and display, two processes must be undertaken Discretisation and Quantization as described in figure 3.7.

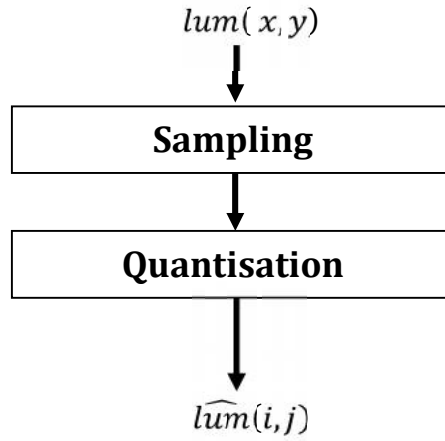


Figure 3.8: Sampling and Quantisation of Analogue Images

First, through the sampling process, the luminance is transformed as:

$$\widehat{lum}(i, j) = lum(x, y) \cdot comb(x, y; \Delta x, \Delta y) \quad (3.42)$$

where $\Delta x = \frac{1}{2f_{x0}}$ is the horizontal raster discretisation; $\Delta y = \frac{1}{2f_{y0}}$ is the vertical raster discretisation, f_{x0} is horizontal cut-off frequency and f_{y0} is vertical cut-off frequency.

$$comb(x, y; \Delta x, \Delta y) \triangleq \sum_{i=1}^I \sum_{j=1}^J \delta(x - i\Delta x, y - j\Delta y) \quad (3.43)$$

where I, J are the number of image points sampled vertically and horizontally respectively. Combining equation 5.36 and 5.37:

$$\widehat{lum}(i, j) = \sum_{i=1}^I \sum_{j=1}^J \delta(x - i\Delta x, y - j\Delta y) \quad (3.44)$$

In frequency domain, equation 5.38 can be expressed as:

$$\widehat{LUM}(f_x, f_y) = LUM(f_x, f_y) COMB(f_x, f_y) \quad (3.45)$$

After sampling process, the next process is quantisation. But before displaying it to screen, a non linear transformation needs to be applied [15]. For medical purpose, this transformation is Hounsfield scale or CT number [16, 17], which is in honour of CT scanner inventor. The range of value of this scale is from - 1000 to 3000, which makes it necessary to apply window. The window selection is nothing but the selection of scale by two parameters window centre C and window width W. Some of the CT number common used to view human tissue are as follow as for example for human bone is C=1000 HU and W=2500 HU and C=-600 HU and W=1700 HU for the lung imaging.

During the comprehensive topographic examination a series of actions are performed which produces the set of images from the slices of the tissue. During the scan the patient is laid on the table and table will move into the gantry as per the requirement set by the radiologist. The places where the image slices are planned are indicated as *Field of view (FOV)* markers.

In some of the cases in order to enhance the contrast of the iodine based dye is injected in the body of the patient [18] especially in case of tumours in soft tissue. After obtaining the set of tomography images the next step is to diagnosis by radiologist often it is necessary to measure the distance between the tissues and enlarge the particular tissue which in medical terms is known as region of interest (ROI).

3.4 Concluding Remarks

Thus, chapter discusses various aspects of basic reconstruction problem along with the two approaches analytical and algebraic to solve the problem. This chapter also provide necessary frame work for the newly developed approach which is discussed in subsequent chapters along with techniques to display the reconstructed images.

Chapter: 4

Soft Computing Techniques Design and Development Tools

This chapter gives the theoretical background for various soft computing techniques like Artificial Neural Network and Genetic Algorithm. Researchers across the globe use MATLAB® and its Toolboxes for implementing their research work. The research work presented in the present thesis is also implemented on the same platform, and so chapter also presents an overview regarding the same.

4.1 Introduction

In recent years, soft computing techniques have evolved as most efficient tools to solve complex engineering and scientific problems. Soft Computing includes Fuzzy Logic (FL), Neural Networks (NN), and Genetic Algorithms (GAs) methodologies. It also combines these methodologies as FL and NN (FL-NN), NN and GA (NN-GA) and FL and GA (FL-GA). These techniques essentially solve the problems by the “human” approach as opposite to the conventional “hard” computing technique which is tolerant of imprecision, uncertainty, partial truth and approximation. Fuzzy logic is based on the human reasoning and language to solve the problems, while in Neural Network; problems are solved by using the artificial neurons, whose structure resembles to biological neurons. Similarly, Genetic Algorithm uses Darwin’s theory of evolution for the solution. The present research work uses Neural Network and Genetic Algorithm and so the basic theoretical background needs to be understood. In the following sections, basic theoretical background is explained.

4.2 Artificial Neural Network

Human brain is capable of solving very complex and non-linear real world problems. Fundamental unit of human brain is neuron, which is also functional unit of human brain. Researchers have developed mathematical model of the neuron and mimicked its functioning that has resulted into a very efficient problem solving network, Artificial Neural Network popularly known as Neural Network. The functioning of Neural Network is very similar to that of human brain; it is capable to

learn, store, adapt, respond and map. These functions are essential to solve the complex problems. The fundamental unit of the NN is the neuron which is information processing unit.

4.2.1 Model of Neuron

As compared to the human neuron, the artificial neuron also consists of three fundamental components; synaptic weights, summing junction and activation function. These functions are graphically represented in figure 4.1:

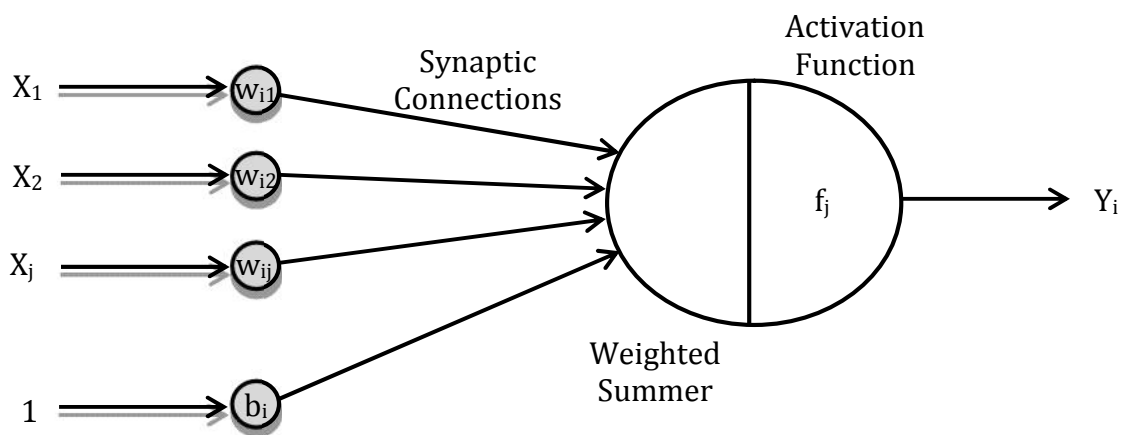


Figure 4.1: Basic Artificial Neuron

From the above figure, input x_i is connected to the summing junction by the synaptic weight w_{ji} popularly known as weight. These weights have specific values. The second component is the adder that is summing junction which is adding all the inputs with bias b_j . The most important component is activation function f_i that will control output of neuron and is also known as squashing function and Y_i is the output. Mathematically, it can be written as:

$$S_j(t) = \sum_{i=1}^n w_{ij} x_i(t) + b_j \quad (4.1)$$

and,

$$S_j(t) = w_j x + b_j \quad (4.2)$$

The activation function f_i defines the output of a neuron in terms of induced field. The activation function can be broadly classified into two broad categories: threshold function and sigmoid function. These functions are show in the figure 4.2 and figure 4.3 respectively.

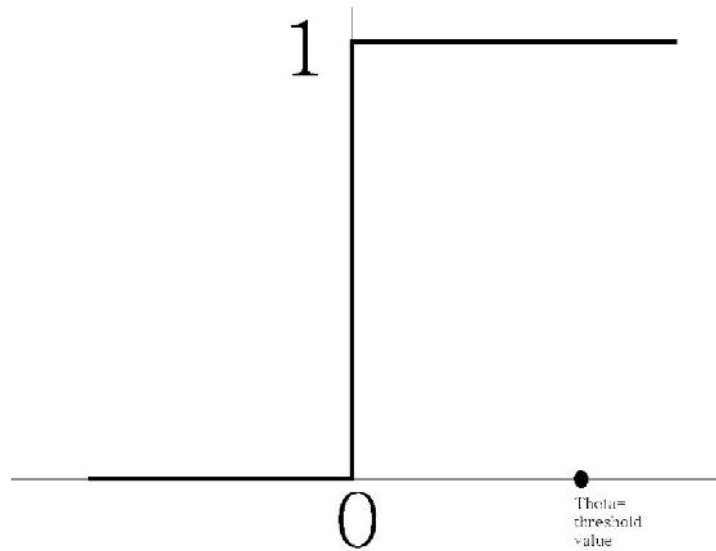


Figure 4.2: Basic Thresholding Function

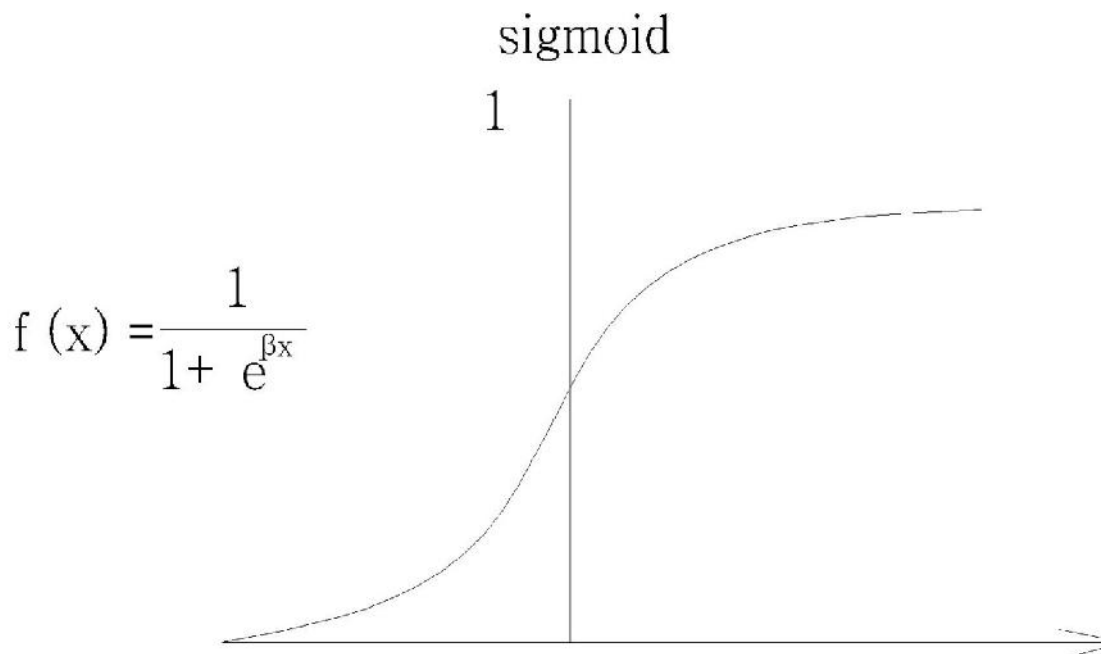


Figure 4.3: Basic Sigmoid Function

4.2.2 Neural Network Architecture

Based on the connection of neuron, the neural network can be classified into two broad categories

- Feed forward Network
- Feedback Network

Feed forward Network

Figure 4.4 shows the basic construction of feedback network. It has multilayer network where first layer has a connection from the network input. Each subsequent layer has a connection from the previous layer. The final layer produces the network's output.

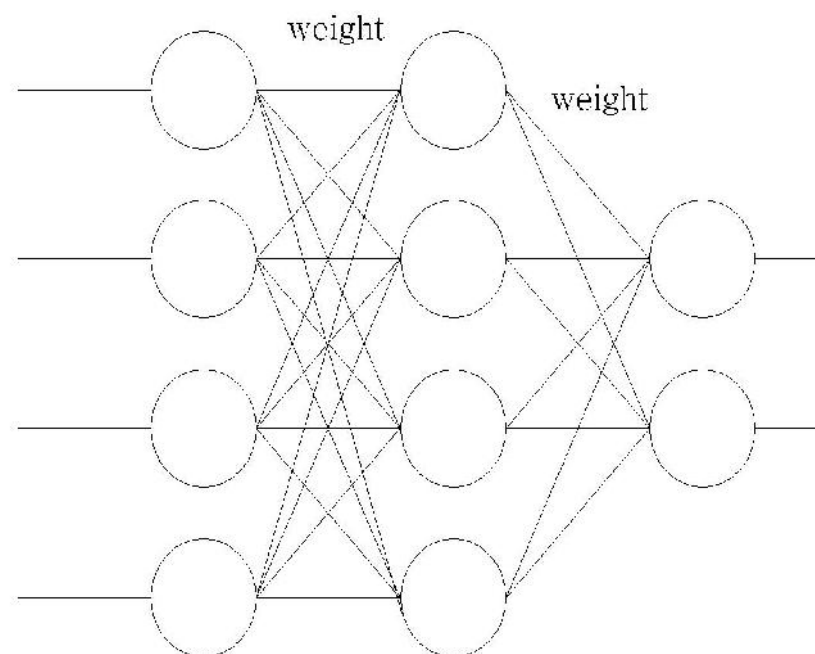


Figure 4.4: Basic Feed Forward Neural Network

Feedback Network

Feedback Network is also popularly known as Recurrent Network and widely used for parallel computing and solving stochastic network. The schematic diagram of feedback network is shown in the figure 4.5. As can be seen in the figure, each neuron is connected to each neuron and activated parallel after taking the feedback.

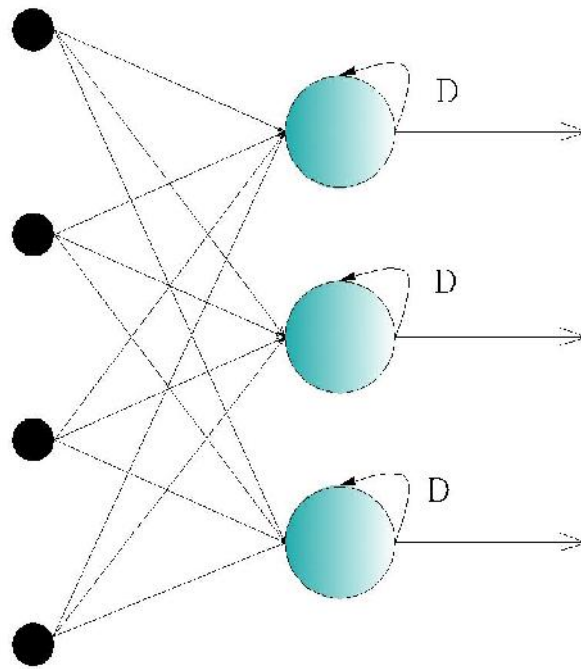


Figure 4.5: Basic Feedback Neural Network

4.2.3 Neural Network Learning

Neural Network learning is algorithm that is used to update weight and bias to obtain the desired response. Neural Network can be trained by two type of learning as:

- Supervised Learning Algorithm
- Unsupervised Learning Algorithm

Supervised Learning Algorithm

In this algorithm, the output of the network is compared to desired output of the network and correspondingly weights are adjusted; so after each cycle the output of network is close to desired output. Some popular neural networks based on supervised learning include:

- ADLINE
- MADALINE
- Perceptron
- Multi-Layer Perceptron (MLP)
- Radial Basic Neural Network(RBFN)
- Probabilistic Neural Network(PNN)

Unsupervised Learning Algorithm

This learning algorithm is based on the concept of self learning, where there is no supervision on the learning. In this algorithm, the weights adjust by themselves and assess their own performances. These networks look for regular patterns in the input signals, and make adaptations according to the function of the network. Even without being told whether it's right or wrong, the network still must have some information about how to organize itself. This type of learning is very much useful to solve stochastic problems as it is impossible to make network learn the infinite pattern and obtain desired output. Some popular neural networks based on unsupervised learning algorithm are:

- Hamming networks;
- Kohonen's self-organizing maps;
- Adaptive Resonance Theory(ART);
- Counter Propagations Networks (CPN), etc.

4.2.4 Hopfield Neural Network

Hopfield Neural Network is type of recurrent network that is used to solve medical problem. In the present research, Hopfield network is extensively used. Hopfield network is set of neurons and corresponding unit time delays creating multiple loop feedback systems as shown in figure 4.6. As discussed in previous section the weights are adjusted.

Hopfield network is an implementation of a learning matrix with recurrent links. The learning matrix is a weight matrix that stores associations between inputs and targets. This network identifies general dependencies in the given incomplete and noisy training data. So, it resembles a learning matrix. This kind of a network is linear model as it can model only linearly separable data.

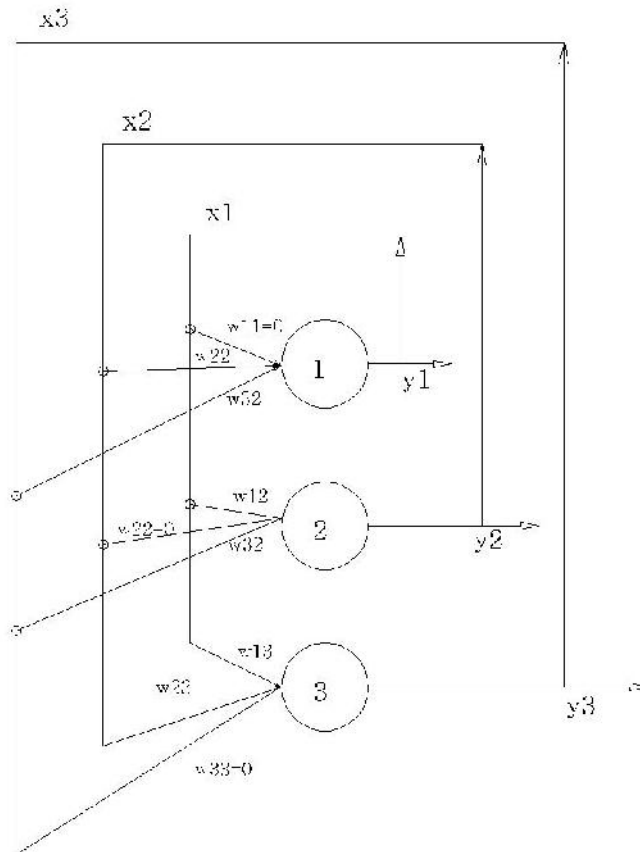


Figure 4.6: Basic structure of Hopfield Network

Hopfield Type Network is a multiple-loop feedback neural computation system. The neurons in this network are connected to all other neurons except to themselves that is there are no self-feedbacks in the network. A connection between two neurons N_i and N_j is a two way connection which is denoted by w_{ij} . The connection w_{ij} from the output of neuron i to the input of neuron j has the same strength as the connection w_{ji} from the output of neuron j to the input of neuron i , in other words the weight matrix is symmetric. Each neuron computes the summation:

$$s_{ij} = \sum_{j=1}^n w_{ji} x_j \quad (4.3)$$

Hopfield network can be made to operate in either continuous or discrete mode.

Learning and Training Algorithm for Hopfield networks

Learning: Present the given training (binary) vectors to the Hopfield net, and calculate the weights using the Widrow-Hoff rule

$$\text{if } s_i \geq 0 \text{ and } x_i = 0 : w_{ji} = w_{ji} - (0.1 + s_i) / n$$

$$\text{if } s_i < 0 \text{ and } x_i = 1 : w_{ji} = w_{ji} + (0.1 - s_i) / n$$

Initialization: Let the testing vector become initial state $x(0)$

Repeat

-update asynchronously the components of the state $x(t)$

$$x^i(t) = 1 \text{ if } s_i(t) = \sum_j w_{ji} x_j(t) \geq 0 \text{ or } x^i(t) = 0 \text{ if } s_i(t) < 0$$

Continue this updating until the state remains unchanged until convergence generates output: return the stable state (fixed point) as a result.

The energy is a behavioural characteristic that can be used to examine network performance. It is well known that independently from the initial conditions, the network will stabilize; it cannot oscillate even at the same energy level. The convergence of network can be considered as a process of reducing the network energy until reaching energy well; that is the stable network states are energy wells.

4.3 Genetic Algorithm

Genetic algorithms are inspired by Darwin's theory about evolution. Genetic algorithm provides solution to a problem. Algorithm is started with a set of solutions (represented by chromosomes) called population. Solutions from one population are taken and used to form a new population. This is motivated by a hope that the new population will be better than the old one. Solutions which are selected to form new solutions (off springs) are selected according to their fitness – the more suitable they are the more chances they have to reproduce. Implementation of Genetic Algorithm can be summarized into following steps:

1. Generating population of n chromosomes that are suitable solutions for the problem.
2. Evaluating fitness function for each chromosome in the population.
3. Creating new population by Selection, Crossover and Mutation.
4. Put the newly created offspring in the population and creating new population.
5. Using new population to run the algorithm to obtain desired solution if desired solution is not obtained repeat the process.

Graphical, implementation of genetic algorithm is shown in the figure 4.7.

Selection

The first essential step to select the parent population to crossover, the best chromosomes must be selected as per the Darwin's theory of evolution. Some of the popular methods that are used to create the population are roulette wheel selection, Boltzman selection, tournament selection, rank selection, and steady state selection.

Encoding

As discussed, the important task after selection is to encode the chromosomes. This chromosome contains the information regarding the solution it represents. The common way of encoding this information is by creating the binary string; e.g. a chromosome string can look like, 1101100100110110 where each bit represents some characteristic of the solution. Apart from binary encoding, there are many

different ways to encode solution that includes permutation encoding, value encoding and tree encoding.

Crossover and Mutation

Crossover and mutation are two basic operators of Genetic algorithms. Performance of Genetic algorithms depends upon them. Type and implementation of operators work on encoding and also on a problem. Some commonly used crossover techniques, for binary encoded chromosomes, are single point crossover, two point crossover, uniform crossover and arithmetic crossover. The mutation technique that is used for the same purpose consists of inversion, order changing, adding and changing operator. The implementation

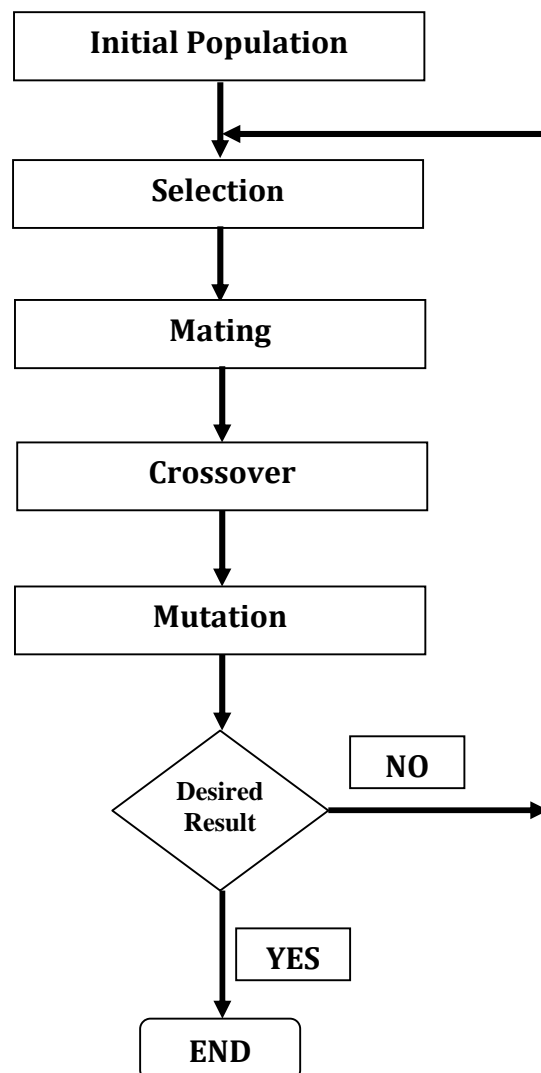


Figure 4.7: Flow Chart showing Implementation of Genetic Algorithm

Some of the common terms of Genetic Algorithms are defined below:

- **Chromosome Length** is the number of genes present on the chromosome. For demo, each gene can take on two values (0 or 1). The default setting is a length of 10. The chromosome length is an important consideration when optimizing a real variable problem. Longer chromosomes allow better conversion from the binary chromosome to the real number variable. However, the longer chromosome is computationally more inefficient and generally takes longer to find the optimal region. This concept can be studied by changing the fitness function to the Bohachevsky function.
- **Population Size** is the number of chromosomes in the population. Larger population sizes increase the amount of variation present in the population at the expense of requiring more fitness function evaluations.
- **Number of Generations** is the maximum number of generations that will be performed.
- **Mutation Rate** is the probability of mutation occurring. Mutation is the random flipping of one of the bits or genes (i.e. change from 0 to 1). Mutation is employed to give new information to the population. It also prevents the population from becoming saturated with chromosomes that all look alike (premature convergence). Large mutation rates increase the probability of destroying a good chromosome, but prevent premature convergence. The best mutation rate is application dependent and related to both the length of the chromosome and the size of the population. For most applications, a mutation rate of 0.1 to 0.01 is employed.
- **Fitness Function** allows the user to decide which fitness function the Genetic algorithms should employ. The first fitness function is called the simple function and consists of the summation of the chromosomes. The second fitness function finds chromosomes which optimize the Bohachevsky function. The third fitness function finds chromosomes which optimize the Rosenbrock function.

4.4 MATLAB® Platform

MATLAB® is the most popular technical platform for engineers worldwide. Most of the complex engineering problems are solved with lot of ease compared to other technical languages. In field of Image Processing and Optimization, the complex tasks are performed with help of the tool box which is developed by various experts. This section gives an overview about the specialized tool boxes for Neural Network and Genetic Algorithm. MATLAB® contains a vast collection of computational algorithms ranging from simple trigonometric function to various complex matrix operations.

One of the major advantages of MATLAB® platform, as a programming language, is that it allows both "programming in the small" to rapidly create quick programs. It can also do "programming in the large" to create complex application programs intended for reuse.

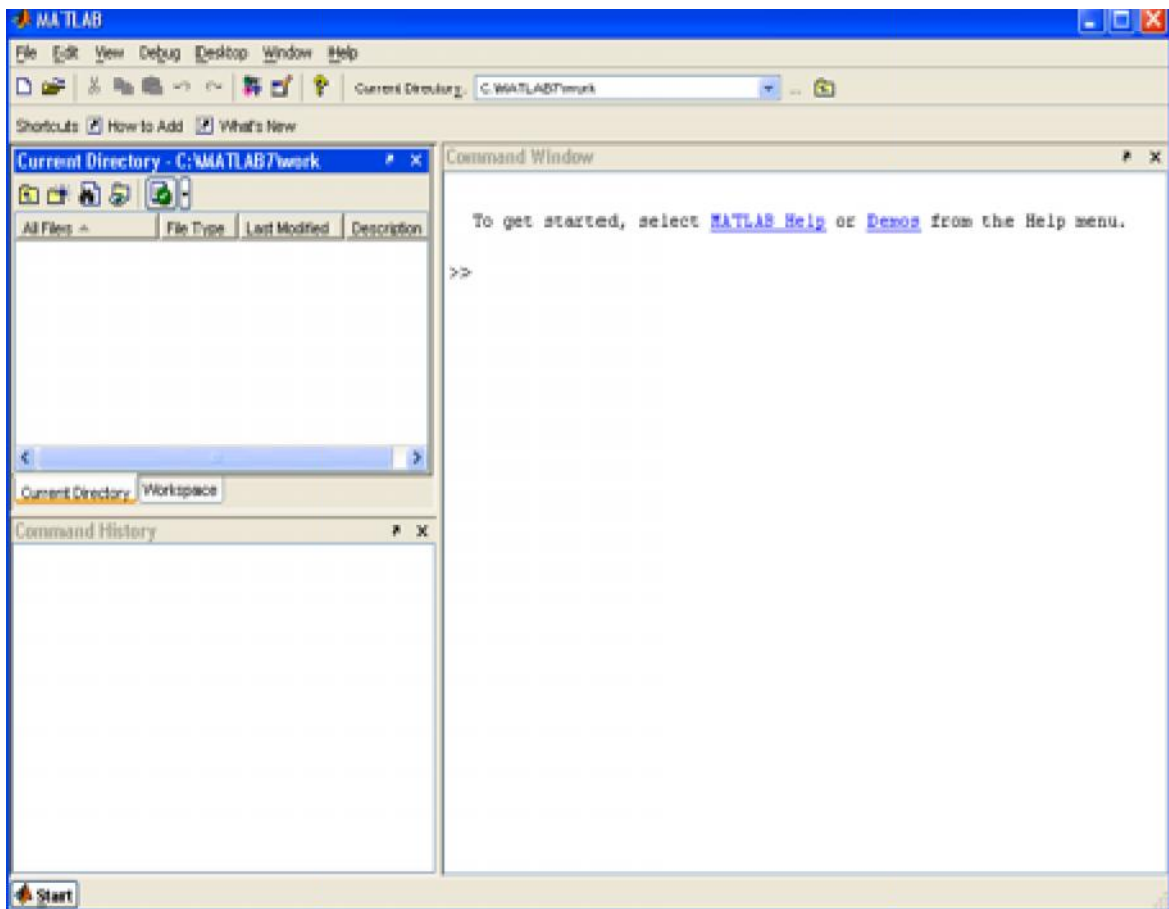


Figure 4.8: Screen shot of typical MATLAB Desktop Window.

MATLAB® also offers a whole host of external interface library which allows to write C/C++ and Fortran programs that interact with MATLAB. It includes facilities for calling routines from MATLAB (dynamic linking), for calling MATLAB as a computational engine, and for reading and writing MAT-files. The most powerful feature of MATLAB® platform is its ability to display vectors matrix in graphical way. It gives user a unique capability to visualize data in two and three dimensions which makes it very useful for interpretation of data in real time. MATLAB® Toolbox software is a collection of functions that extend the capability of the MATLAB® numeric computing environment. The toolboxes used for the implementation of the research work are briefly discussed in following subsections:

4.4.1 Neural Network Toolbox

The Toolboxes developed for Neural Network have high degrees of user interface. It is used to perform some of Neural Network task such as initialising networks, training the network and assessing the results. Some of the key features of the Neural Network are:

1. It supports large variety of supervised and unsupervised network architecture. Modular approach helps user to build its own network and even to customise as per the requirement. It supports mainly four types of supervised learning network namely feed forward, radial basis, dynamic, and learning vector quantization. Similarly, it supports two unsupervised learning algorithms which include competitive layers and self-organizing maps.
2. Neural Network can be trained by a wide range of training algorithms like gradient descent methods, conjugate gradient methods, the Levenberg-Marquardt algorithm (LM), and the resilient backpropagation algorithm (Rprop); and learning functions like gradient descent, Hebbian learning, LVQ, Widrow-Hoff, and Kohonen.
3. Toolbox has unique feature of pre-processing and post processing the data, thereby making the neural network efficient. Simulink(R) blocks can be used to build and evaluate the neural network function.

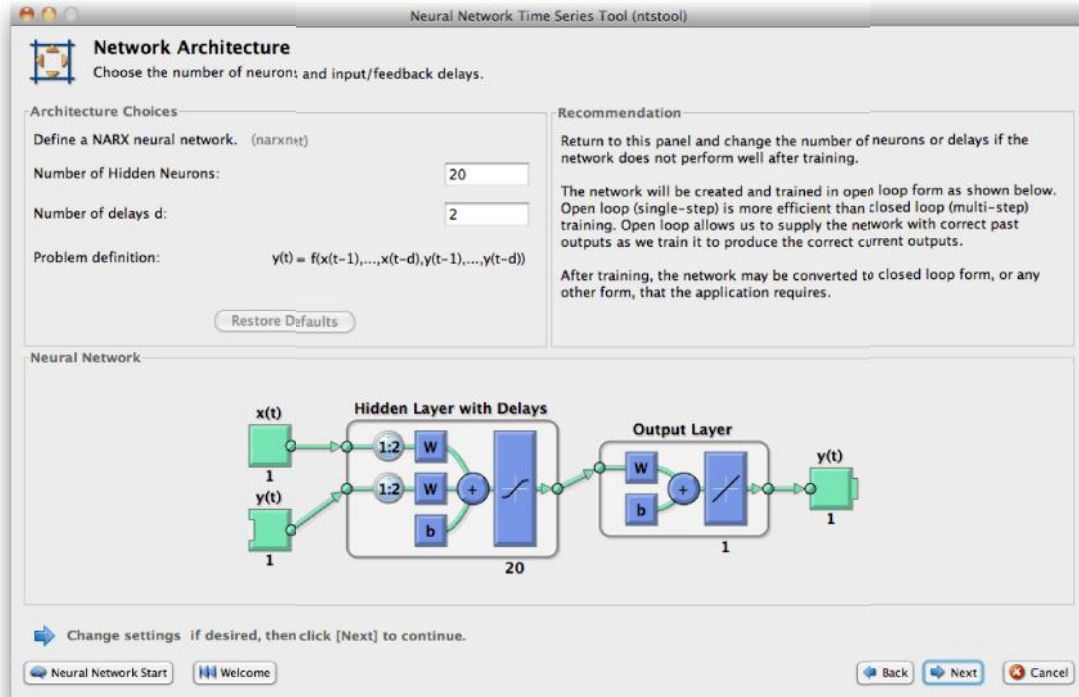


Figure 4.9: Screen Shot of Neural Network Toolbox

Toolbox can be used by the user in many different ways. First and foremost is by using the predefined user interface, in which user has to provide the necessary input. But, the disadvantage of this feature is that it provides less flexibility to overcome. The user can customise toolbox by creating own neural network and using all the features of the toolbox. Apart from the above discussed ways to use the toolbox, it can also be used though command line operations.

4.4.2 Global Optimisation Toolbox

Global Optimisation toolbox contains the function, which can be used for defining, solving and assessing optimization problem. Optimization solving techniques, which are implemented, include Global Search, Mutistart, Pattern Search, Simulated Annealing and Genetic Algorithm. Out of these, Genetic Algorithm has been used in the present research work. The Global Optimisation toolbox allows user to define population size, number of elite children, crossover fraction, Migration and the various constrains.

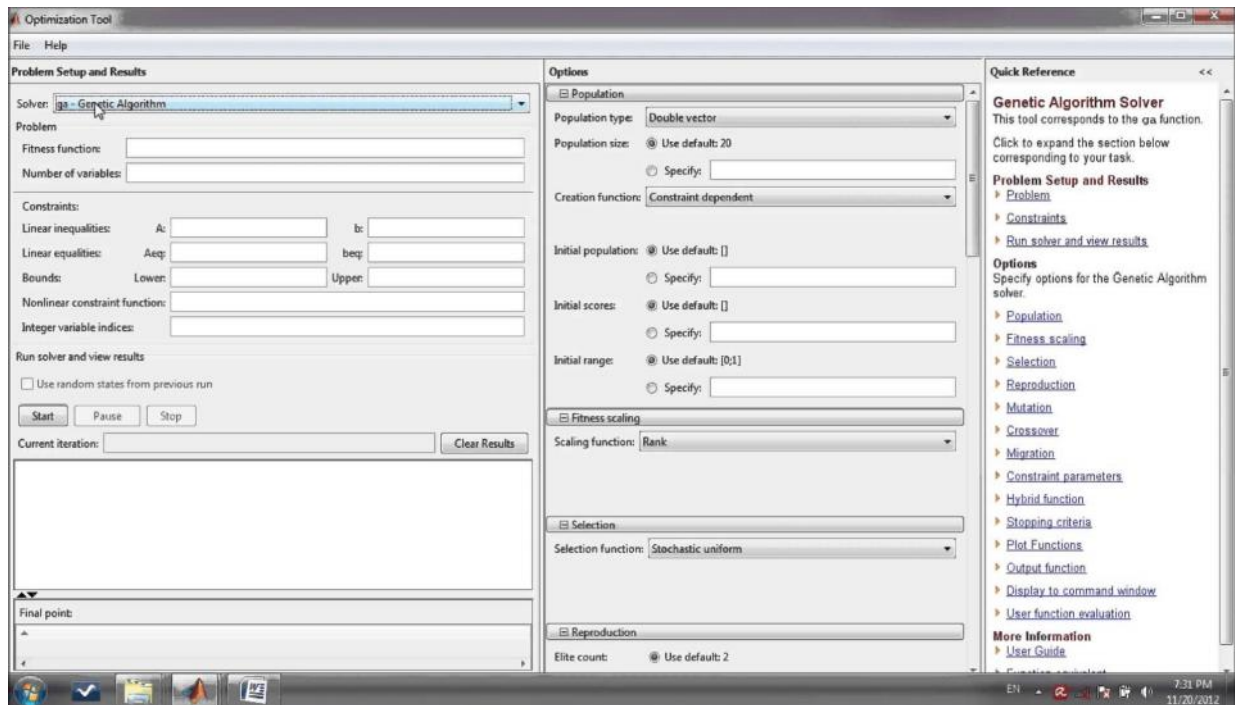


Figure 4.9: Screen Shot of Genetic Algorithm Solver

4.5 Concluding Remarks

Soft Computing techniques are Fuzzy Logic, Neural Network and Genetic Algorithm out of which Neural Network and Genetic Algorithm are widely used to solve stochastic problems. MATLAB® due to its relative advantage is used by researchers worldwide to implement their work. These tools are used for implementation of the present research work.

Chapter: 5

Problem Formulation

This chapter provides an extended mathematical frame work for the formulating the problem of reconstruction for the different beam profiles along the various approaches to solve the problem. The results obtained after the implementation are also discussed.

5.1 Problem Formulation for Parallel Beam Scanner

Parallel Beam profile is most used beam profile for all generation of CT scanner. Hence, the problem for reconstruction needs to be modelled and implemented. [1, 2]

5.1.1. Geometry of Parallel beam Scanner

Figure 5.1 shows pictorial representation of the parallel beam scanner, which is the moveable part of the scanner and is consisting of an emitter of X-rays and a screen on which radiation detectors are placed. This revolves around the body being examined. The detectors measure the attenuated intensity and it is evaluated relative to the original radiation intensity as defined in equation 3.13. This value of projection is represented by $p^p(s, \alpha^p)$ where α^p is the angle at which the projection is carried out and s is the position of a particular place on the screen.

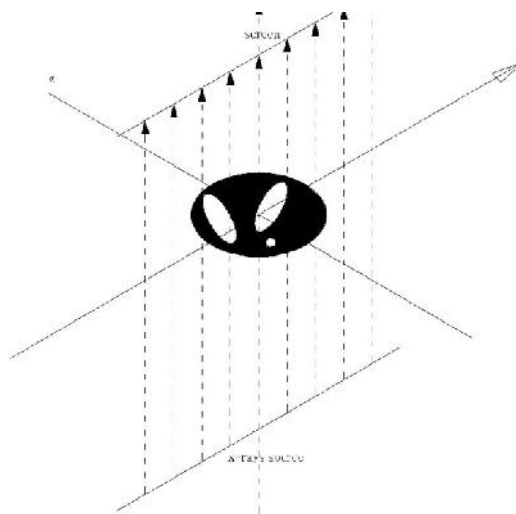


Figure 5.1: Basic Geometry of Parallel Beam Scanner

This method of scanning allows obtaining the image of the attenuation coefficient distribution for one cross-section of the body under examination. As shown in the figure 5.2, the scanner geometry is in the plane x and y coordinates, that is in the plane perpendicular to z-axis. Using the standard definition of Radon transform [1] it can be derived:

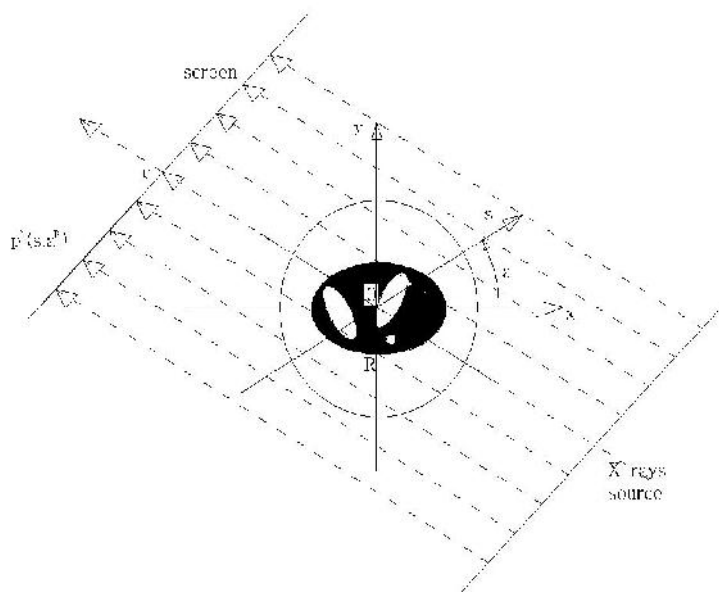


Figure 5.2: Scanner Geometry in X-Y Plane

$$p^p(s, \alpha^p) = \int_{-\infty}^{+\infty} \mu(s \cos \alpha^p - u \sin \alpha^p, s \sin \alpha^p + u \cos \alpha^p) du \quad (5.1)$$

This allows easy interpretation of value at each point on the screen. The above equation in the frequency domain can be represented by:

$$p^p(s, \alpha^p) = F_1\{p^p(s, \alpha^p)\} = \int_{-\infty}^{\infty} p^p(s, \alpha^p) e^{-j2\pi f_s s} ds \quad (5.2)$$

As mentioned in equation 3.36, the practical implementation of the above problem can be solved by using two approaches as below:

- Convolution and back projection method;
- Filtration and back projection method.

5.1.2. Convolution and Back projection method

Out of two approaches, reconstruction by convolution and back projection is most popular [3-5] due to its simplicity and its implementation. In this approach, filtering takes place in s-domain and this can be mathematically expressed as:

$$\mu(x, y) = \int_0^\pi F_1^{-1}(P(f, \alpha^p) \cdot f \cdot \text{sign}(f)) \alpha^p \quad (5.3)$$

By applying the Fourier transform, it is converted into form:

$$\mu(x, y) = \int_0^\pi F_1^{-1}(P(f, \alpha^p) * F_1^{-1}(f \cdot \text{sign})) \alpha^p \quad (5.4)$$

This will lead to:

$$\mu(x, y) = \int_0^\pi P^p(s, \alpha^p) * F_1^{-1}(f \cdot \text{sign}) d\alpha^p \quad (5.5)$$

Comparison of equation 3.36 and 5.5 will result into:

$$\hat{P}^p(x \cos \alpha^p + y \sin \alpha^p, \alpha^p) = P^p(s, \alpha^p) * F_1^{-1}(f \cdot \text{sign}) d\alpha^p \quad (5.6)$$

By using Hebert transformation, it can be stated:

$$\tilde{H} \left(\frac{1}{2\pi} \frac{dP^p(\dot{s}, \alpha^p)}{ds} \frac{1}{s - \dot{s}} d\dot{s} \right) = \tilde{p}^p(s, \alpha^p) \quad (5.7)$$

The values of $\tilde{p}^p(s, \alpha^p)$ obtained in this process need to be subjected to the process of back-projection in order to reconstruct the final image. Mathematically, it can be expressed as:

$$\mu(x, y) = B(P^p(s, \tilde{p}^p(s, \alpha^p)) * F_1^{-1}\{|f|\}) \quad (5.8)$$

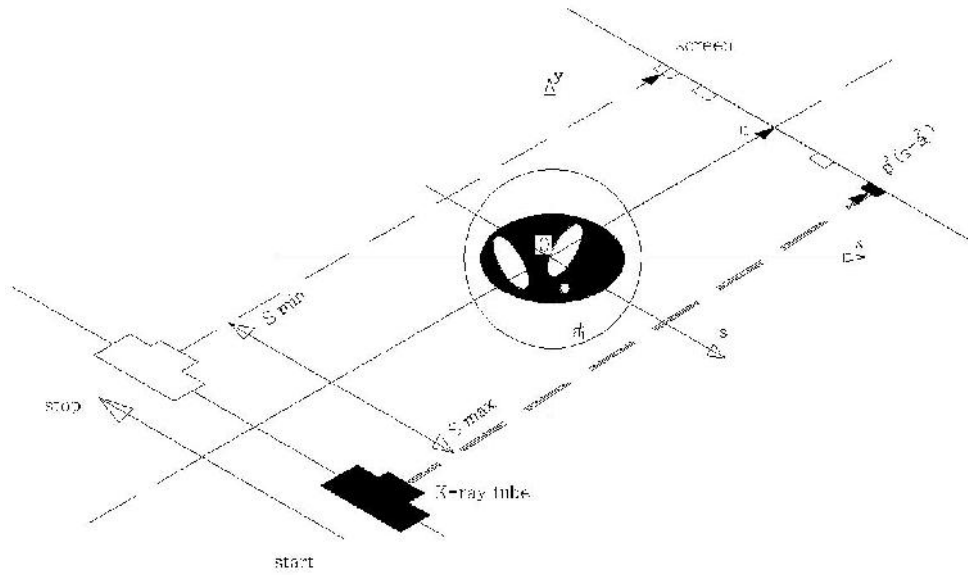


Figure 5.3: Projection at various Angle

If it is assumed that $\tilde{\mu}(x, y)$ is a function approximating to the $\mu(x, y)$, then equation 5.8 can be modified as:

$$\mu(x, y) = \int_0^\pi \left(\int_{-\infty}^{\infty} W(f) \cdot \text{rect}\left(\frac{f}{2f_0}\right) \cdot P(f, \alpha^p) \cdot f \cdot \text{sgn}(f) \cdot e^{-j2\pi f s} df \right) \cdot d\alpha^p \quad (5.9)$$

where f_0 is cut off frequency function. Hence, finally it can be written as:

$$\tilde{\mu}(x, y) = \int_0^\pi P^p(s, \alpha^p) * h^{XX}(s) \cdot d\alpha^p \quad (5.10)$$

where $h^{XX}(s)$ is the point spread function of the selected convolution kernel. Considering the practical implementation, equation 5.10 needs to be converted into discrete form as there are limited number of projections which are carried out during each revolution of X-ray tube and limited resolution, at which the radiation intensities are measured. The angles at which discrete projections are carried out are represented by:

$$\alpha_\psi^p = \psi \Delta_\alpha^p \quad (5.11)$$

where $\psi = 0, \dots, \Psi - 1$ and the detectors are placed at equal distance $s_l = l \cdot \Delta_s^p$ hence the index variable $l = -\frac{L-1}{2}, \dots, L - \frac{1}{2}$. The equation 5.10 can be implemented as shown in figure 5.4:

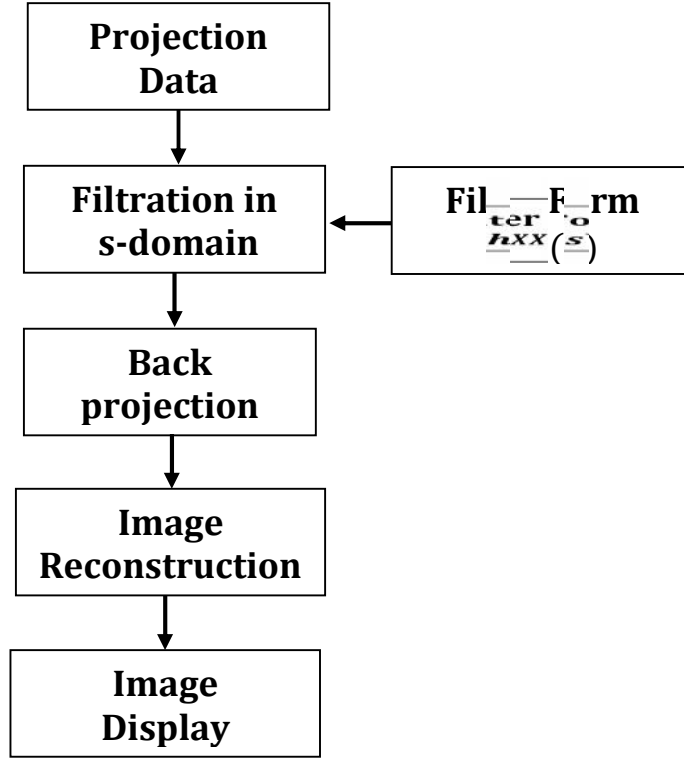


Figure 5.4: Flow chart for Convolution Back projection Method

5.1.3. Filtration and Back projection Method

In this approach, the filtering is carried out in the frequency domain [6-8] as contrast to s-domain in convolution approach. Applying Fourier transform to individual projection, the equation 5.4 can be written as:

$$\mu(x, y) = \int_0^\pi (F_1^{-1} (F_1(P^p(s, \alpha^p)))) \cdot f \cdot \text{sign}(f) \cdot d\alpha^p \quad (5.12)$$

So,

$$\hat{P}^p(x \cos \alpha^p + y \sin \alpha^p, \alpha^p) = F_1^{-1} F_1(P^p(s, \alpha^p)) \cdot f \cdot \text{sign}(f) \quad (5.13)$$

Hence,

$$\hat{P}^p(s, \alpha^p) = F_1^{-1} (|f| \cdot F_1(P^p(s, \alpha^p))) \quad (5.14)$$

Mathematically, it can be expressed as:

$$\mu(x, y) = B(F_1^{-1}(|f| \cdot F_1(P^p(s, \alpha^p)))) \quad (5.15)$$

As seen in section 5.1.2, for the limited band spectrum, we approximate $\tilde{\mu}(x, y)$ for the function $\mu(x, y)$. mathematically, it can be written as:

$$\tilde{\mu}(x, y) = \int_0^\pi \int_{-\infty}^\infty P(f, \alpha^p) * H^{XX}(f) e^{j2\pi f_s df} d\alpha^p \quad (5.16)$$

where $H^{XX}(f)$ is spectrum of selected convolution kernel. Hence, the sequence of operation to implement reconstruction algorithm can be written as:

$$\tilde{\mu}(x, y) = B\{F_1^{-1}\{P^p(s, \alpha^p)\} \cdot H^{XX}(f)\} \quad (5.17)$$

For practical implementation, the above form is converted into discrete form as discussed in section 5.1.2 and flow chart for the implementation is shown in figure 5.5.

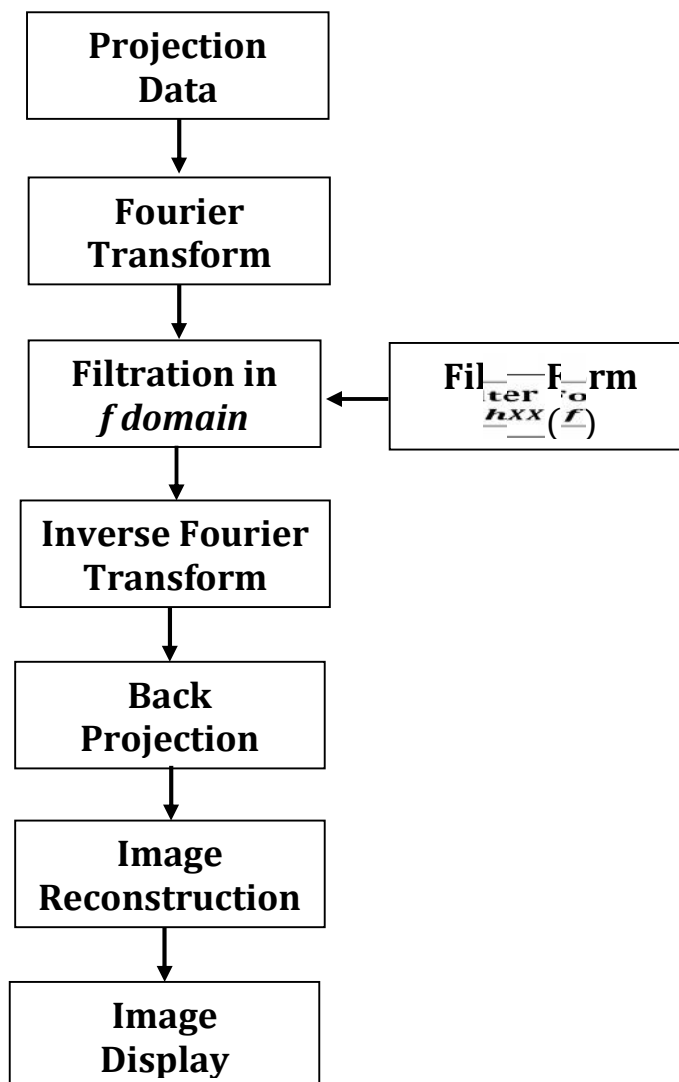


Figure 5.5: Flow chart for Filtration Back projection Method

5.2 Problem Formulation for Fan Beam Scanner

One of the major disadvantages of parallel beam scanner is the lateral movement of the source and detector which leads to artefacts in the reconstructed image. This can be overcome by using fan beam shaped detectors array as discussed in chapter 3. The reconstruction problem can be formulated on the same line as for the parallel beam scanner. Before problem formulation, it is necessary to understand the geometry of scanner as discussed in the next section.

5.2.1. Geometry of Fan beam Scanner

As the name suggests, the beam profile is in fan shaped as opposite to parallel beam as can be seen in figures 5.6. [9]

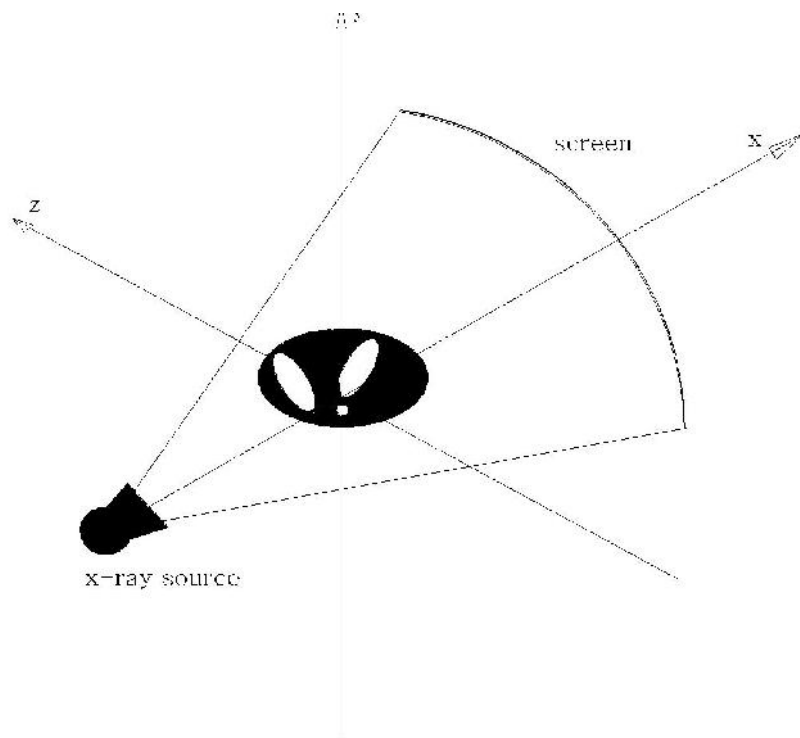


Figure 5.6: Basic shape of Fan Beam Profile

It is evident that axis of rotation of the system and the axis of symmetry of radiation beam plays very vital role in geometrical relationship. The axis of rotation is directed along the line perpendicular to the cross section. A ray emitted from the tube at a given angle of rotation and reaching a particular detector can be identified

by parameter (β, α^f) , where β is the angle that the ray makes with the principal axis of the radiation beam and α^f is angle of rotation.

As in the parallel beam, the motion of the tube detector arrangement is rotational. The angle will be in the range of $[0, 2\pi)$, and thus the corresponding range for the β will be:

$$\beta_{max} = \beta_{min} = \arcsin\left(\frac{R}{R_f}\right) \quad (5.18)$$

where R is the radius of the circle and R_f is the radius of circle describing the focus of the tube. In most of cases, the β lies within the range of $[-\frac{\pi}{6}, \frac{\pi}{6}]$. The projection function for the fan beam profile is mathematically represented as:

$$P^f(\beta, \alpha^f) \quad (5.19)$$

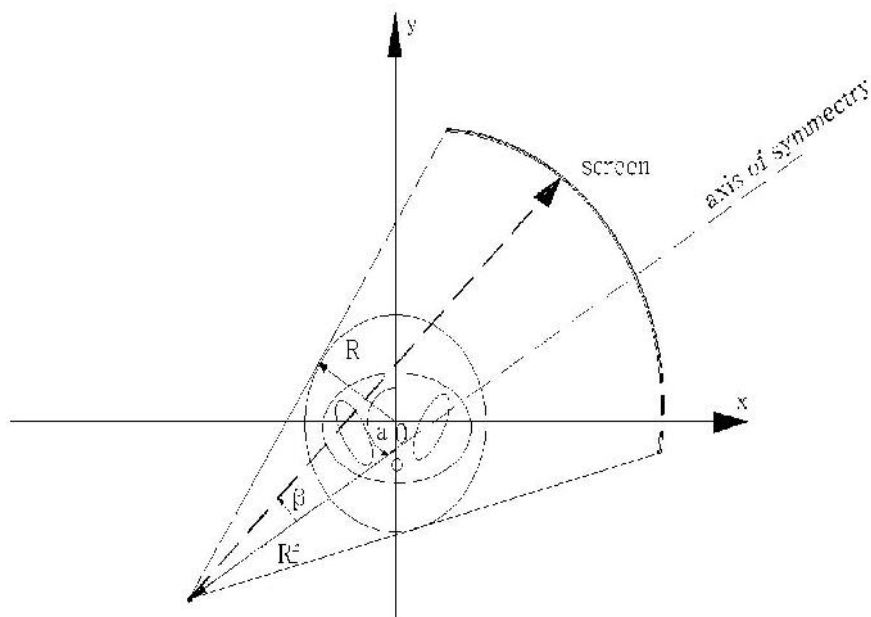


Figure 5.7: Basic Geometrical Relationship for Fan Beam

For the practical implementation, the problem must be addressed into the discrete domain. Hence, the geometry of discrete projection system must be analysed. The fan beam scanner can be divided into two broad categories; equiangular sampling

and equidistance sampling. But, for practical reasons and due to limitation of the X-ray tube, equidistance sampling systems are widely used. In the equidistance sampling system, the projection is obtained at predetermined angles α_γ^f . Hence, the angular distance β_η is determined by the location of the detectors. As the system is equidistance, the angular distance between the detectors is equal and is obtained by Δ_β .

The discrete angles at which projections are made can be given by:

$$\alpha_\gamma^f = \gamma \Delta_\alpha^f \quad (5.20)$$

where Δ_α^f is the angle through which tube screen system is rotated and $\gamma = 0, 1, \dots, \Gamma - 1$ is the sample index for each projection. The location of the arc is defined by an angle:

$$\beta_\eta = \eta \Delta_\beta \quad (5.21)$$

where Δ_β is the distance between the radiation detector, η is the index of detector matrix. Hence, the projection value for the fan beam profile can be expressed mathematically as:

$$\hat{P}^f(\eta, \gamma) = P^f(\eta \Delta_\beta, \gamma \Delta_\alpha^f) \quad (5.22)$$

5.2.2 Rebinning Reconstruction Method

This method uses re-shortening for [10-12] reconstruction of image. In this method, all the projections $P^f(\beta, \alpha^f)$, which correspond to the hypothetical parallel beam projection $p^p(s, \alpha^p)$ are identified. The rays which would be equivalent to the parallel rays will be considered and collected. The projection data obtained will be used for the reconstruction as per the methods described in section 5.1. The flow chart for the implementation of this method is shown in the figure 5.8. Mathematically,

$$p^f(\beta, \alpha^f) = p^p(s, \alpha^p) = p^p(R_f \sin \beta, \alpha^f + \beta) \quad (5.23)$$

which is simplified as:

$$p^p(s, \alpha^p) = p^f(\beta, \alpha^f) = P^f\left(\arcsin\frac{s}{R_f}, \alpha^p - \arcsin\frac{s}{R_f}\right) \quad (5.24)$$

Using equation 5.25, the equivalent ray of fan beam systems to parallel beam system is:

$$\beta = \arcsin\frac{s}{R_f} \quad (5.25)$$

However, for practical implementation, discrete domain must be considered.

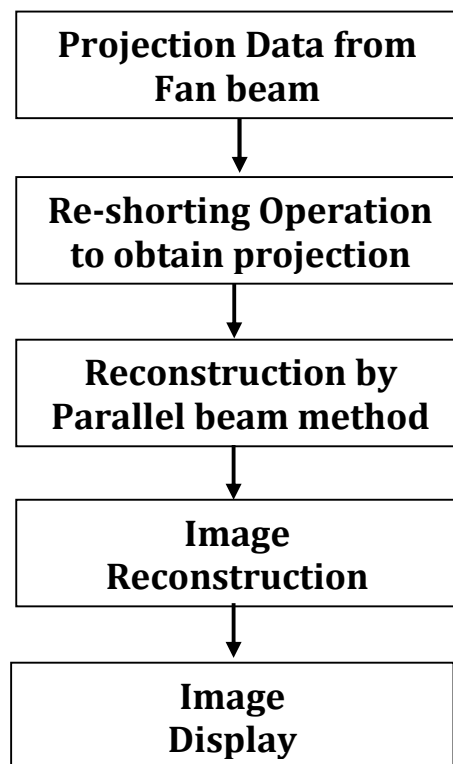


Figure 5.8: Flow chart for Implementation of Rebinning Method

5.2.3 Direct Fan Beam Reconstruction Method

In opposite to the using the reconstruction methods developed for the parallel beam systems, here a direct approach is used to solve the problem [13,14]. Here, the formula for the parallel beam method is found in which the values obtained from the fan beam can be directly used. In other words, this method can be considered as the extension of the parallel beam reconstruction method. Using the equation 5.5, the relationship between the quantities of two approaches can be expressed as:

$$s = R_f \cdot \sin \alpha^f \quad (5.26)$$

$$\alpha^p = \alpha^f + \beta \quad (5.27)$$

Converting the equation to polar form, using equation 5.26 and equation 5.27:

$$r \cos (\alpha^p - \phi) - s = \dot{u} \sin(\dot{\beta} - \beta) \quad (5.28)$$

where $\dot{\beta} = \arctan \left(\frac{\alpha^f - \phi}{R_f + r \sin(\alpha^f - \phi)} \right)$. The following sequence of equation based on Radon transforms can be derived:

$$\mu(x, y) = \int_{-\infty}^{\infty} \int_{-\infty}^{\infty} M(f_1, f_2) \cdot e^{j2\pi(f_1 x + f_2 y)} df_1 df_2 \quad (5.29)$$

Converting above into polar form:

$$\mu(x, y) = \int_0^{\pi} \int_{-\infty}^{\infty} |f| P(f, \alpha^p) \cdot e^{j2\pi(x \cos \alpha^p + y \sin \alpha^p)} d\alpha^p \quad (5.30)$$

As the system is using fan beam profile, the limit of integration changes:

$$\mu(x, y) = \frac{1}{2} \int_0^{2\pi} \int_{-\infty}^{\infty} |f| P(f, \alpha^p) \cdot e^{j2\pi(x \cos \alpha^p + y \sin \alpha^p)} d\alpha^p \quad (5.31)$$

Converting above equation 5.31 into frequency domain, it is reformulated to:

$$\mu(x, y) = \frac{1}{2} \int_0^{2\pi} \int_{-\infty}^{\infty} |f| P(f, \alpha^p) \cdot e^{j2\pi(x \cos \alpha^p + y \sin \alpha^p)} e^{-j2\pi f_s} ds df d\alpha^p \quad (5.32)$$

As discussed in above sections, the above method can be implemented in discrete domain. The implementation steps are shown in the figure 5.9

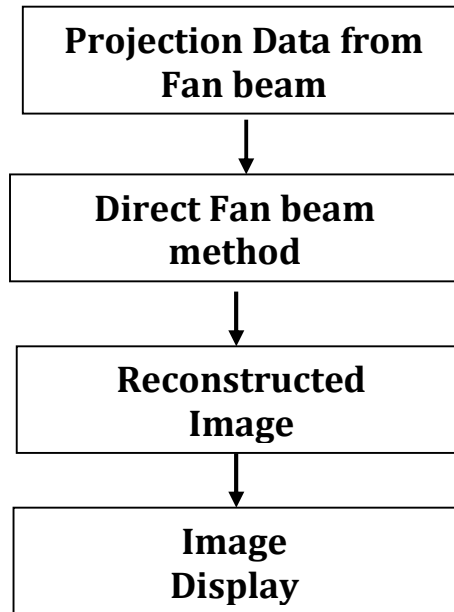


Figure 5.9: Flow chart for implementation of Direct Fan Beam Method

5.3 Implementation

As discussed in previous sections most of CT scanner either uses the Parallel beam profile or Fan beam profile. But it is evident that if scanner uses the fan beam profile but in one form or other reconstruction problem is reformulated to parallel beam reconstruction problem. Hence, it is logical to address parallel beam reconstruction problem and implement the same. As stated in Chapter 4, MATLAB®(R) platform is used to implement the research.

In order to implement and test the reconstruction method user defined phantom with the resolution 256X256 is used [15], the detail description is discussed in Chapter 7 in detail. The user defined phantom is shown in the figure 5.10:



Figure 5.10: User defined Phantom.

Before applying the method discussed in previous section is interesting, to view reconstructed image by only applying the back projection algorithm the result obtained can be viewed in the figure 5.11:



Figure 5.11: Reconstructed User defined Phantom using Back projection

Implementing the method discussed in section 5.1.2 on the MATLAB®(R) platform the phantom reconstructed is shown in the figure 5.12:



Figure 5.12: Reconstructed User defined Phantom using Convolution and Back projection

On similar lines the method discussed in section 5.1.3 the result obtained is shown in figure 5.12. From the result it can be concluded that by employing the methods discussed in the chapter the quality of the image has improved significantly and thus making the diagnosis more accurate.



Figure 5.13: Reconstructed User defined Phantom using Filtration and Back projection

The details analysis and comparative analysis of the results obtained by the implementation of this work is being discussed in Chapter 8. The function files that are developed to implement the existing techniques are listed in table 5.1:

Sr. No	Name of Function File	Purpose
01	ct_reconstruction	It is main function file which takes required input from the user and produces the output.
02	phtantom_data	It creates the phantom data as per the choice of the user.
02	radon	It converts the generated phantom data into projection data.
03	simple_backprojection	It performs back projection operation on the pre-processed image.
04	filtered_backprojections_con	It performs convolution operation on the projection data
05	filtered_backprojection_fd	It performs filtration operation in frequency domain on projection data.

Table 5.1: Table listing the MATLAB® Function Files Developed for Implementation.

5.4 Concluding Remarks

Chapter discusses mathematical derivation for existing reconstruction techniques and the step wise implementation and testing of these techniques was done on MALTLAB platform and corresponding results obtained as shown in the above shown figures.

Chapter: 6

Artificial Neural Network Implementation

This chapter discusses regarding the novel approach developed to solve the problem of image reconstruction by using the soft computing technique Neural Network (NN) and its implementations and testing.

6.1 Approach

As discussed in Chapter 5, the reconstruction techniques used to solve the problem of reconstruction from projection can be classified into two broad approaches; the transformation based reconstruction techniques and algebraic method based reconstruction techniques. Out of these two techniques, algebraic reconstruction techniques are not used widely due to difficulty in implementation. [1] Hence, the present research is based on the transformation technique convolution and back projection for its simplicity in implementation.

As it is evident from the discussions in Chapter 4, the soft computing techniques are widely used to solve many complex engineering problems where conventional solving techniques have not resulted into the good performance. Out of various soft computing techniques, Artificial Neural Networks popularly known as ANN are used to solve many non linear optimization problems. Due to its relative advantages, ANN is used to solve the problem of reconstruction [2]. ANN can be classified into two broad categories based on the learning algorithm; the supervised learning networks and unsupervised learning networks.

Extending the usage of ANN to solve problem of reconstruction, it can be classified into two broad categories viz. Algebraic Neural Network and Transform Neural Network which can be further classified into two sub categories based on the type of training i.e supervised neural network and unsupervised neural network. For image reconstruction problem, supervised neural networks are not efficient because it is difficult to learn all the possible images[3,4,5]. Hence, reconstructing image using the supervised learning algorithm will not lead to good performance. Moreover, algebraic neural networks are not computationally efficient, as during

solving the problem of projection, a huge size of the variable matrix is used. The size of the matrix is directly proportional to square size of image multiplied by number of projections; hence the number of neural connection also increases.

One of the solutions to this problem is using transform method based neural network which uses unsupervised learning. One possible ANN which can be used is Hopfield network[6,23]. One of the advantages of employing this network is that it decreases the computational complexity as the number of neuron is proportional to size of the image and not on the resolution.

6.2. Parallel Beam Projection System

As discussed in the earlier Chapter the fundamental problem of reconstruction used the Parallel beam profile hence it is essential that any new algorithm for solving the reconstruction problem must be developed and implemented before using for Fan beam profile[6,7,19]. In the present work also the problem using neural network is solved for the parallel beam profile as discussed in subsequent sections:

6.2.1 Mathematical Remodelling

As discussed, the distribution of attenuation is defined by $\mu(x, y)$ and the mathematical equation can be written as:

$$p(s, \alpha) = \int_{-\infty}^{\infty} \int_{-\infty}^{\infty} \mu(x, y) \delta(x \cos \alpha + y \sin \alpha - s) dx dy \quad (6.1)$$

The accumulations due to the projection carried out at various angles are described by the equation:

$$\tilde{\mu}(x, y) = \int_0^{\pi} p(x \cos \alpha + y \sin \alpha, \alpha) d\alpha \quad (6.2)$$

where $\tilde{\mu}(x, y)$ is the image of distribution of the X-ray attenuation in object of interest, but as described in section 5.2.1, the image reconstruction by this method are subject to distortion and hence, mathematically it is expressed as:

$$\tilde{\mu}(x, y) = \mu(x, y) * (x^2 + y^2)^{-\frac{1}{2}} \quad (6.3)$$

As only limited number of projections can take place, the equation 6.3 must be converted to discrete domain as:

$$\mu(x, y) = \hat{\mu}(i, j) \quad (6.4)$$

$$\tilde{\mu}(x, y) = \hat{\tilde{\mu}}(i, j) \quad (6.5)$$

where i, j are integers. The discrete equivalent of equation 6.3, therefore, can be written as:

$$\hat{\tilde{\mu}}(i, j) \cong \sum_{k=1}^K \sum_{l=1}^L h_{ijkl} \hat{\mu}(k, l) \quad (6.6)$$

where h_{ijkl} represents the discrete impulse response of the signal, responsible for geometric distortion of original image. Implementing interpolation, the equation 6.6 is expressed as:

$$\hat{\tilde{\mu}}(i, j) \cong \sum_{k=1}^K \sum_{l=1}^L h_{i-k, j-l} \hat{\mu}(k, l) \quad (6.7)$$

In order to remove the distortion, the image filtering is performed on the image which will result into removal of geometrical distortion. This problem can be viewed as problem of optimization, where least square error needs to be reduced. The popular solution to this problem of optimization is entropy criterion[8-11]. Entropy criterion is efficient for the method to find out the direction and rate of change in algorithm. It is widely used in the domain of image processing to remove the distortion[11,20]. Thus it can be extended to solve problem of reconstructed image[15]. The problem can be reformulated to reconstruct the image in discrete domain as under:

$$\begin{cases} \max Ent(F) \\ \tilde{F} = HF \end{cases} \quad (6.8)$$

where $F = [\hat{\mu}(k, l)]$ is the matrix with element from the original image, \tilde{F} is the matrix from distorted image and $H = [h_{ijkl}]$ is the matrix of impulse response. The $Ent(F)$ can be written as:

$$Ent(F) = - \sum_{k=1}^K \sum_{l=1}^L \chi(k, l) \ln(\chi(k, l)) \quad (6.9)$$

where

$$\chi(k, l) = \frac{\hat{\mu}(k, l) - \hat{\mu}(k, l)_{min}}{\sum_{n=1}^I \sum_{m=1}^J (\hat{\mu}(n, m) - \hat{\mu}(k, l)_{min})} \quad (6.10)$$

where $\hat{\mu}(k, l)_{min}$ is the lowest value among negative $\hat{\mu}(k, l)$, thus the penalty function for the equation 6.8 can be expressed as:

$$\min_F (-w_1 Ent(F) + w_2 \sum_{i=1}^I \sum_{j=1}^J f(e_{ij}(F))) \quad (6.11)$$

where

$$e_{ij}(F) = \sum_{k=1}^I \sum_{l=1}^J h_{i-k, j-l} \hat{\mu}(k, l) - \hat{\mu}(k, l)_{min} \quad (6.12)$$

The penalty function $f(\cdot)$ can be defined as:

$$f(e) = \lambda \ln \cosh\left(\frac{e}{\lambda}\right) \text{ where } \lambda > 0 \quad (6.13)$$

Implementing equation 6.11 in form on Neural Network, it can be expressed as:

$$E^t = -w_1 Ent(F^t) + w_2 \sum_{l=1}^I \sum_{j=1}^J f(e_{ij}(F^t)) \quad (6.14)$$

Applying the derivation to equation 6.14, following form is obtained:

$$\frac{dE^t}{dt} = - \sum_{k=1}^I \sum_{l=1}^J \frac{d\hat{\mu}^t(k, l)}{dt} \quad (6.15)$$

where t represents the learning progress of the neural network. Further:

$$\frac{d\hat{\mu}^t(k, l)}{dt} = w_1 \frac{\partial Ent(F^t)}{\partial \hat{\mu}^t(k, l)} - w_2 \sum_{i=1}^L \sum_{j=1}^J \frac{\partial f(e_{ij}(F^t))}{\partial e_{ij}^t} \frac{\partial e_{ij}^t}{\partial \hat{\mu}^t(k, l)} \quad (6.16)$$

Implementing neural network to above equation, below mentioned structure is obtained:

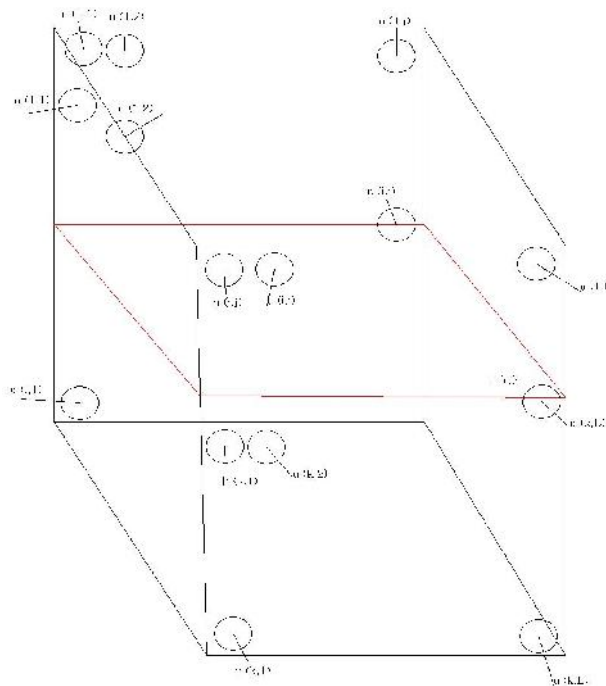


Figure 6.1: Structure of Developed Neural Network

It is advantageous to consider the neighbourhood of the given kernel instead of considering the entropy of the whole image. This will lead to modification of equation 6.15 into:

$$Ent_{kl}(F) = - \sum_{m=-k}^K \sum_{n=-k}^K \chi(k+m, l+n) \ln(\chi(k+m, l+n)) \quad (6.17)$$

where

$$\chi(k+m, l+n) = \frac{\hat{\mu}(k, l) - \hat{\mu}(k, l)_{min}}{\sum_{n=k}^K \sum_{n=k}^K (\hat{\mu}(k+m, l+n) - \hat{\mu}(k, l)_{min})} \quad (6.18)$$

The cross section of the neural network is shown in the figure 6.2. For the discrete implementation, the following values were used for the discussion of the results in the subsequent chapters.

Quantity	Layer 1	Layer 2
Weight of the connection	$w_{klj}^{(1)} = h_{j-kj-1}$	$w_{klj}^{(2)} = w_2 h_{j-kj-1}$
Weight of the sum	$s_{ij}^{(1)} = \sum_k \sum_l w_{klj}^{(1)} \hat{\mu}^{(k,l)} - \hat{\mu}^{(i,j)}$	$s_{kl}^{(2)} = \frac{d\hat{\mu}^{(k,l)}}{dt}$
Output of Neuron	$y_{ij}^{(1)} = thg\left(\frac{s_{ij}^{(1)}}{\lambda}\right)$	$\hat{\mu}^{(k,l)} = \int s_{kl}^{(2)} dt$

Table 6.1: Parameters for the Developed Neural Network

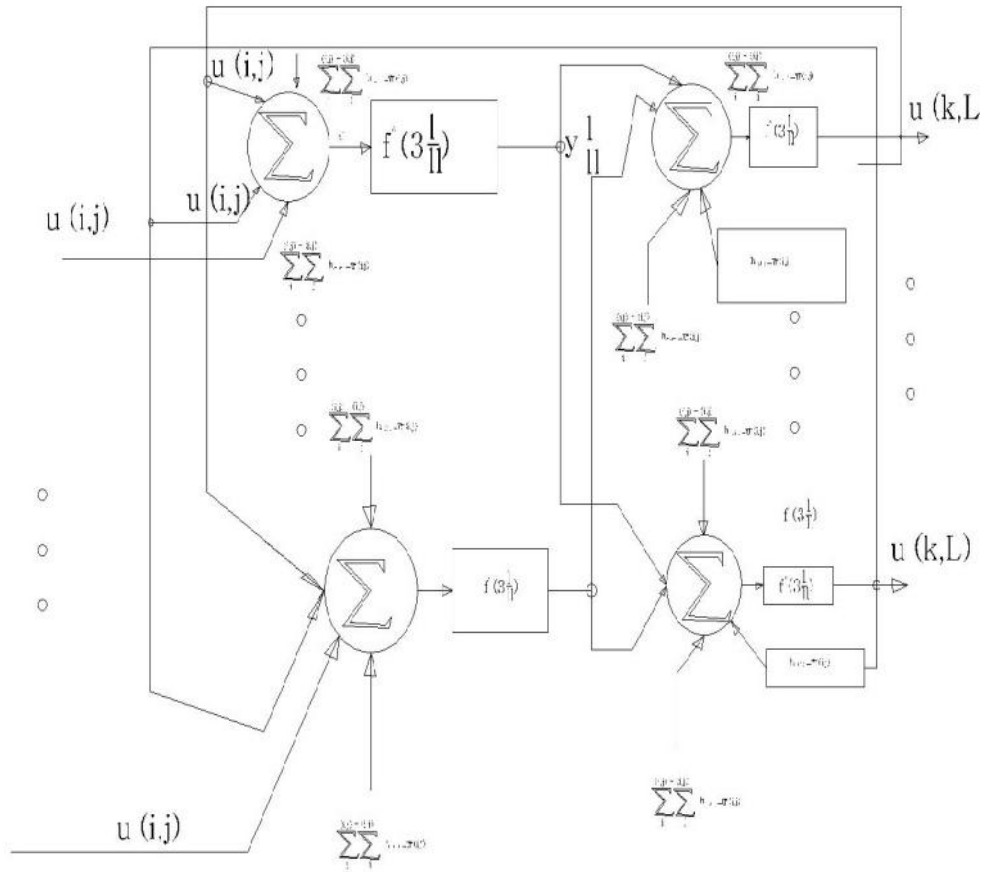


Figure 6.2: Cross Section of the Developed Neural Network

6.2.1 Implementation

In continuous, of previous section the theory developed was implemented on the MATLAB®(R) platform. To test any medical reconstruction algorithm Sheep-Logan phantom is standard volume used [12]. But for the present work a User defined phantom is used the detail regarding the modelling of phantom is discussed in Chapter 7. Based on the previous section the implementation of developed approach is done as show in the figure 6.3.[14,15]:

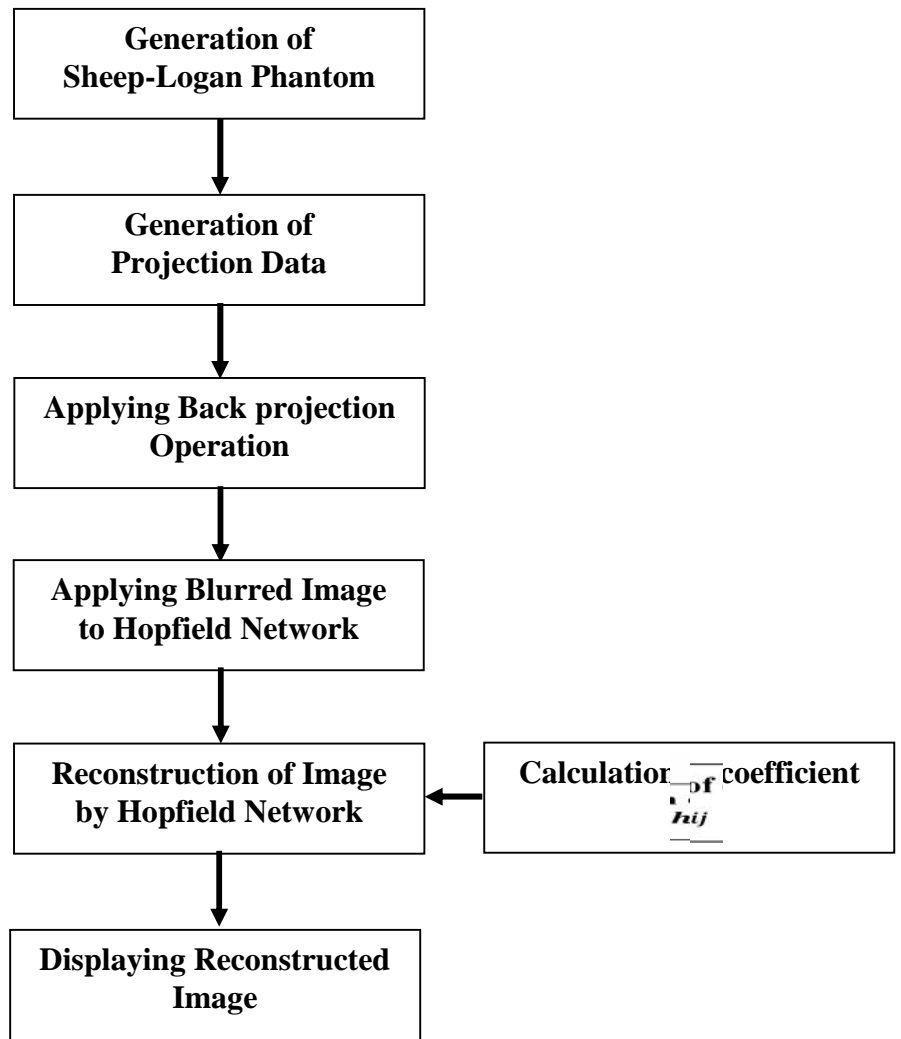


Figure 6.3: Flow chart for Reconstructing Image for Parallel Beam Scanner

As seen from the figure the first step is to generate User defined Phantom of the desired resolution in the present work the phantom of resolution 256X256 is used as shown in the figure 6.4:



Figure 6.4: User defined Phantom with Resolution of 256X256

The next step is obtained the projection data from the volume by Radon transform. As opposite to the convention method of reconstruction here the back projection operation is applied, that results reconstruction of the volume. The reconstructed image will be subject of lot of geometric distortion making it impossible for interpretation of the information as seen from the figure 6.5:



Figure 6.5: Reconstructed Image by Back projection Operation

In order, to recover the image by removing geometric distortion by employing Hopfield neural network which replaces the conventional two dimensional filtering techniques. It is very much essential to calculate the weights for the neural network as discussed previous section. Before starting the neural network algorithm it is essential to establish h matrix the convolution kernel. The pseudo code for the generation of h matrix for the image with size of 256 X256 is as below:

```
//initialization  
h:array[-255..255,-255..255] of double;  
  
//establishing of the h matrix  
for i:=-255 to 255 do  
    for j:=-255 to 255do  
        begin  
            h[i,j]:=0;  
        end  
    end  
end  
for k:=0 to 71999 do
```

```

begin
s:=i*cos(k*Pi/36000)+j*sin(k*PI/36000);
if ABS(s)<=1 then
h[i,j]:=h[i,j]+(Pi/36000)*(1-ABS(s));
end;
end;
//symmetrization of the matrix h
for i:=0 to 1023 do
for j:=0 to 1023 do
if j>i then h[j,i]:=h[i,j];
for i:=0 to 1023 do
for j:=0 to 1023 do
begin
h[i,-j]:=h[i,j];
h[-i,j]:=h[i,j];
h[-i,-j]:=h[i,j];
end;
end;
end;
end;

```

These weights are calculated by numerical method and value of these weigh are $w_1 = 100$ and $w_2 = 6 \times 10^{10}$ and slope for the penalty function $\lambda = 10^{10}$ with suitable value for the window as discussed in Chapter 3. The phantom reconstruction is done for various iteration are shown below:



Figure 6.6: Reconstructed Image by Hopfield Network after 100 iteration for Parallel Beam



Figure 6.7: Reconstructed Image by Hopfield Network after 1000 iteration for Parallel Beam

After the 10,000 iteration the network stabilizes and the reconstructed image is obtained as shown in the figure 6.7[16]:



Figure 6.8: Reconstructed Image by Hopfield Network after 10000 iteration for Parallel Beam

The comparisons of the image reconstructed is with the existing method has been discussed in Chapter 9.

6.3 Fan Beam Projection System

As most of the modern scanner uses the Fan beam projection hence the research work must be extended for the Fan beam scanner[21]. As discussed in Chapter 5, to solve the reconstruction problem for fan beam profile the methods used for the parallel beam profile with some modification. These modification and implementation are discussed in following sections.

6.3.1 Mathematical Remodelling

As discussed in the Chapter 5, the basic problem of for the fan beam can be solved by using two approaches viz. Rebinning and direct fan method. For the present research work, rebinning method is used. As stated earlier, in rebinning method only those rays which can be modelled into the parallel beam projection are considered. These projection values are given by $p^f = (\beta, \alpha^f)$ and the corresponding geometry is shown in the figure 6.8:

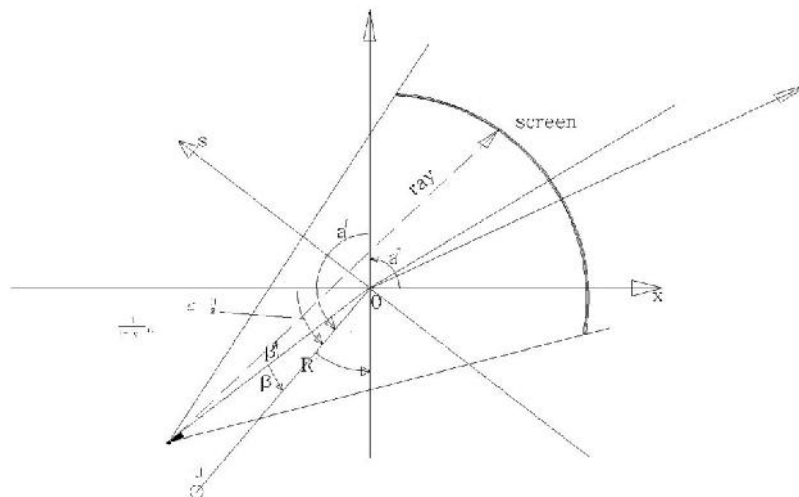


Figure 6.8: Geometric Relationship between Variables for Fan Beam

As discussed in previous chapters and using the definition of Radon transformation [13], the values of projection are obtained by:

$$p^p(s, \alpha^p) \int_{-\infty}^{\infty} \int_{-\infty}^{\infty} \mu(x, y) \cdot \delta(x \cos \alpha^p + y \sin \alpha^p - s) dx dy \quad (6.19)$$

Using the geometry described in the figure, it is obtained:

$$p^p(s, \alpha^p) = p^f = (\beta, \alpha^f) = p^f \left(\arcsin\left(\frac{s}{R_f}\right), \alpha^p - \arcsin\left(\frac{s}{R_f}\right) \right) \quad (6.20)$$

As the limited parallel projections are taken into consideration, the values of projection and indexed angle are represented as:

$$\widehat{p}^p = (l, \psi) \quad (6.21)$$

where l is uniform sampling point and ψ is the indexed angle. The space between each parallel ray from the origin is calculated by:

$$s(i, j) = l \cdot \Delta_s \quad (6.22)$$

where Δ_s is sampling interval. Once the resorting is completed, the next step implemented is back projection as discussed in section 5.3.2. Mathematically it is represented as:

$$\tilde{\mu}(x, y) = \int_0^{\pi} \widehat{p}^p(s_{xy}, \alpha^p) \cdot d\alpha^p \quad (6.23)$$

when considering the finite sum the equation 6.23 is modified as:

$$\widehat{\tilde{\mu}}(i, j) = \frac{1}{\alpha} \sum_{\psi=0}^{\psi-1} \widehat{p}^p(s_{ij}, \alpha_{\psi}^p) \quad (6.24)$$

where $s_{ij} = i l_s^p \cos \alpha_{\psi}^p + j l_s^p \sin \alpha_{\psi}^p$.

As discussed in previous section, the image obtained contains the information regarding the original image along with the geometric distortion. Hence, the next step involves removing the geometric distortion by employing conventional

filtering technique. In the present work, this conventional filtering is replaced by the Hopfield neural network. Before establishing the neural network, it is necessary to convert reconstruction problem into discrete domain. Mathematically [13], it can be expressed as:

$$\tilde{\mu}(x, y) = \int_0^\pi \left(\int_{-\infty}^{\infty} \left(\int_{-\infty}^{\infty} \int_{-\infty}^{\infty} (\mu(\tilde{x}, \tilde{y}) \cdot \delta(\tilde{x} \cos \alpha^p + \tilde{y} \sin \alpha^p - s) d\tilde{x}d\tilde{y}) \cdot I(\dot{s} - s) ds \right) d\alpha^p \right) \quad (6.25)$$

Approximating function and using the finite range $[1, I]$ and $[1, J]$, the equation 6.25 is reformulated as:

$$\hat{\mu}(i, j) = \sum_i \sum_j \hat{\mu}(\tilde{i}, \tilde{j}) \cdot h_{i\tilde{i}j\tilde{j}} \quad (6.26)$$

which can be further simplified into:

$$\hat{\mu}(i, j) = \sum_i \sum_j \hat{\mu}(\tilde{i}, \tilde{j}) \cdot h_{i\tilde{i}j\tilde{j}} \quad (6.27)$$

where $h_{i\tilde{i}j\tilde{j}}$ is used to calculate weight for the developed network.

By using above derivation, the problem of reconstruction is reformulated into problem of optimization as discussed in section 6.2. Mathematically, it can be expressed as:

$$\min_M \left(v \cdot \sum_{i=1}^I \sum_{j=1}^J f(e_{ij}(M)) \right) \quad (6.28)$$

where $e_{ij}(M) = \sum_{i=1}^I \sum_{j=1}^J h_{\Delta i l j} \hat{\mu}(\tilde{i}, \tilde{j}) - \hat{\mu}(i, j)$ $M[\hat{\mu}(k, l)]$ is the matrix with element from the original image, \tilde{M} is the matrix from distorted image, $H = [h_{ijkl}]$ is the matrix of impulse response, and v is suitable large positive coefficient. The penalty function can be expressed as:

$$f(e_{ij}) = \lambda \ln \cosh\left(\frac{e_{ij}}{\lambda}\right) \text{ where } \lambda > 0 \quad (6.29)$$

Applying derivation to equation 6.29, it takes form:

$$\dot{f}(e_{ij}) = \frac{1 - \exp(-\frac{2e_{ij}}{\lambda})}{1 + \exp(-\frac{2e_{ij}}{\lambda})} \quad (6.30)$$

Converting equation 6.27 into energy function for solving the problem as optimization problem, it is expressed as:

$$E^t = v \cdot \sum_{i=1}^I \sum_{j=1}^J f(e_{ij}(M)) \quad (6.31)$$

In order to find out the minimum function, derivative operation is applied to equation 6.31 and the equation obtained is:

$$\frac{dE^t}{dt} = - \sum_{i=1}^I \sum_{j=1}^J \left(\frac{d\hat{\mu}^t((i,j))}{dt} \right)^2 \quad (6.32)$$

The schematics of implementation of above are shown in the figure 6.9

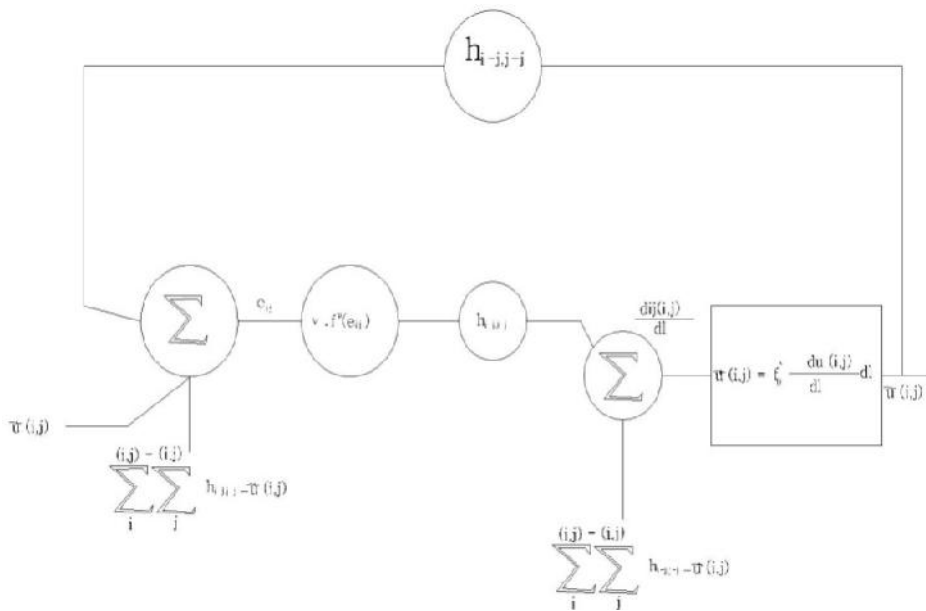


Figure 6.9: Cross Section of Neural Network for solving the Problem for Fan Beam

6.3.2 Implementation

As discussed in the section 6.2.1 the problem of reconstruction for the fan beam is also implemented on the same line. The steps of implementation are as shown in figure 6.8[14,17]. The pseudo code for Hopfield network is as follow:

Selection of Coefficient w_i and w_j

```
for i:=0 to 255 do
  for j:=0 to 255 do
    x2[i,j]:=1.01;
```

image obtained after back-projection operation is $y_2[i,j]$

```
repeat
  for i:=0 to 255 do
    for j:=0 to 255 do
      begin
        e2[i,j]:=0;
```

```
for k:=0 to 255 do
  for l:=0 to 255 do e2[i,j]:=e2[i,j]+h[i-k,j-l]*x2[k,l];
```

```
for i:=0 to 255 do
```

```
for j:=0 to 255 do
  e2[i,j]:= (1-exp((-e2[i,j]+y2[i,j])/w_i))/(1+exp((-e2[i,j]+y2[i,j])/w_i));
```

```
for i:=0 to 255 do
for j:=0 to 255 do
  begin
    z2[i,j]:=0;
```

```
for k:=0 to 255 do
for l:=0 to 255 do z2[i,j]:=z2[i,j]+h[k-i,l-j]*e2[k,l];
end;
```

```
for i:=0 to 255 do
for j:=0 to 255 do x2[i,j]:=x2[i,j]-w_j*z2[i,j];
x2[i,j] display on the screen.
```

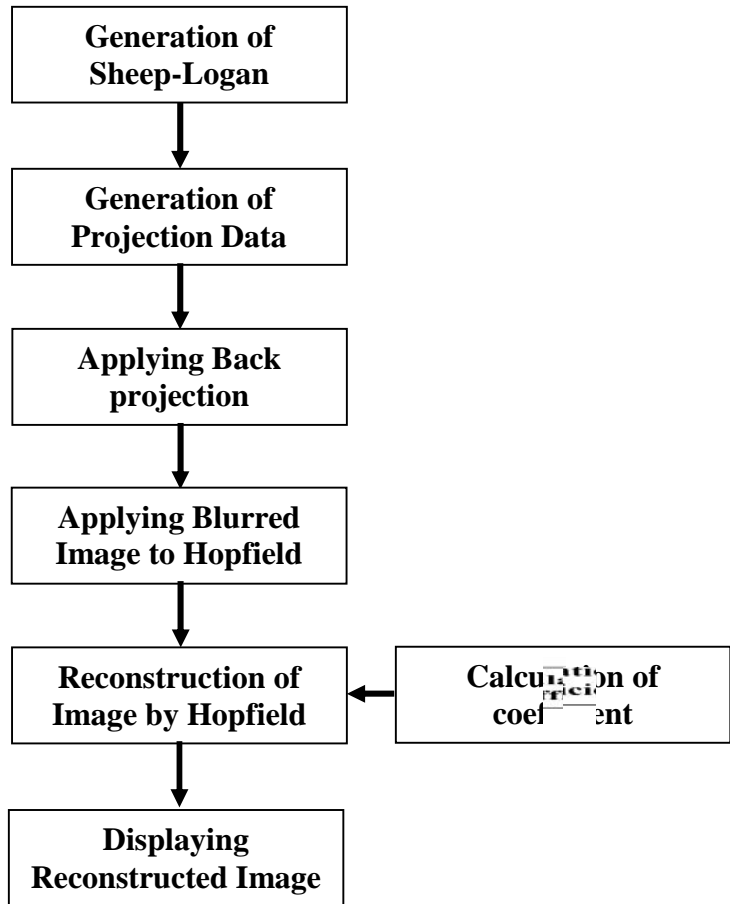


Figure 6.10: Flow chart for Reconstructing Image for Fan Beam Scanner

As seen the same philosophy is used to implement the problem for fan beam profile. The reconstructed image obtained after the implementation of neural network is shown in the below:



Figure 6.11: Reconstructed Image by Hopfield Network after 100 iteration for Fan Beam Profile



Figure 6.12: Reconstructed Image by Hopfield Network after 1000 iteration for Fan Beam Profile



Figure 6.13: Reconstructed Image by Hopfield Network after 10000 iteration for Fan Beam Profile.

The table 6.2 enlists the MATLAB® function file developed to solve the problem of reconstruction:

Sr. No	Name of Function File	Purpose
01	ct_reconstruction_nn	It is main function file takes required input from the user and produces the output.
02	phtantom_data	Creates the phantom data as per the choice of the user.
02	radon_transformation	Generates projection data from phantom data.
03	backprojection_operation	Performs backprojection and reconstruct the image.
04	h_matrix	Creates convolution kernel for the Hopfield network.
05	hop_nn_parallel_beam	Main function files for implementing neural network for parallel beam.
06	hop_nn_fan_beam	Main function files for implementing neural network for fanbeam.

Table 6.2: List of the MATLAB® Function Files Developed for the Implementation using Neural Network.

6.4 Concluding Remarks

The chapter discusses the novel approach developed to solve the problem of image reconstruction by reformulating it to the problem of optimization and solving it by using recurrent neural network as opposite to the traditional methods. It also discusses the result obtained after the implementation.

Chapter: 7

Advance Neural Network

This chapter discusses the user defined phantom construction used for testing the developed techniques. It also discusses the application of Genetic Algorithm application for Neural Network.

7.1 User Defined Phantom

As CT scanner uses the X-rays as the energy source, the over exposure of these radiation are harmful to human organisms. Hence, to ensure that the over dosage is avoided; all the techniques are tested in simulated environment. Hence, all the newly developed or modified techniques need to be verified by computer simulation. Moreover, it is nearly impossible to obtain the physical projection data from the CT scanner and hence, simulation is very much useful.

In order to standardize the testing of the entire algorithm, Sheep Logan phantom is used to obtain the virtual projection values [1,2]. This makes it possible to standardise the data for the reconstruction algorithms, which makes it possible to compare the result. Moreover, the reconstruction image can easily be compared to the original image, which helps to evaluate the quality of the reconstruction algorithm.

In order test the developed techniques in previous chapter, a user defined phantom is developed, which provides the projection value data needed for the simulation. The phantom developed resembles to human head, a multi density tissue organ. It may be noted that the elements in the phantom are additive. The mathematical modelling for the different beam profile is discussed in the following sections.

The phantom developed is made up of ellipse shape, which allows user to obtain the projection values for all points of interest on the screen for any projection angle. The topology of the mathematical model is shown in the figure 7.1:

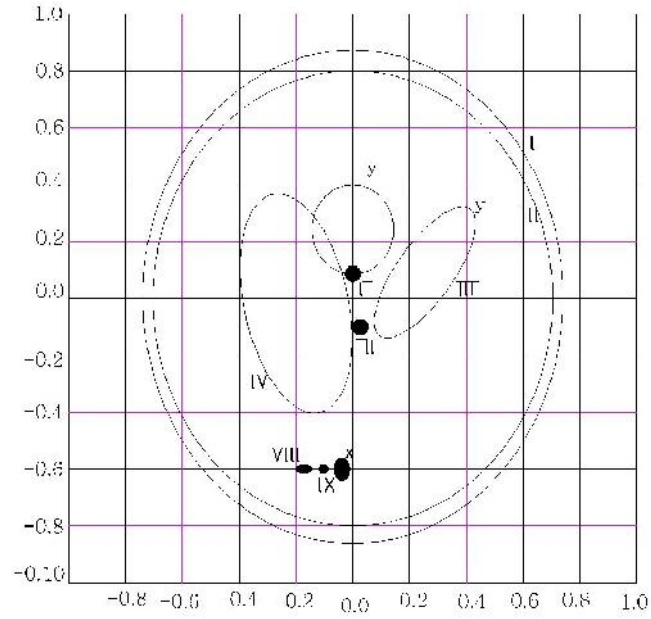


Figure 7.1: Topology of User defined Phantom

As seen from the figure, the model consists of elliptical elements, which are having constant attenuation coefficient. The mathematical equation describing the individual three categories of ellipses are given below:

- a) For ellipse centred at origin:

$$\frac{x^2}{a^2} + \frac{y^2}{b^2} \leq 1 \quad (7.1)$$

- b) For ellipse with its centre displayed to the point (x_0, y_0) :

$$\frac{(x - x_0)^2}{a^2} + \frac{(y - y_0)^2}{b^2} \leq 1 \quad (7.2)$$

- c) For ellipse displayed to point (x_0, y_0) and rotated at angle α_0 :

$$\frac{((x - x_0) \cos \alpha_0 + (y - y_0) \sin \alpha_0)^2}{a^2} + \frac{(-(x - x_0) \cos \alpha_0 + (y - y_0) \sin \alpha_0)^2}{b^2} \leq 1 \quad (7.3)$$

The image of the model user defined phantom is developed by superimposing successive elements of the phantom using ellipses defined in the equation below:

a) For ellipse centred at origin:

$$\mu_i(x, y) = \begin{cases} \mu_i^{const} & \text{for } \frac{x^2}{a^2} + \frac{y^2}{b^2} \leq 1 \\ 0 & \text{for } \frac{x^2}{a^2} + \frac{y^2}{b^2} > 1 \end{cases} \quad (7.4)$$

b) For ellipse with its centre displayed to the point (x_0, y_0) :

$$\mu_i(x, y) = \begin{cases} \mu_i^{const} & \text{for } \frac{(x - x_0)^2}{a^2} + \frac{(y - y_0)^2}{b^2} \leq 1 \\ 0 & \text{for } \frac{(x - x_0)^2}{a^2} + \frac{(y - y_0)^2}{b^2} > 1 \end{cases} \quad (7.5)$$

c) For ellipse displayed to point (x_0, y_0) and rotated at angle α_0 :

$$\mu_i(x, y) = \begin{cases} \mu_i^{const} & \text{for } \frac{((x - x_0) \cos \alpha_0 + (y - y_0) \sin \alpha_0)^2}{a^2} + \frac{(-(x - x_0) \cos \alpha_0 + (y - y_0) \sin \alpha_0)^2}{b^2} \leq 1 \\ 0 & \text{for } \frac{((x - x_0) \cos \alpha_0 + (y - y_0) \sin \alpha_0)^2}{a^2} + \frac{(-(x - x_0) \cos \alpha_0 + (y - y_0) \sin \alpha_0)^2}{b^2} > 1 \end{cases} \quad (7.6)$$

Using the Radon theory [3] for a given angle of incidence α^p , one can sum the separately evaluated projection values $p_i^p = (s, \alpha^p)$. For the individual figure, each point s is given by:

$$p^p = (s, \alpha^p) = \sum_{i=1}^{\text{number of ellipese}} p_i^p = (s, \alpha^p) \quad (7.7)$$

With presented mathematical background, the user defined phantom is created in the MATLAB® giving the user flexibility to decide regarding the resolution of the image. In the present work, the image resolution of 256 X 256 pixels is used, which provides adequate validly for the developed approach.

Using the above, user defined phantom was simulated. The parameters which were used are listed below:

Number of Ellipse	Coordinates		Angle of Rotation α_0	Attenuation μ^{const}
	x^0	y^0		
I	0.00	0.00	0.00	2.00
II	0.00	-0.01	0.00	-0.98
III	0.22	0.00	-18.00	-0.02
IV	0.00	0.00	18.00	-0.02
V	0.00	0.35	0.00	0.01
VI	0.00	0.10	0.00	0.01
VII	0.00	-0.10	0.00	0.01
VIII	-0.08	-0.60	0.00	0.01
IX	0.00	-0.60	0.00	0.01
X	0.06	-0.60	0.00	0.01

Table 7.1: Parameters used to Simulate the User Defined Photon.

The phantom generated is shown in the figure 7.2:



Figure 7.2: Cross Section of User defined Phantom

7.2 Advance Neural Network

As discussed in previous chapters, the problem of reconstruction was reformulated as problem of optimisation. Genetic Algorithm emerged as most powerful tool to solve the problem of optimisation particularly when the problem is stochastic [3]. Since, it is evident that problem of reconstruction is stochastic in nature, it is logical to employ genetic algorithm to solve the problem[4].

It very important to assesses the quality of the image after any type of processing. There are number of parameters by which the quality of the image can be assessed. Out of these parameters, it is worth to mention that two parameters, signal to noise ratio and mean square error, are significantly important [5].

As discussed in Chapter 6, the image reconstructed is subject to assessment by these two parameters. Signal to noise ratio (SNR) and mean square error (MSE) for the reconstructed image are defined as:

$$SNR = 10 \log_{10} \left(\frac{\sum_{i=1}^I \sum_{j=1}^J [\mu(i,j)^2]}{\sum_{i=1}^I \sum_{j=1}^J [\mu(i,j) - \hat{\mu}(i,j)]^2} \right) \quad (7.6)$$

$$MSE = \frac{1}{IJ} \sum_{i=1}^I \sum_{j=1}^J [\mu(i,j) - \hat{\mu}(i,j)]^2 \quad (7.7)$$

where $\mu(i,j)$ is the original image. The performance of the Neural Network developed greatly depends on the weights w_1 and w_2 which are used to tune the neural network[8,9]. Genetic Algorithm due to its advantage can be used for tuning these weights[7].

In implementation of the Genetic Algorithm, it is worth to remember that two parameters namely chromosomes and fitness function play very vital role in the performance. In the present research work, the fitness function is defined on basis of mean square error of the reconstructed image and the chromosomes are decided on the basis of the resolution of the image i.e. if the resolution of the image is 128

X128 the length of the chromosome will be the same. The implementation of the Genetic Algorithm and Neural Network is similar to the strategy discussed in the previous chapter. However, the major difference is, instead of calculating the weights numerically, they are tuned by the GA[8]. The flow of implementation is shown in the figure 7.3:

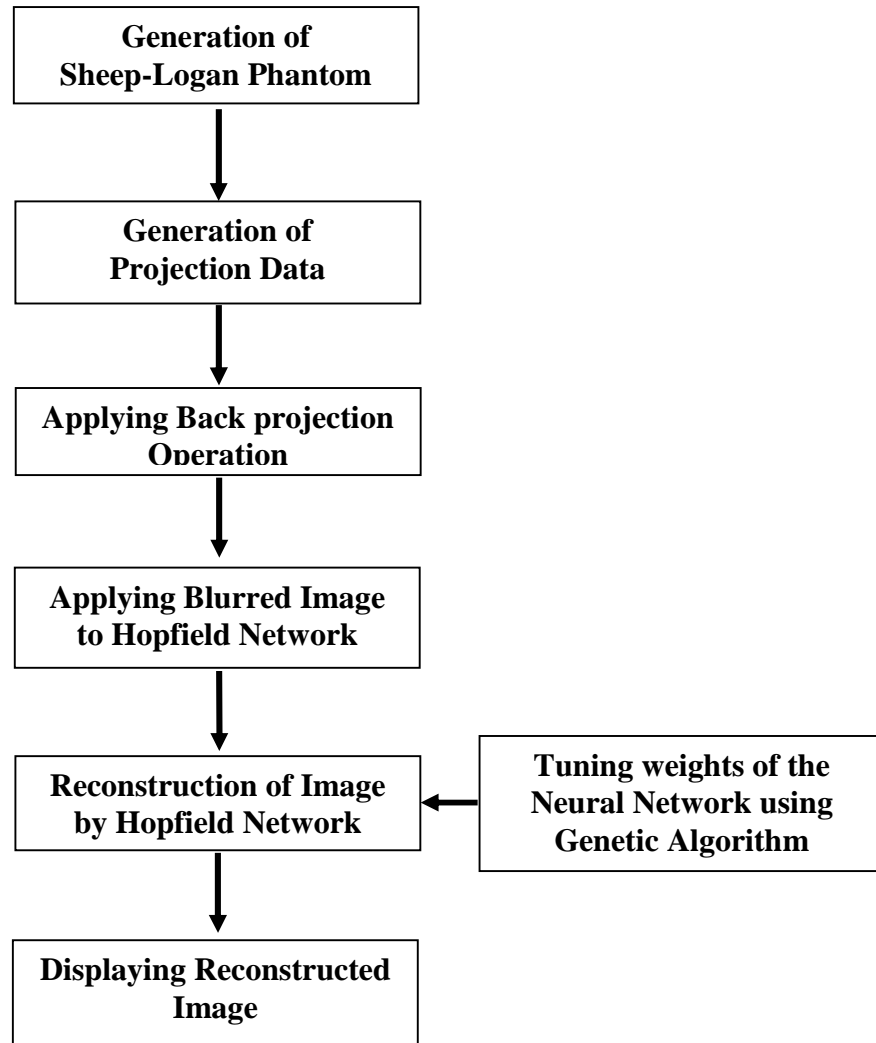


Figure 7.3: Flow chart for Implementing Advance Neural Network using Genetic Algorithm

The pseudo code for the implementing the GA to the problem is as follow:

Creation of the initial population of chromosomes.

for (all weights)

Evaluate the fitness of all the chromosomes of the population.

The best chromosomes will be selected to reproduce, using mutation and crossover.

With the new chromosomes created from the fittest of the previous generation, a new generation is created.

end for

Evaluate the fitness for all the chromosomes of the population.

Select the fittest chromosome of the population as the new weight.

end for

end for

As discussed earlier, the algorithm was tested by user defined phantom. The result obtained is shown in figure 7.4 [4]. The assessment of all the reconstructed phantoms are discussed in the Chapter 9 in details along with the relative comparison.



Figure 7.4: Reconstructed user defined phantom by using GA

The function files developed for the implementation of GA are listed in table 7.2 below:

Sr. No	Name of Function File	Purpose
01	ct_reconstruction_nn_ga	Main function file to execute image reconstruction using neural network and genetic algorithm.

Sr. No	Name of Function File	Purpose
02	phtantom_data	Generated phantom data.
02	radon_transformation	Obtains the projection data for further processing.
03	backprojection_operation	Reconstruct the image by backprojection operation.
04	h_matrix	Generates convolution matrix.
05	nn_ga	Main function file to use genetic algorithm to tune weights.
06	crossover_nn_ga	Performs crossover operation
07	mutate_nn_ga	Executes mutation operation.
08	fitness_nn_ga	Defines fitness function for the GA.

Table 7.2: List of the MATLAB® Function Files developed for the Implementation using Genetic Algorithm

7.4 Concluding Remarks

Chapter provides the necessary frame work to make user defined phantom, which is used to test the newly developed algorithmis and assesing them by comparing the reconstruted image with the original image. Chapter also dicusses application of Genetic Algorithm in the present research work.

Chapter: 8

User Interface Development

This chapter discusses feature and development procedure for Graphical User Interface using MATLAB®. Chapter also describes the User Interface developed for the presented research work.

8.1 Graphical User Interface Environment (GUI)

A graphical user interface (GUI) is a pictorial interface to a program. A good GUI can make programs easier to use by providing them with a consistent appearance and with intuitive controls like pushbuttons, list boxes, sliders, menus, and so forth. The GUI behaves in an understandable and predictable manner, so that a user knows what to expect when he or she performs an action. For example, when a mouse click occurs on a pushbutton, the GUI should initiate the action described on the label of the button. This section introduces the basic elements of the MATLAB® GUIs.

8.1.1. Working of Graphical User Interface [1-4]

A graphical user interface provides the user with a familiar environment in which to work. This environment contains pushbuttons, toggle buttons, lists, menus, text boxes, and so forth, all of which are already familiar to the user, so that he or she can concentrate on using the application rather than on the mechanics involved in doing things. However, GUIs are harder for the programmer because a GUI-based program must be prepared for mouse clicks (or possibly keyboard input) for any GUI element at any time. Such inputs are known as events, and a program that responds to events is said to be event driven. The three principal elements required to create a MATLAB® Graphical User Interface are:

1. **Components:** Each item on a MATLAB® GUI (pushbuttons, labels, edit boxes, etc.) is a graphical component. The types of components include graphical controls (pushbuttons, edit boxes, lists, sliders, etc.), static elements (frames and text strings), menus, and axes. Graphical controls and static elements are created by the function `uicontrol`, and menus are

created by the functions `uimenu` and `uicontextmenu`. Axes, which are used to display graphical data, are created by the function `axes`.

2. **Figures:** The components of a GUI must be arranged within a figure, which is a window on the computer screen. In the past, figures have been created automatically whenever data is plotted. However, empty figures can be created with the function `figure` and can be used to hold any combination of components.
3. **Callbacks:** Finally, there must be some way to perform an action if a user clicks a mouse on a button or types information on a keyboard. A mouse click or a key press is an event, and the MATLAB® program must respond to each event if the program is to perform its function. For example, if a user clicks on a button, that event must cause the MATLAB® code that implements the function of the button to be executed. The code executed in response to an event is known as a callback. There must be a callback to implement the function of each graphical component on the GUI.

MATLAB® GUIs are created using a tool called `guide`, the GUI Development environment. This tool allows a programmer to layout the GUI, selecting and aligning the GUI components to be placed in it. Once the components are in place, the programmer can edit their properties: name, color, size, font, text to display, and so forth. When `guide` saves the GUI, it creates working program including skeleton functions that the programmer can modify to implement the behavior of the GUI.

When `guide` is executed, it creates the Layout Editor, shown in Figure 8.1. The large white area with grid lines is the layout area, where a programmer can layout the GUI. The Layout Editor window has a palette of GUI components along the left side of the layout area. A user can create any number of GUI components by first clicking on the desired component, and then dragging its outline in the layout area. The top of the window has a toolbar with a series of useful tools that allow the user to

distribute and align GUI components, modify the properties of GUI components, add menus to GUIs, and so on.

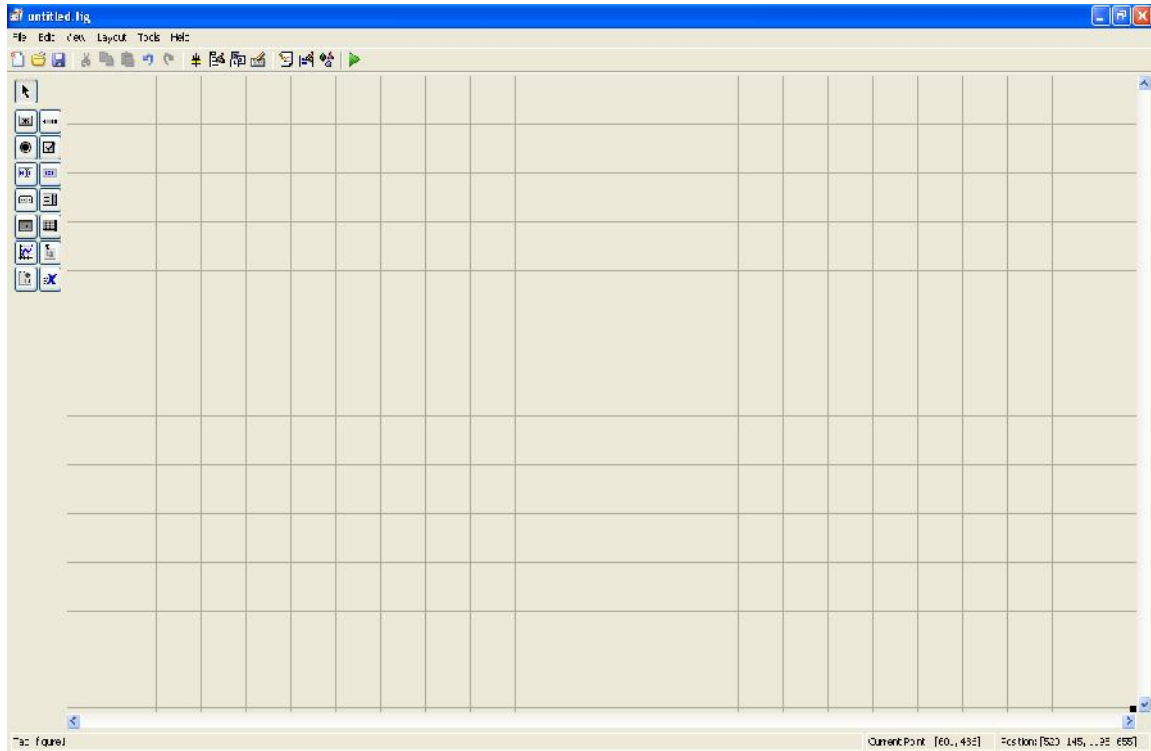


Figure 8.1: Layout of Guide in MATLAB®

8.1.2 GUI Components

This section summarizes the basic characteristics of common Graphical User Interface components. It describes how to create and use each component, as well as the types of events each component can generate. The components discussed in this section are

- **Text Fields:** A text-field is a graphical object that displays a text string. User can specify how the text is aligned in the display area by setting the horizontal alignment property. By default, text fields are horizontally centered. A text field is created by creating a uicontrol whose style property is 'edit'. A text field may be added to a GUI by using the text tool in the Layout Editor. Text fields do not create callbacks, but the value displayed in the text field can be updated in a callback function by changing the text field's String property.

- **Edit Boxes:** An edit box is a graphical object that allows a user to enter a text string. The edit box generates a callback when the user presses the Enter key after typing a string into the box. An edit box is created by creating a uicontrol whose style property is 'edit'. An edit box may be added to a GUI by using the edit box tool in the Layout Editor.
- **Frames:** A frame is a graphical object that displays a rectangle on the GUI. User can use frames to draw boxes around groups of logically related objects. A frame is created by creating a uicontrol whose style property is 'frame'. A frame maybe added to a GUI by using the frame tool in the Layout Editor. Frames do not generate callbacks.
- **Pushbuttons:** A pushbutton is a component that a user can click on to trigger a specific action. The pushbutton generates a callback when the user clicks the mouse on it. A pushbutton is created by creating a uicontrol whose style property is 'pushbutton'. A pushbutton may be added to a GUI by using the pushbutton tool in the Layout Editor.
- **Toggle Buttons:** A toggle button is a type of button that has two states: on (depressed) and off (not depressed). A toggle button switches between these two states whenever the mouse clicks on it, and it generates a callback each time. The 'Value' property of the toggle button is set to max (usually 1) when the button is on, and min (usually 0) when the button is off. A toggle button is created by creating a uicontrol whose style property is toggle button. A toggle button may be added to a GUI by using the toggle button tool in the Layout Editor. When a user clicks on the toggle button, it automatically calls the function ToggleButton_Callback, This function locates the toggle button using the handles structure and recovers its state from the 'Value' property. Then, the function locates the text field and displays the state in the text field

- **Checkboxes and Radio Buttons:** Checkboxes and radio buttons are essentially identical to toggle buttons except that they have different shapes. Like toggle buttons, checkboxes and radio buttons have two states: on and off. They switch between these two states whenever the mouse clicks on them, generating a callback each time. The 'Value' property of the checkbox or radio button is set to max (usually 1) when they are on, and min (usually 0) when they are off.
- **Popup Menus:** Popup menus are graphical objects that allow a user to select one of a mutually exclusive list of options. The list of options that the user can select among is specified by a cell array of strings, and the 'Value' property indicates which of the strings is currently selected. A popup menu may be added to a GUI by using the popup menu tool in the Layout Editor.
- **List Boxes:** List boxes are graphical objects that display many lines of text and allow a user to select one or more of those lines. If there are more lines of text than can fit in the list box, scroll bar will be created to allow the user to scroll up and down within the list box. The lines of text that the user can select among are specified by a cell array of strings, and the 'Value' property indicates which of the strings are currently selected. A list box is created by creating a uicontrol whose style property is 'listbox'.
- **Slide Sliders:** Slide Sliders are graphical objects that allow a user to select values from a continuous range between a specified minimum value and a specified maximum value by moving a bar with a mouse. The 'Value' property of the slider is set to a value between min and max depending on the position of the slider.

8.2 Designing of User Interface

In view to provide better user interface the techniques developed user interface is developed in the MATLAB® the screen shot of the main window of the GUI developed is shown in the figure 8.2[5]:

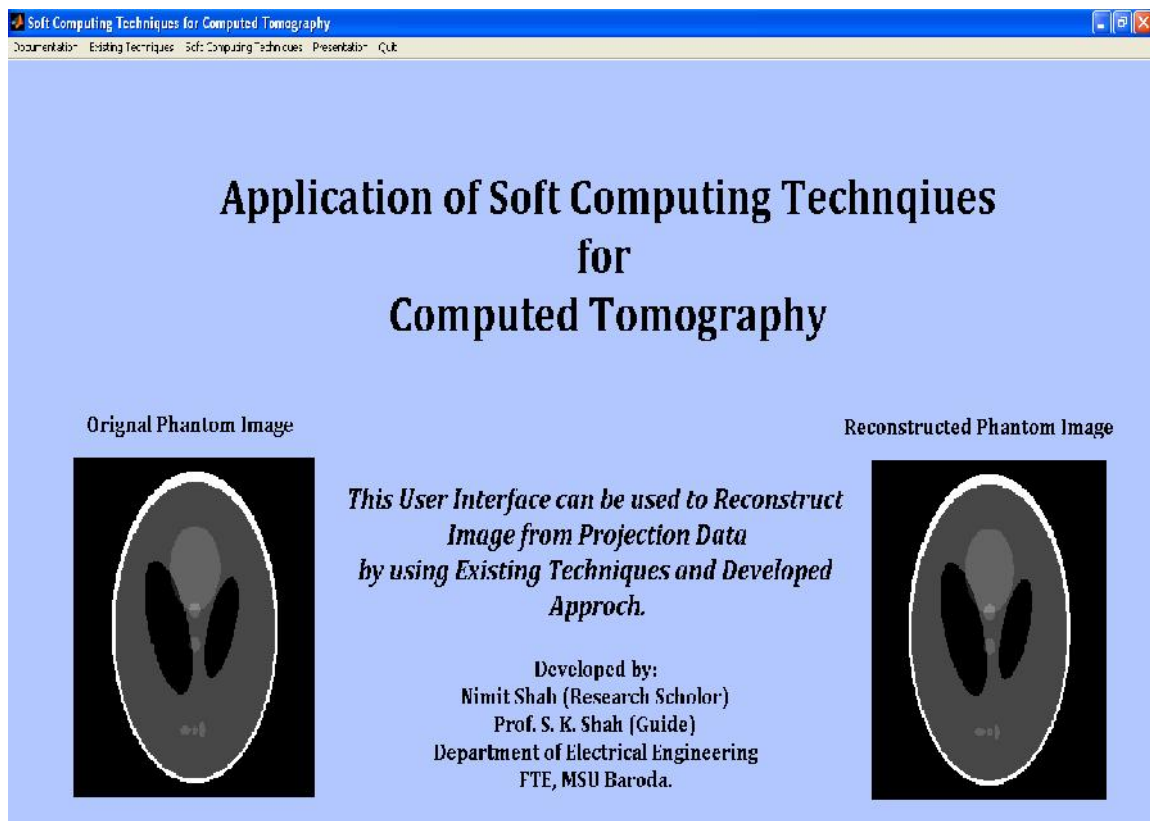


Figure 8.2: Main Window of the Developed Interface

As seen from the figure the user interface contains five main menu namely documentation, existing techniques, Soft computing techniques , presentation and quit. Documentation menu contains two sub menu synopsis and thesis related to the research work, presentation contains two sub menus for presentation and the publication based on the research.

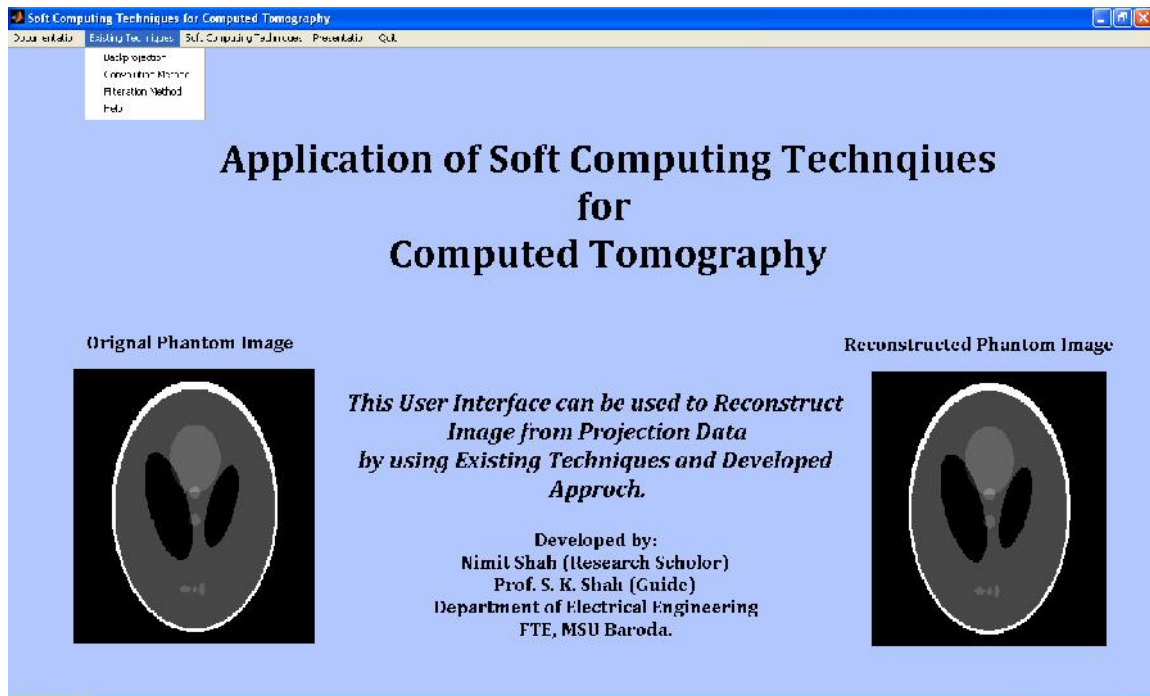


Figure 8.3: Window showing sub menus in Existing Techniques

As seen it the module which is developed to implement existing reconstruction techniques which are described in the Chapter 5, these techniques are implemented to compare the results obtained with developed technique. The three technique implemented are simple back projection, convolution and back projection and filtration and back projection.

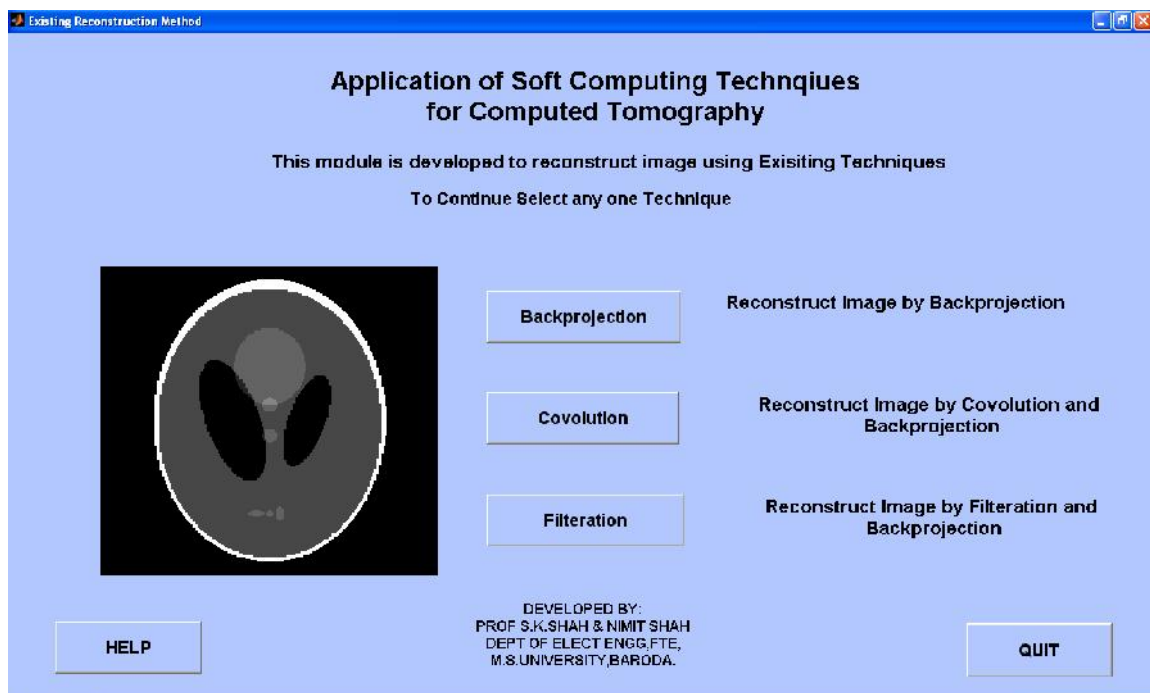


Figure 8.4: Window showing Implementation of Existing Techniques

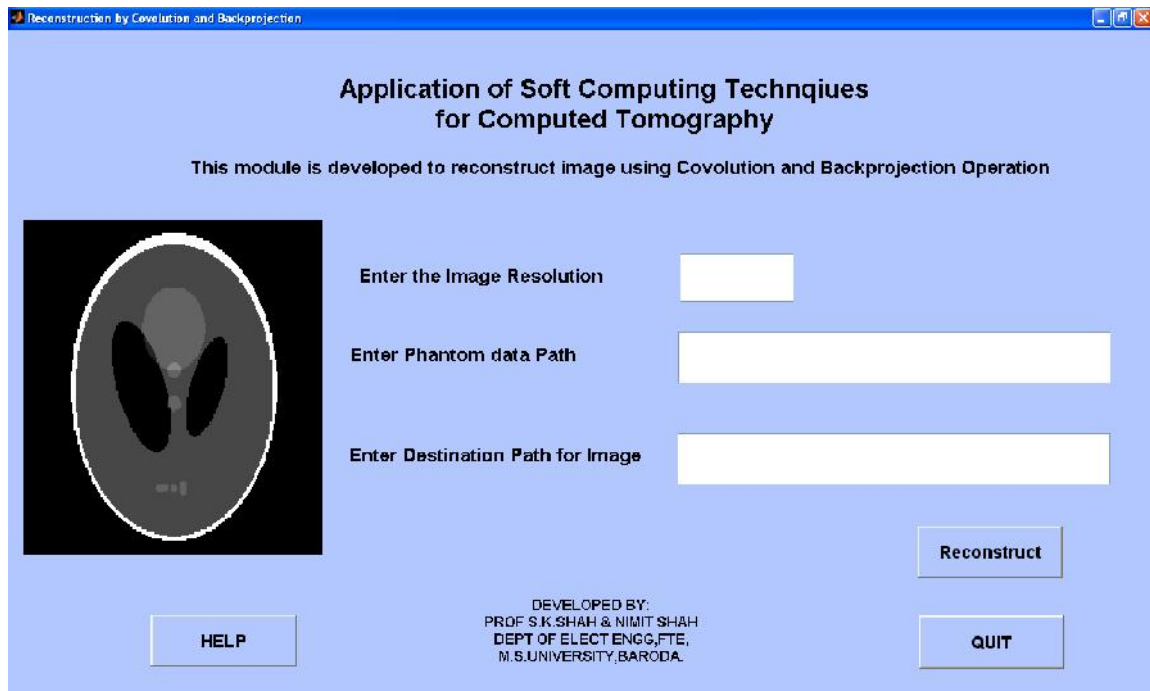


Figure 8.5: Window showing Implementation of Convolution Method

The input parameter required for implementing technique are the image resolution pre-defined phantom data and destination path were reconstructed image will be saved. The other techniques are implemented in the same manner.

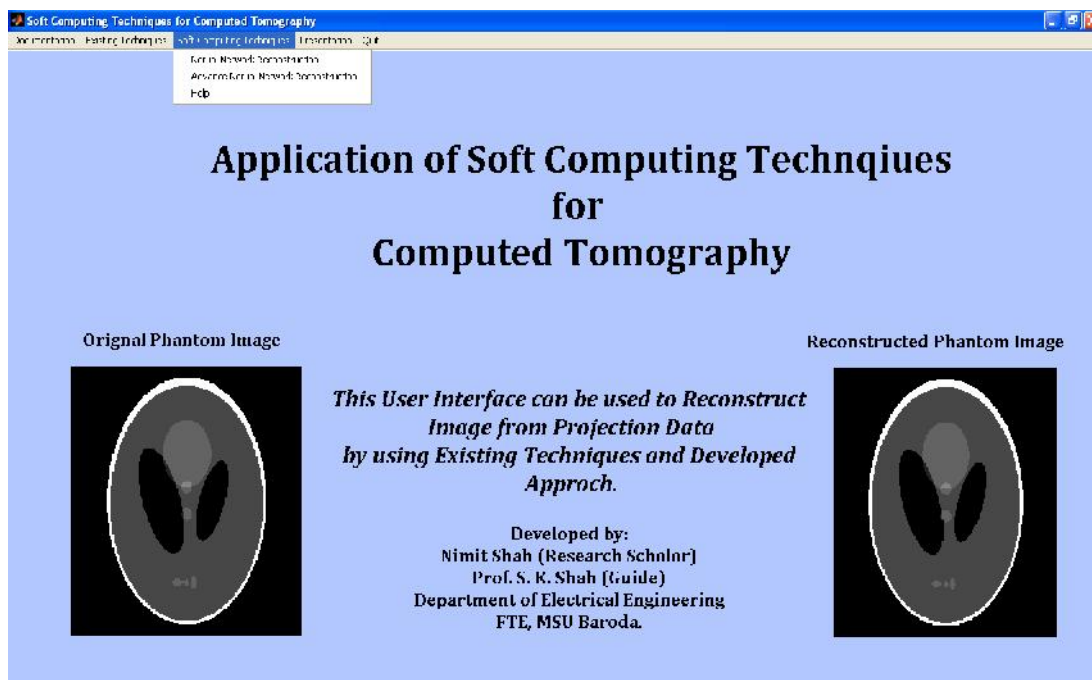


Figure 8.6: Window showing sub menus in Developed Techniques

As seen from the figure 8.6 under the menu of soft computing techniques two sub menu are given namely Neural Network Reconstruction and Advance Neural Network which implements the techniques discussed in Chapter 6 and Chapter 7 respectively.

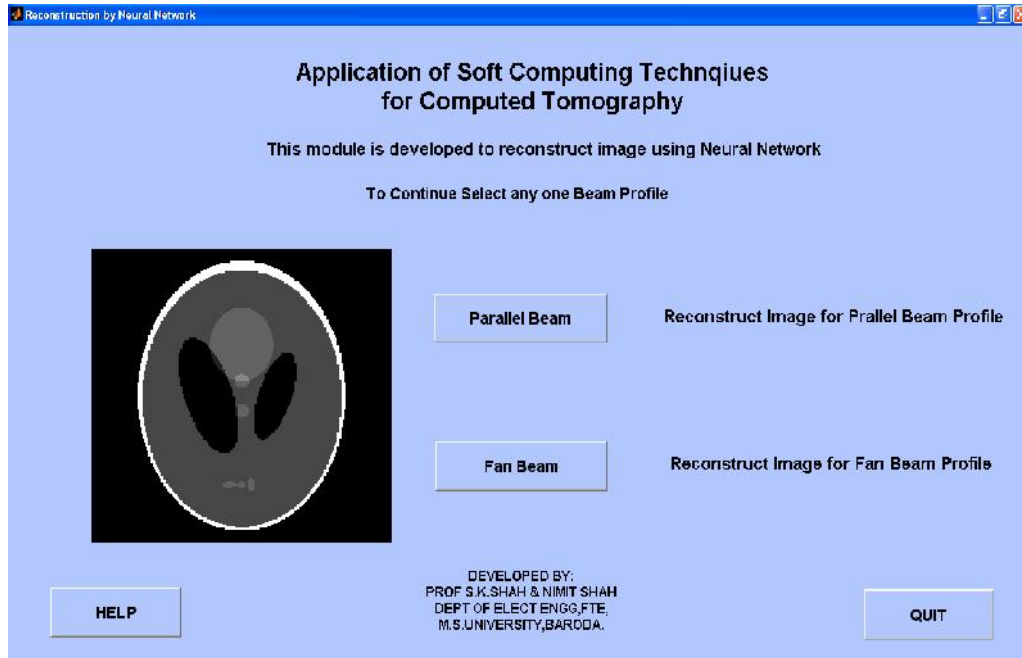


Figure 8.7: Window showing selection of Beam Profile

The problem of reconstruction is solved for two beam profile Parallel beam and Fan beam. The user is able to select the type of the beam profile for which image is to be reconstructed.

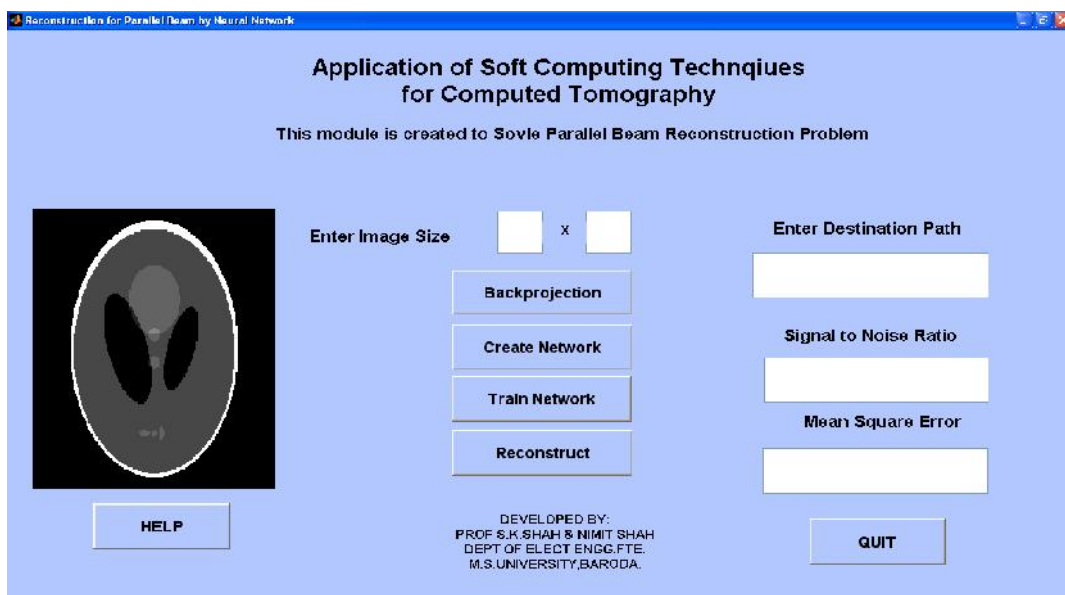


Figure 8.8: Window showing solving Parallel Beam Profile

The user needs to provide the image size i.e. resolution from which corresponding user defined phantom will be generated. Next step to perform back projection operation followed by creating the neural network. As the network needs to be trained this is followed by the reconstruction. At the end of the reconstruction process the two parameters Signal to Noise Ratio and Mean Square Error will be given to the user.

The module for the Advance Neural Network is developed on the similar line where user needs to provide the image resolution and destination path to save the reconstructed image. The next chapter discusses the performance assessment.

8.3 Concluding Remarks

This chapter gives the brief overview regarding the features of GUIDE the tool used to develop the user interface in MATLAB®. Chapter also discusses the features of the developed user interface for the research along with some of the screen shots of the windows of interface

Chapter: 9

Conclusions and Future Scope

This chapter discusses the results obtained, research contribution, limitations and assumptions made. Suggestions for future scope of the research work are also given in the chapter.

9.1 Research Contribution

On the basis of the work carried out for this research, following outcomes have emerged:

1. Understanding the technical aspects of the CT Scanners and the diagnostic importance of the information which can be inferred from the output.
2. Modelling the basic reconstruction problem by the conventional techniques provides basic mathematical frame work to reformulate the problem of reconstruction for better solution.
3. The existing problem is being modified as problem of optimization to enable usage of soft computing techniques to solve problem more efficiently.
4. Implementation of novel developed algorithm through the use of Neural Network and Genetic Algorithm.
5. Testing the developed approach by standard testing techniques and comparing results with exiting methods.

9.1.1 Problem Formulation

Accurate and fast medical diagnosis is very essential for providing better health care. Out of many diagnostic techniques, non invasive radiological techniques are of great importance because of their non invasive philosophy. CT scanner, out of many modalities to view the inside of the human body, is most powerful and widely used modality. In CT scanner, the image is reconstructed by processing the projection data, which is obtained from the gantry of the scanner. The mathematical frame work to execute this process is popularly known as reconstruction problem.

This reconstruction problem is divided into two categories on beam profile which is used for acquiring projection data. Based on the geometrical relations and the attenuation property of X-rays, the problem is solved by two approaches; analytical method like back projection and algebraic technique like algebraic reconstruction technique (ART).

9.1.2 Problem Reformulation

Optimization techniques are widely used in solving many complex problems and its application can be extended to medical field also. The problem of reconstruction can be reformulated as problem of optimization. The problem was formulated first for the parallel beam projection system followed by the problem solving for fan beam projections system.

The least square error and steepest decent are two popular techniques used to solve the problem when two constrains direction and rate of change of algorithm is to be calculated. The basic reconstruction algorithm uses these two constraints. As soft computing techniques are used to solve non linear stochastic problems, the usage can be extended to solve this reformulated problem by considering the maximizing entropy criterion.

9.1.3 Implementation of Problem

Using Entropy criterion, the problem of optimisation was solved and based on the maximizing entropy criterion, the Hopfield neural network was developed. Hopfield network, a recurrent neural network, was used because it is evident that, for the problem of reconstruction, supervised learning networks cannot be employed because it is impossible to train the network.

Moreover, the transform method is used to solve the problem as the popular algebraic methods are computationally costly. Moreover, the networks formed, based on the algebraic method, are large and very complicated making it impossible to implement. It is observed that the novel algorithm developed can be used to reconstruct the standard phantom by simulating it on the MATLAB® platform. The algorithm developed can be used to reconstruct other volumetric data.

9.1.4. Overall Conclusion

The reconstruction method developed can be used to reconstruct the volumetric data from projection data. The reconstructed image developed is having good diagnostic value. The quality of the image reconstructed is better as compared to the image reconstructed from the conventional approach. The same can be seen by comparing the results obtained by various approaches discussed in the thesis.



Figure 9.1: Cross Section of User defined Phantom

As shown above Figure 9.1 shows the cross section of the image of the phantom generated and Figure 9.2 show the image reconstructed by simple back projection. It can be seen from the figure no interpretation of the data is possible as it contains geometric distortion.



Figure 9.2: Cross Section of User defined Phantom reconstructed by Back Projection.

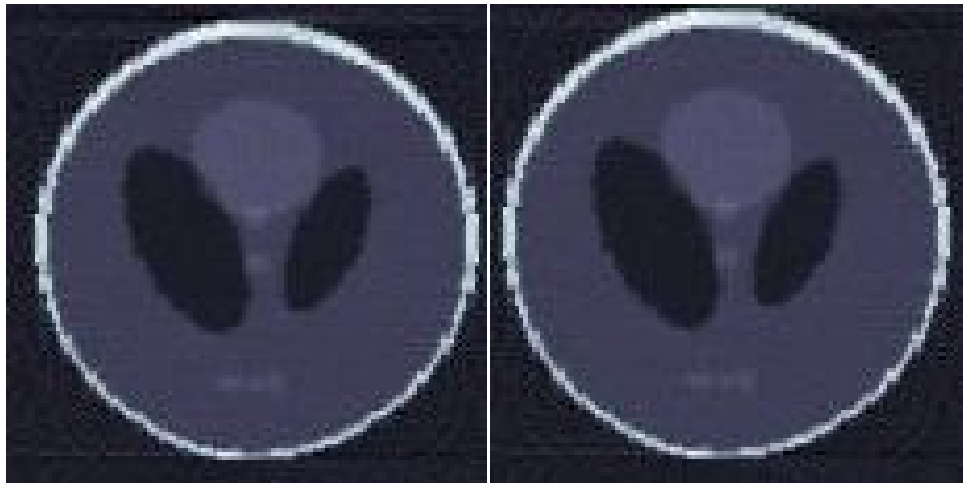


Figure 9.3: Cross Section of User defined Phantom reconstructed by a) Convolution and Back projection b) Filtration and Back projection

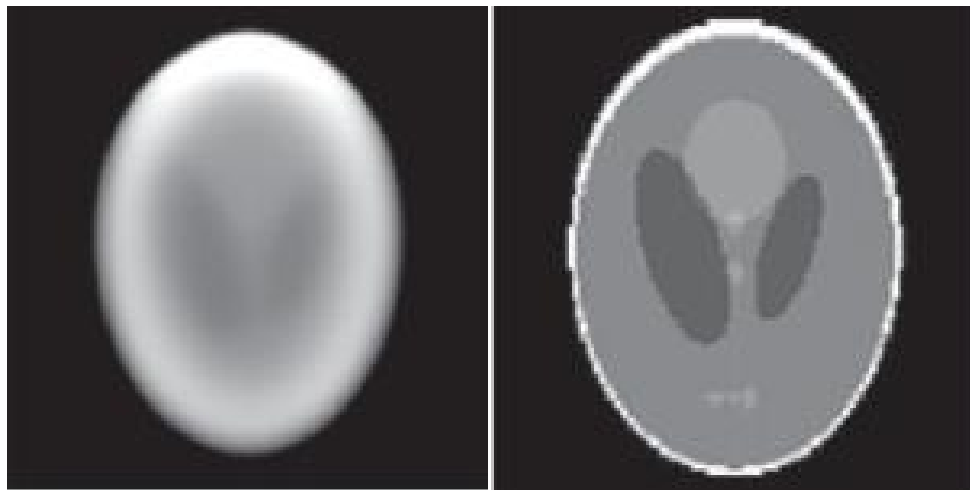


Figure 9.4: Cross Section of User defined Phantom reconstructed by a) Neural Network with 100 iterations b) Neural Network with 10000 iterations

Similarly, Figure 9.3 shows the reconstructed image by using conventional approaches. From the image, it is evident the reconstructed image contains artefacts. The image reconstructed by the developed approach shown in figure 9.4 b resembles to the original image shown in the figure 9.1. Hence, it can be concluded image reconstructed by the developed approach is having the better diagnostic value as compared to the other approaches. Moreover, the reconstructed image by the exiting techniques are having less distorting as compared to the simple back projection but the values of two assessment parameters signal to noise ration and mean square error are not satisfactory. The evaluation parameters obtained are shown in table 9.1:

Particular	Conventional Approach	Developed Approach
SNR	19.23	17.00
MSE	0.0167	0.0150

Table 9.1: Values obtained for Evaluation Parameters

As seen from the above results from the reconstructed phantom image by simple back projection is having large distortion making it difficult to interpret any information from the image. The reconstructed image by the exiting techniques are having less distorting as compared to the simple back projection but the values of two assessment parameters signal to noise ration and mean square error are not satisfactory. While the in the image reconstructed from the developed approach is of better quality as the objects of phantoms are distinctly visible and the assessment parameters are good as compared to exiting approach.

For better interface, the user interface is developed which includes the implementation and testing of the existing techniques and developed approaches. Developed approaches contain solution for parallel beam and fan beam profiles. This solution is obtained by using neural network and combination of neural network and genetic algorithm, as shown in the figure below:

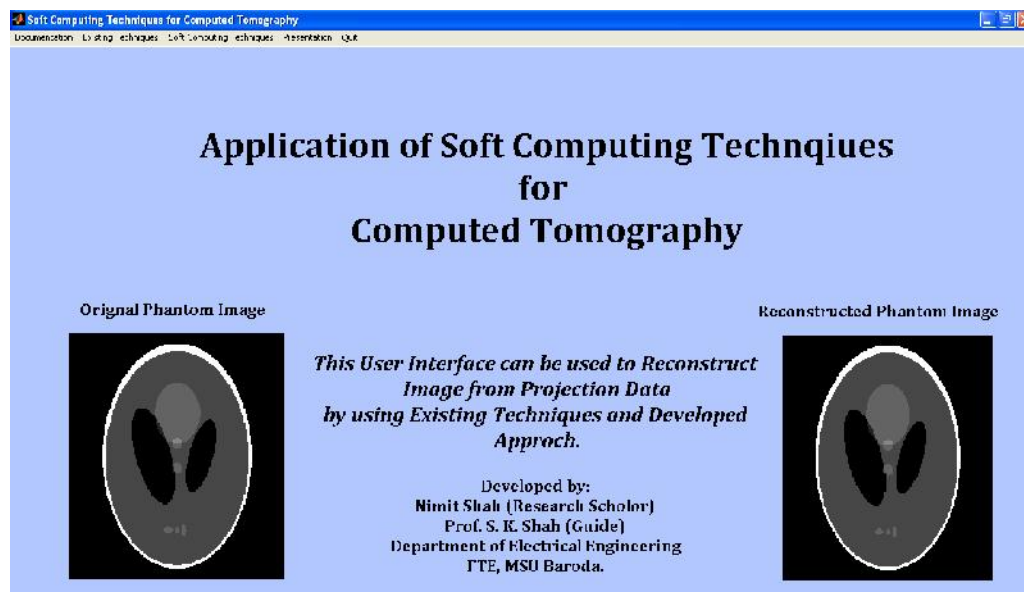


Figure 9.5: Main Window of the Developed Interface

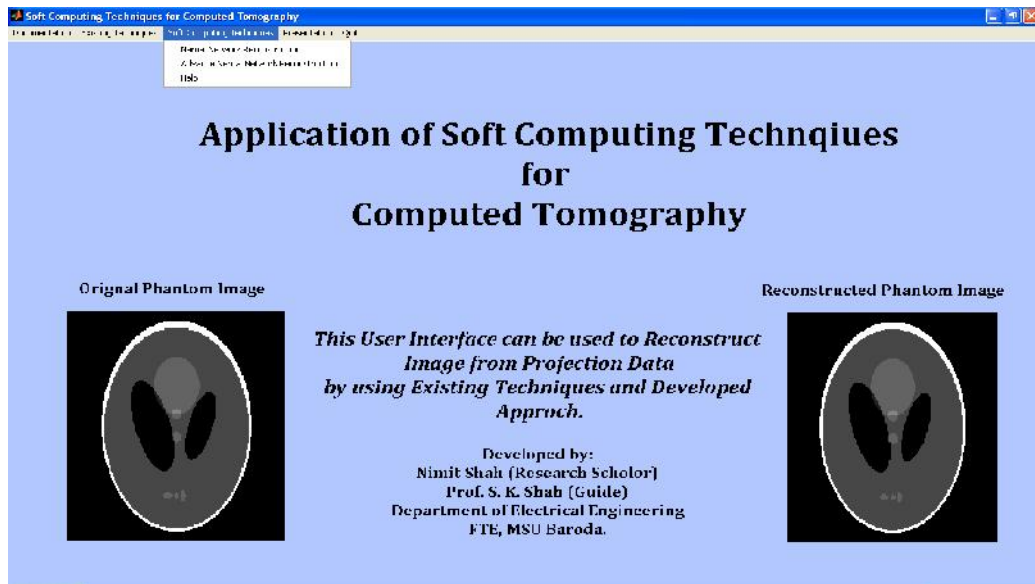


Figure 9.6: Window showing sub menus in Developed Techniques

9.2 Future Scope

As the reconstruction problem is formulated, implemented and tested; it is possible to carry out further research in the areas suggested below:

1. The reconstruction algorithm was tested using the user defined phantom resembling to standard testing phantom Sheep Logan. The algorithm needs to be tested for more data sets to test robustness of the algorithm. As in present study, real projection data is not used due to non availability of the raw data sets from the existing scanner.
2. The present algorithm is developed for the parallel beam and fan beam profile. The approach can be further extended by modifying to spiral scanner geometry.
3. The reformulated problem can be solved by employing unsupervised neural network configuration which can be optimized by using other popular algorithms such as Particle Swarm Optimization.

4. For research, problem was realised on MATLAB® platform. In view, to make it more universal, the problem must be realised on the popular open source software. It will include the necessary simulation study to understand CT scanning techniques and the reconstruction from the projection data.
5. The corresponding hardware realisation by using DSP or FGPA platform can be explored, which will enable to use the developed algorithm in real time for existing CT scanners.

Chapter: 10

Bibliography

Thesis ends with bibliography for each chapter.

Chapter 1

- [1] Pratt, W.K, Digital Image Processing. 2nd ed. 1991, New York: Wiley & Sons.
- [2] Shung, N, S, "Fundamental of Computed Tomography", 2nd ed. 200, New York : Wiley & Sons.
- [3] Bankman, N,I, "Handbook of Medical Image Processing", 2010, Academic Press.
- [4] Cormack A.M.: "Reconstruction Of Densities From Their Projections, With Applications" in radiological physics, Phys. Med. Biol., vol. 18, no. 2, pp.195–207, 1973.
- [5] Hounsfield G. N.: "Computerized Transverse Axial Scanning: Tomography", British Institute Conference, London, 1973.
- [6] Jain A K(1989) "Fundamentals of Digital Image Processing". Prentice-Hall, Englewood Cliffs
- [7] Lewitt RM. "Reconstruction algorithms: Transform methods". Proceeding of the IEEE, vol. 71, no. 3; 1983. p. 390—408.
- [8] Kak AC, Slanley M (1988) "Principles of Computerized Tomographic Imaging". IEEE Press, New York
- [9] Gordon R, Bender R, Herman GT (1970) "Algebraic reconstruction techniques (ART)for three-dimensional electron microscopy and X-ray photography". J Theor Biol 29:471-481
- [10] Eggermont PPB, Herman GT, Lent A (1981) "Iterative algorithms for large partitioned linear systems, with application to image reconstruction". Linear Algebra Its Appl 40:37-67.
- [11] D.E. Goldberg, "Genetic Algorithms in Search: Optimization and Learning", Addison-Wesley Publishing Co., Reading, 1989.

- [12] Kerr JP, Bartlett EB. "A statistically tailored neural network approach to tomography image reconstruction". *Med Phys* 1995;22:601—10.
- [13] Kerr JP, Bartlett EB. "Medical image processing utilizing neural networks trained on a massively parallel computer". *Comput Biol Med* 1995;25:393—403.
- [14] Knoll P, Mirzaei S, Mueller A, Leitha T, Koriska K, Koehn H, et al. "An artificial neural net and error back propagation to reconstruct single photon emission computerized tomography data". *Med Phys* 1999;26:244—8.
- [15] Srinivasan V, Han YK, Ong SH. "Image reconstruction by Hopfield neural network". *Image Vis Comput* 1993;11(5278—82).
- [16] Jaene B. *Digital image processing—concepts, algorithms and scientific applications*. Berlin, Heidelberg: Springer-Verlag;
- [17] Q. Tang, G. L. Zeng, and G. T. Gullberg, "Analytical fan-beam and cone-beam reconstruction algorithms with uniform attenuation correction," Rome, 2004, pp. 35463550.
- [18] S.F. Yau, S.H. Wong, "Limited angle tomography using artificial neural networks", *SPIE 2664* (1996) 170–179
- [19] Munley MT, Floyd CE, Bowsher JE, Coleman RE. "An artificial neural network approach to quantitative single photoemission computed topographic reconstruction with collimator, attenuation and scatter compensation". *MedPhys* 1994;21:1889—99.
- [20] S.F. Yau, S.H. Wong, "Limited angle tomography using artificial neural networks", *SPIE 2664* (1996) 170–179
- [21] S. K. Shah, N. D. Shah, "Reconstruction of 3D Medical Images by Neural Network," , at Control, Microcomputer, Electronics and Communication by Institute of Electronics & Telecommunication Engineers , Vadodara, February 2011.
- [22] N. D. Shah, S. K. Shah "Radon Transform Based Improved Algorithm For Computed Tomography To Reconstruct Volume From Real 2d Data Gathered Over Arbitrary Path using Matlab® With Graphical User Interface" , Accepted for publication at Institution of Engineers, India.

[23] N.D. Shah, S. K. Shah , D. Rathod, “ Computed Tomography Reconstruction by using Unsupervised Artificial Neural Network” , Submitted for publication for International Journal of Automation and Control Engineering (IJACE, ISSN Print: 2325-7407)

Chapter 2

[1] G. T. Herman, Image Reconstruction from Projection: The Fundamental of Computerized Tomography, Academic Press, San Francisco, 1980.

[2] Peschmann KR, Couch JL, Parker DL (1981) “New developments in digital X-ray detection”. SPIE 314:50–54

[3] Arenson JS (1995) Data collection strategies: gantries and detectors. In:Goldman LW,Fowlkes JB (ed) Medical CT and Ultrasound. Advanced Medical Publishing

[4] Hahn G, Hupke R, Kohl G et al (1997) “Ultra-fast detector for computed tomography”. Res Innov 1:15–22

[5] Greskovich CD, Cusano D, Hoffman Det al (1992) “Ceramic scintillators for advanced, medical x-ray detectors”. Am Ceramic Soc Bull 71:1120–1130

[6] Fuchs T, Kachelrieß M, Kalender WA (2000) “Direct comparison of a xenon and asolid-state CT detector system: Measurements under working conditions”. IEEE Trans Med Imag 19(9):941–948

[8] Peschmann KR (1981) Xeneon gas ionization detectors. In: Newton TH, Potts DG(ed) Radiology of the Skull and Brain: Technical Aspects of Computed Tomography,Mosby, Saint Louis

[9] Lewitt RM. “Reconstruction algorithms: transform methods”. Proceeding of the IEEE, vol. 71, no. 3; 1983. p. 390—408.

[10] Hsieh J, Gurmen OE, King KF (2000) “Investigation of a solid-state detector for advanced computed tomography”, IEEE Trans Med Imag 19(9):930–940

[11] Suryanarayana C, Grant Norton M (1998) X-Ray diffraction: A practical approach. Plenum Press, Ney York

[12] Brooks RA, DiChiro G (1976) “Principles of computer assisted tomography (CAT) in radiographic and radioisotopic imaging”. Phys Med Biol 21:689–732

[13] Cullity BD, Stock SR (2001) Elements of X-ray diffraction, 3rd edn. Addison-Wesley Publishing Comp Inc

[14] Glover GH, Pelc NJ (1981) "An algorithm for the reduction of metal clip artifacts reconstructions". *Med Phys* 8:799–807

[15] www.imp.uni-erlangen.de/phantoms/

[16] Shepp LA, Logan BF (1974) "The Fourier reconstruction of a head section". *IEEE Trans Nucl Sci NS-21:21–43*

Chapter 3

[1] Jain AK (1989) *Fundamentals of digital image processing*. Prentice-Hall.

[2] Kak AC, Slanley M (1988) *Principles of computerized topographic imaging*. IEEE Press, New York

[3] Ludwig D (1966) "The Radon Transform on Euclidean space". *Commun Pure Appl Math* 19:49–81

[4] Lewitt RM (1983) "Reconstruction algorithms: transform methods". *Proc IEEE* 71(3):390–408

[5] Censor Y (1983) "Finite series-expansion reconstruction methods". *Proc IEEE* 71:409–419

[6] Gubarieny N (2010) "Generalized model of asynchronous iterations for image reconstruction". *Proc Confer PPAM'99, Kazimierz Dolny*

[7] Tanabe K (1982) "Projection method for solving a singular system of linear equations and its applications". *Numer Math* 17:203–214

[8] Kudo H, Noo F, Defrise M (1998) "Cone-beam filtered-backpropagation algorithm for truncated helical data". *Phys Med Biol* 43: 2885–2909

[9] Herman GT, Lent A (1976) "Iterative reconstruction algorithms", *Comput Biol Med* 6:273–294

[10] Gordon R, Bender R, Herman GT. "Algebraic reconstruction techniques (ART) for three-dimensional electron microscopy and X-ray photography". *J Theor Biol* 1970;29:471–81.

[11] Herman GT, Lung H-P (1990) "Reconstruction from divergent beams: a comparison of algorithms with and without rebinning". *Comput Biol Med* 10:131–139

- [12] Peters TM, Lewitt RM (1977) Computerized tomography with fan beam geometry. *J Comp Assist Tomogr* 1:429–436
- [13] Herman GT, Lakshminarayanan AV, Naparstek A (1997) “Convolution reconstruction techniques for divergent beams”. *Compute Biol Med* 6:259–271
- [14] Kak AC, Slanley M (1988) Principles of computerized tomography imaging. IEEE Press, New York
- [15] Elvins TT (1982) “A survey of algorithm for volume visualization”. *Compute Graph* 26(3):194–201
- [16] Buzug TM (2008) “From photon statistics to modern cone-beam CT”. Springer-Verlag, Belin, Heidelberg
- [17] Gonzalez RC, Woods RE (1992) Digital Image Processing, Addison-Wesley Publishing Company, Reading, Menlo Park, New York
- [18] Wilson O, Gelder van A, Wilhelms J (1994) “Direct volume rendering via 3D textures”. Tech Rep USCS-CRL-94-19

Chapter 4

- [1] S.N. Sivanandam, S. Sumathi, S.N. Deepa, “Introduction to neural networks using MATLAB 6.0”, Tata McGraw-Hill Publishing Company Limited, New Delhi, ISBN: 0-07-059112-1, 2006.
- [2] Anil K Jain, Jianchang Mao and K.M Mohiuddin, “Artificial Neural Networks: A Tutorial”, Michigan State university, 1996
- [3] Yardimci, A., Applications of soft computing to medical problems, in Ninth International Conference on Intelligent Systems Design and Applications. 2009. p. 614-619.
- [4] Azvine, B., N. Azarmi, and K.C. Tsui, An introduction to soft computing — A tool for building intelligent systems, in Lecture Notes in Computer Science. 1997, Springer Berlin / Heidelberg.
- [6] Rudolf Seising “Soft Concepts” for Soft Computing in “Soft Sciences” On 20 years of “Soft Computing” IEEE2010
- [7] Lotfi, A.Z., The Roles of Fuzzy Logic and Soft Computing in the Conception, Design and Deployment of Intelligent Systems, in Software Agents and Soft

Computing: Towards Enhancing Machine Intelligence, Concepts and Applications. 1997, Springer-Verlag

[8] V. RaoVemuri “Main Problems and Issues in Neural Networks Application” IEEE1993

[9] Yardimci, A., Soft computing in medicine. Applied Soft Computing, 2009. 9: p. 1029–1043.

[10] Holland, J.H., Adaptation in Natural and Artificial Systems. University of Michigan Press, Ann Arbor, Michigan, 1975. Reprinted: MIT Press, Cambridge, Massachusetts,, 1992.

[11] Simon Haking “ Neural Network and Learning machine: 3 ed. PHI. India.

[12] Harikumar, R., R. Sukanesh, and P.A. Bharathi. Genetic algorithm optimization of fuzzy outputs for classification of epilepsy risk levels from EEG signals. in Conference Record of the Thirty-Eighth Asilomar Conference on Signals, Systems and Computers 2004.

[13] D.E. Goldberg, “Genetic Algorithms in Search: Optimization and Learning”, Addison-Wesley Publishing Co., Reading, 1989.

[14] XinjianQiang, Guojian Cheng, Zheng Wang “An Overview of Some Classical Growing Neural Networks and New Developments” 2nd International Conference on Education Technology and Computer (ICETC) 2010

[15]Hamada R. H. Al-Absi, Azween Abdullah and MahamatIssa Hassan “Soft Computing in Medical Diagnostic Applications:” 2011 IEEE Proceedings.

[16] Matlab software, www. mathworks.in, 2013

Chapter 5

[1] Jain AK (1989) Fundamentals of digitals image processing. Prentice-Hall, Englewood Cliffs

[2] Kak AC, Slanley M (1988) Principles of computerized tomographic imaging. IEEE Press, New York

[3] Ludwig D (1966) The Radon Transform on Euclidean space. Commun Pure ApplMath 19:49–81

[4]. Lewitt RM (1983) Reconstruction algorithms: transform methods. Proc IEEE71(3):390–408

- [5] Ramachandran GN, Lakshminarayanan AV (1971) Three-dimensional reconstruction from radiographs and electron micrographs: II. Application of convolutions instead of Fourier Transforms. *Proc Nat Acad Sci* 68:2236–2240
- [5] K. Mueller, M. Kaveh, and G. Wade, “Reconstructive tomography and applications to ultrasonics,” *Proc. IEEE*, vol. 67, pp. 567-587, 1979.
- [6] P. A. Rattey and A. G. Lindgren, “Sampling the 2-D Radon transform,” *IEEE Trans. Acoust., Speech, Signal Processing*, vol. ASSP-29, pp. 994-1002, 1981.
- [7] Naparstek, “Short-scan fan-beam algorithms for CT,” *IEEE Trans. Nucl. Sci.*, vol. NS-27, pp. 1112-1120, 1980
- [8] Y. Wang and W. Lu, “Multicriterion image reconstruction and implementation,” *Computer Vision, Graphics, Image Processing*, vol. 46, no. 2, pp. 131–135, 1989.
- [9] R. Jaszczak, “Tomographic Radiopharmaceutical Imaging”, *Proceedings of The IEEE*, vol. 76(9), pp. 1079-1094, September 1988.
- [10] A. Alessio, P. Kinahan, and T. Lewellen, “Modeling and Incorporation of System Response Functions in 3D Whole Body PET,” submitted to *IEEE Trans Med Imaging*, 2005.
- [11] Noo F, Defrise M, Clackdoyle R and Kudo H 2002 Image reconstruction from fan-beam projections on less than a short scan *Phys. Med. Biol.* 47 2525–46
- [12] Crawford C F and King K F 1990 Computed tomography scanning with simultaneous patient translation *Med. Phys.* 17 967–82
- [13] A. Brandt, J. Mann, M. Brodski, and M. Galun, “A fast and accurate multilevel inversion of the Radon transform,” *SIAM J. Appl. Math.*, vol. 60, no. 2, pp. 437–462, 2000.
- [14] A. Averbuch, R. R. Coifman, D. L. Donoho, M. Israeli, and Y. Shkolnisky, “A framework for discrete integral transformations I—the pseudo-polar Fourier transform,” *SIAM J. Sci. Comput.*, vol. 30, no. 2, pp. 764–784, Feb. 2008.
- [15] N. D. Shah, S. K. Shah “Radon Transform Based Improved Algorithm For Computed Tomography To Reconstruct Volume From Real 2d Data Gathered Over Arbitrary Path using Matlab® With Graphical User Interface”
- [16] I. Hein, K. Taguchi, M. D. Silver, M. Kazama, and I. Mori, “Feldkamp-based cone beam reconstruction for gantry-tilted helical multislice CT,” *Medical Physics*, vol. 30, no. 12, pp. 3233–3242, 2003.

[17] Nitin Kothari, Yogesh K. Bhatshvar, AbsishekKatariya,, Shilpa Kothari “3D Image Reconstruction Using X-Rays For CT Scan” International Conference on Computational Intelligence and Communication 2011.

Chapter 6

[1] Jain AK. Fundamentals of digital image processing. New Jersey: Prentice Hall; 1989.

[2] Kerr JP, Bartlett EB. A statistically tailored neural network approach to tomographic image reconstruction. *Med Phys* 1995;22:601—10

[3] Kerr JP, Bartlett EB. Medical image processing utilizing neural networks trained on a massively parallel computer. *Comput Biol Med* 1995;25:393—403

[4] Knoll P, Mirzaei S, Mueller A, Leitha T, Koriska K, Koehn H, et al. An artificial neural net and error backpropagation to reconstruct single photon emission computerized tomography data. *Med Phys* 1999;26:244—8.

[5] Munley MT, Floyd CE, Bowsher JE, Coleman RE. An artificial neural network approach to quantitative single photon emission computed tomographic reconstruction with collimator, attenuation and scatter compensation. *Med Phys* 1994;21:1889—99.

[6] Srinivasan V, Han YK, Ong SH. Image reconstruction by Hopfield neural network. *Image Vis Comput* 1993;11(5):278—82.

[7] Lewitt RM. Reconstruction algorithms: transform methods. *Proceeding of the IEEE*, vol. 71, no. 3; 1983. p. 390—408.

[8] F. Natterer, *The Mathematics of Computerized Tomography*. New York: Wiley, 1986

[9] Ingman D, Merlis Y. Maximum entropy signal reconstruction with neural networks. *IEEE Trans Neural Netw* 1992;3:195—201.

[10] Elfing T. On some methods for entropy maximization and matrix scaling. *Linear Alg Appl* 1980;35:321—38.

- [11] Xia Y, Feng G, Wang J. A recurrent neural network with exponential convergence for solving convex quadratic program and linear piecewise equation. *IEEE Trans Neural Network* 2004;17(7):1003—15
- [12] Shepp LA, Logan BF (1974) “The Fourier reconstruction of a head section”. *IEEE Trans Nucl Sci NS-21:21-43*
- [13] Y. Wang, F.M. Wahl, Vector-entropy optimization-based neural-network approach to image reconstruction from projections, *IEEE Trans. Neural Networks* 8 (5) (1997) 1008–1014.
- [14] S. K. Shah, N. D. Shah, “Reconstruction of 3D Medical Images by Neural Network,” , at *Control, Microcomputer, Electronics and Communication* by Institute of Electronics & Telecommunication Engineers , Vadodara, February 2011.
- [15] N.D. Shah, S. K. Shah , D. Rathod, “ Computed Tomography Reconstruction by using Unsupervised Artificial Neural Network” , Submitted for publication for *International Journal of Automation and Control Engineering (IJACE, ISSN Print: 2325-7407)*
- [16] N. D. Shah, “Reconstruction of 3D Medical Images by Neural Network,” , at *Control, Microcomputer, Electronics and Communication* by Institute of Electronics & Telecommunication Engineers , Vadodara, February 2011.
- [17] Elfing T. On some methods for entropy maximization and matrix scaling. *Linear Alg Appl* 1980;35:321—38.
- [18] Verma, B. and P. Zhang, A novel neural-genetic algorithm to find the most significant combination of features in digital mammograms. *Applied Soft Computing*, 2007. 7: p. 612–625.
- [19] Xinjian Qiang, Guojian Cheng, Zheng Wang “An Overview of Some Classical Growing Neural Networks and New Developments” 2nd International Conference on Education Technology and Computer (ICETC) 2010
- [20] Zhenghao Shi, and Lifeng He “Application of Neural Networks in Medical Image Processing” *Proceedings of the Second International Symposium on Networking and Network Security (ISNNS 2010)*
- [21] Hsieh, “Tomography reconstruction for tilted helical multislice CT,” *IEEE Transactions on Medical Imaging*, vol. 19, no. 9, pp. 864–872, 2000.

[22] Bouman, C. A. and Sauer, K. D. (1996). A unified approach to statistical tomography using coordinate descent optimization, IEEE Transactions on Image Processing 5(3): 480–492.

[23] J.J. Hopfield, Neural networks and physical systems with emergent collective computational abilities, in: Proceedings of National Academy of Science USA, vol. 79, 1982, pp. 2554–2558.

Chapter 7

[1] www.imp.uni-erlangen.de/phantoms/

[2] Shepp LA, Logan BF (1974) “The Fourier reconstruction of a head section”. IEEE Trans Nucl Sci NS-21:21–43.

[3] D.E. Goldberg, “Genetic Algorithms in Search: Optimization and Learning”, Addison-Wesley Publishing Co., Reading, 1989.

[4] N. D. Shah, “A novel approach for Computer Tomography Reconstruction Algorithm using Unsupervised Neural Network,” , at Control, Microcomputer, Electronics and Communication by Institute of Electronics & Telecommunication Engineers , Vadodara, February 2014.

[5] S. K. Shah, N. D. Shah, “Reconstruction of 3D Medical Images by Neural Network,” , at Control, Microcomputer, Electronics and Communication by Institute of Electronics & Telecommunication Engineers , Vadodara, February 2011

[6] Cierniak, R. (2008b). A new approach to image reconstruction from projections problem using a recurrent neural network, International Journal of Applied Mathematics and Computer

[7] N. D. Shah, “Development of User Interface for 3D Reconstruction Algorithm using Soft Computing Techniques,” , under publication.

[8] Bouman, C. A. and Sauer, K. D. (1996). A unified approach to statistical tomography using coordinate descent optimization, IEEE Transactions on Image Processing 5(3): 480–492.

[9] J.J. Hopfield, Neural networks and physical systems with emergent collective computational abilities, in: Proceedings of National Academy of Science USA, vol. 79, 1982, pp. 2554–2558.

Chapter 8

[1] Digital Signal and Image Processing Using MATLAB - Gerard Blanchet & Maurice Charbit.

[2] Biosignal and Biomedical Image Processing MATLAB based Applications - John L. Semmlow

[3] Graphics and GUIs with MATLAB- Patrik Marchand :CRC Press

[4] Matlab software, www.mathworks.in, 2013

[5] N. D. Shah, "Development of User Interface for 3D Reconstruction Algorithm using Soft Computing Techniques," , under publication.

Appendix A

Overview of Radon Transform

This appendix discusses the Radon Transform, which is used for solving the problem of reconstruction irrespective of the solution technique.

When a CT scan is made, the X-rays are absorbed by the tissues and bones in the body. The absorption is described by a linear attenuation function, which at a fixed point has the value of the linear attenuation coefficient of the tissue. The linear attenuation function is approximately proportional to the density of the body, so it is this function which is to be displayed from the data obtained. Radon transform plays very vital role to display the images.

A.1 Mathematical Framework

When an X-ray beam is sent through a body, it is assumed that it follows a straight line, L , from a source S to a detector R . The linear attenuation function is denoted by f , and is a function of a position $x = (x_1, x_2)$ in a Cartesian coordinate system. The intensity of beam at a point x is expressed by $I(x)$, the attenuation of the intensity within a distance dl along the line L , is written as:

$$dI(x) = -f(x)I(x)dl \quad (A.1)$$

$$\frac{dI(x)}{I(x)} = -f(x)dl \quad (A.2)$$

The solution of the above equation is given by Beer's Law as shown below:

$$\ln(I(x)) = \int_L -f(x)dl \quad (A.3)$$

The intensity of the beam denoted as I_s , at the source, is known as difference in intensity from where the beam has emerged to a point on the line L , is expressed as:

$$\ln(I_s) - \ln(I(x)) = - \int_L -f(x)dl \quad (A.4)$$

$$\int_L -f(x)dl = \ln\left(\frac{I_s}{I}\right) \quad (A.5)$$

This described process is repeated on parallel lines. During the number of lines, corresponding to the number source and detectors will be finite. Hence, the inverse problem is to recover $f(x)$ from these equations, which are popularly known as reconstruction problem. Obtaining the integrals means that a slice of the object is being investigated in a certain direction. The integrals represent the projection of $f(x)$. The next step is to define the new direction and through that the other projections are obtained. Graphically it shown in the figure A-1:

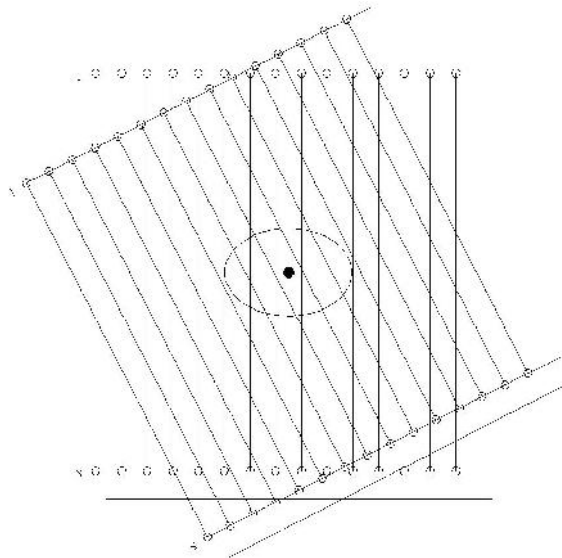


Figure A-1: Example of Projections

When a CT scan is performed, and the sources and receivers move as described, there will be a point of rotation in the middle of gantry. The origin 0 is selected in $x - plane$, considering a single slice. The Cartesian axes are chosen such that $x_1 - axis$ is parallel to the initial direction of the source detector pair movement, as shown in the figure A-2. Figure illustrates new coordinate system which appears when the source detectors are moved at an angle $\phi \in [0, 2\pi]$ from the $x_1 - axis$.

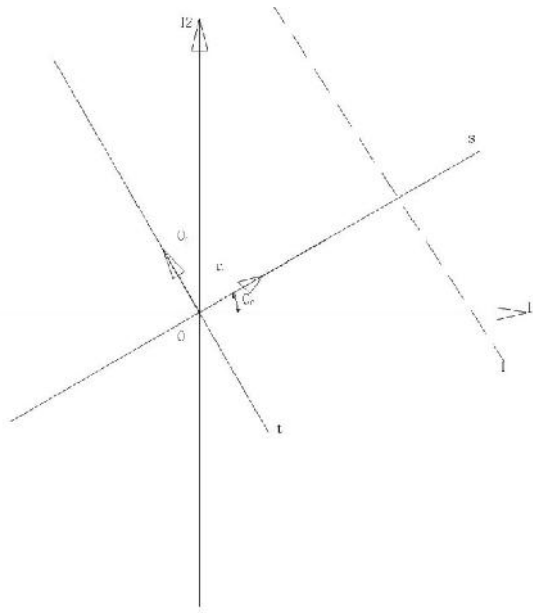


Figure A-2: Geometrical Relationship for Radon Transform

The direction is defined by the vector θ as:

$$\theta = \{\cos \phi, \sin \phi\} \quad (A. 6)$$

$$\theta^\perp = \{-\sin \phi, \cos \phi\} \quad (A. 7)$$

The s – axis will be parallel to the line where the sources are placed and t is the line parallel to the lines of the rays. The dotted line x represents one of these lines. From equation A.6 and A.7, it can be inferred that for a given line s , the Cartesian coordinated system is written as:

$$x = s\theta + t\theta^\perp ; t \in R \quad (A. 8)$$

Hence, the projection of f in the direction θ is given by:

$$(R_\phi f)(s) = \int_{-\infty}^{\infty} f(s\theta + t\theta^\perp) dt \quad (A. 9)$$

where R_ϕ denotes the Radon transform for the specific direction of θ . Considering all the possible directions of θ , the function is defined by two variables as:

$$(Rf)(s, \phi) = (R_\phi f)(s) \quad (A. 10)$$

Hence, all inverse problems are consisting of recovering function of two variables from its line integrals. Expressing the equation A.10 in terms of s and ϕ is given by:

$$(Rf)(s, \phi) = \int_{-\infty}^{\infty} f(s \cos \phi - t \sin \phi, s \sin \phi + t \cos \phi) (A.11)$$

Plotting the value of R_f as the function of s and ϕ is known as Sinogram, when the values of f are represented as grey scale level. Practically, during the scan, the values of Radon transform are discrete and noisy.

It is assumed that density function f is assumed to have the support within a disc of radius a . Thus, the sinogram will have support of a rectangle $-a \leq s \leq a$ and $-\pi < \phi < \pi$. For every point in the sinogram, there is corresponding straight line in the $x - plane$.

For all the lines passing through a fixed point $x_0 = (x_1^0, x_2^0)$, the corresponding points in the sinogram are described as sinusoidal curve in the (s, ϕ) plane. This curve is described by:

$$s = x \cdot \theta = x_1^0 \cos \phi + x_2^0 \sin \phi (A.12)$$

A.2 Implementation

The realization of this problem was done on the MATLAB® platform for two images:

- a) Image with only one non zero pixel
- b) Standard Sheep Logan Phantom

The MATLAB® Code developed for:

a) Image with only one non zero pixel is given below:

% Making a 256x256 matrix, where only one pixel is non-zero:

```
X = zeros(256);
X(100,100) = 255;
figure(1)
```

```

subplot(2,2,1)
imagesc(X), colormap(gray), title('Single Object'), axis square
xlabel('x_1'), ylabel('x_2')
theta = 0:359;
Y = radon(X,theta);
subplot(2,2,2)
imagesc(Y), colormap(gray), xlabel('phi'), ylabel('s'), axis square
title('Sinogram of the single object');

```

b) Sinogram for Sheep Logan Phantom

% Using the Phantom-image to see more sinograms in one image

```

X = phantom(256);
subplot(2,2,3)
imagesc(X), colormap(gray), title('Phantom'), axis square
xlabel('x_1'), ylabel('x_2')
Y = radon(X,theta);
subplot(2,2,4)
imagesc(Y), colormap(gray), xlabel('phi','LineWidth',5), axis square
ylabel('s'), title('Sinogram of Phantom');

```

The results obtained are presented in four figures as under:

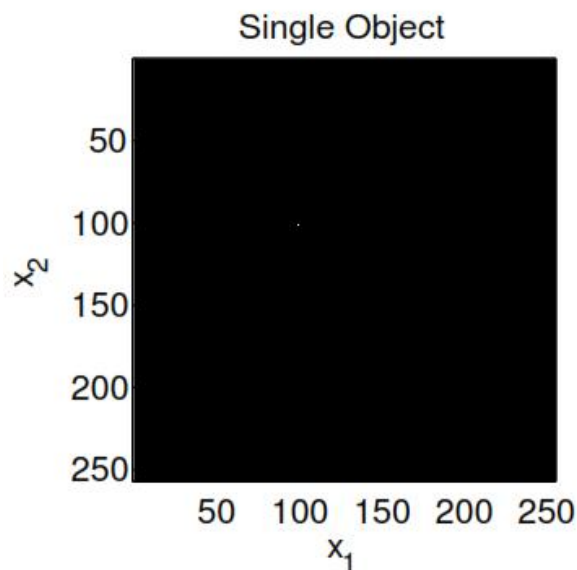


Figure A-3: Image with single pixel

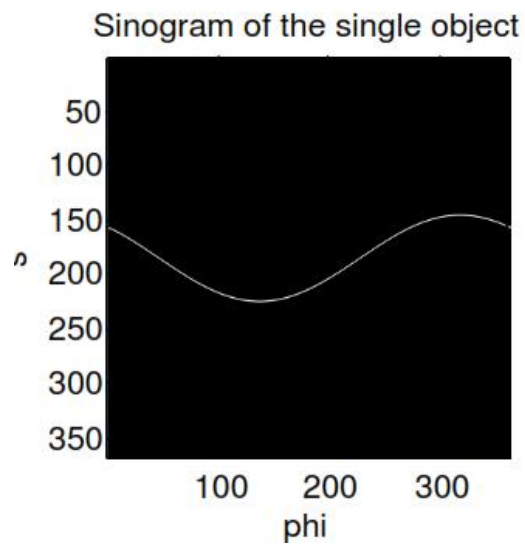


Figure A-4: Sinogram of the Image with single pixel

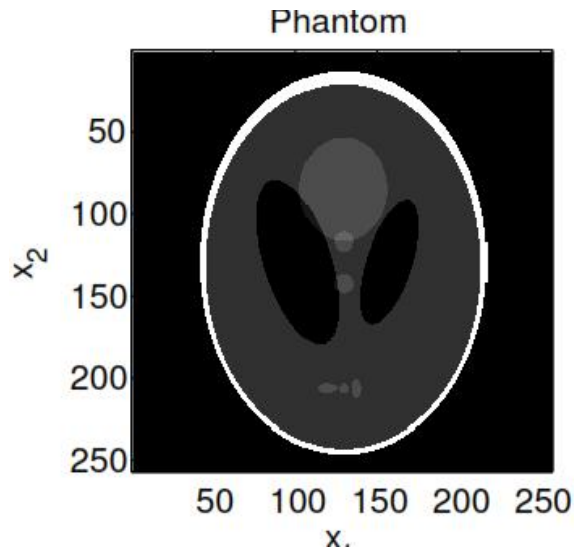


Figure A-5: Image of Sheep Logan Phantom.

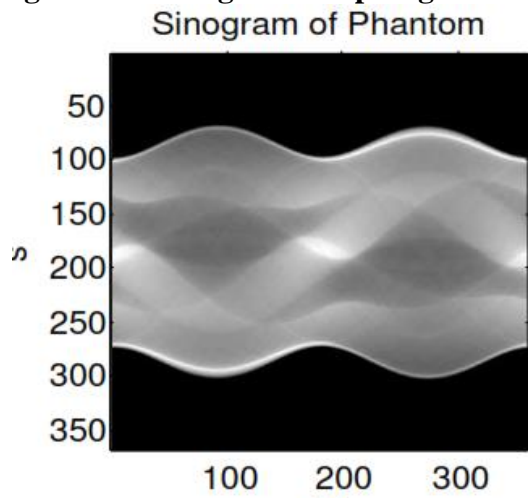


Figure A-6: Sinogram of Sheep Logan Phantom.

Appendix B

List of Publications and Presentations

This appendix provides the details pertaining to the publications, presentations and awards received based on this research work.

Publication Based on Research Work for Ph.D.

1. N. D. Shah, "Reconstruction of 3D Medical Images by Neural Network", a paper presented at a conference on "Control, Microcomputer, Electronics and Communication" organised by Institute of Electronics and Telecommunication Engineers and Institute of Engineering, at Vadodara, Gujarat on 22nd February 2011.
2. N. D. Shah, and S. K. Shah "Development of User Interface for 3D Reconstruction Algorithm Using Modified Grange Method", in the Proceeding of IEEE Symposium on Computers and Informatics, Kuala Lumpur, Malaysia, 20-22 March 2011.
3. N. D. Shah, S. K. Shah "Radon Transform Based Improved Algorithm For Computed Tomography To Reconstruct Volume From Real 2D Data Gathered Over Arbitrary Path using MATLAB® With Graphical User Interface", a paper submitted and is accepted for publication Journal of Institution of Engineers, India.
4. N. D. Shah, S. K. Shah "Soft Computing and Its Application for Medical Images", a paper presented in Soft Computing For Processing, Security, Networking and Communication, SCPSNC_2013, Institute of Electrical & Telecommunication Engineering, Vadoadara, 20th January 2013
5. N.D. Shah, S. K. Shah , D. Rathod, " Computed Tomography Reconstruction by using Unsupervised Artificial Neural Network" ,a paper published in International Journal of Automation and Control Engineering (IJACE, ISSN Print: 2325-7407)

6. N.D. Shah," A Novel Approach for Computed Tomography Reconstruction Algorithm Using Unsupervised Neural Network" published in Proceeding of Target Technologies in Computing, Automation and Communication. TTCAC_2014, Organised by Institute of Electronics and Telecommunication Engineers and Institute of Engineering March 2014.
7. N.D. Shah, A. V. Namsa "Overview of Volume Rendering Techniques for volumetric density data". Published in Proceeding at Target Technologies in Computing, Automation and Communication. TTCAC_2014, Organised by Institute of Electronics and Telecommunication Engineers and Institute of Engineering March 2014.
8. N.D. Shah " A Novel Approach for Image Reconstruction by using Advance Neural Network" published in International Journal for Science and Technology ISSN: 2229-7577 IRISC 2014 Volume No:01 Issue No: 01

International Presentation

1. "Development of User Interface for 3D Reconstruction Algorithm Using Modified Grange at Method", IEEE Symposium on Computers and Informatics, Kuala Lumpur, Malaysia, 20-22 March 2011.

National Presentation

1. N. D. Shah, "Reconstruction of 3D Medical Images by Neural Network," , at National Conference Control, Microcomputer, Electronics and Communication by Institute of Electronics & Telecommunication Engineers , Vadodara, February 2011.
2. N. D. Shah, "Soft Computing and Its Application for Medical Images", at Conference on Soft Computing For Processing, Security, Networking and Communication, SCPSNC_2013, Institute of Electrical & Telecommunication Engineering, Vadoadara, 20th January 2013.

3. N.D. Shah," A Novel Approach for Computed Tomography Reconstruction Algorithm Using Unsupervised Neural Network" at Target Technologies in Computing, Automation and Communication. TTCAC_2014, Organised by Institute of Electronics and Telecommunication Engineers and Institute of Engineering, March 2014.
4. N.D. Shah, A. V. Namsa "Overview of Volume Rendering Techniques for volumetric density data". at Target Technologies in Computing, Automation and Communication. TTCAC_2014, Organised by Institute of Electronics and Telecommunication Engineers and Institute of Engineering , March 2014

Technical Workshop

1. Industry- Institute Interactive Workshop on " Embedded System & VLSI Design" organized by Electrical Engineering Department, FTE, MSU of Baroda, IETE –Vadodara Center, Edu Tech Systems Vadodara and Advance Microsystems Mumbai during 11-15th April 2011.

National Conferences & Technical Events

1. N. D. Shah (2013) "Soft Computing and Its Application for Medical Images", at Soft Computing For Processing, Security, Networking and Communication, SCPSNC_2013, Institute of Electrical & Telecommunication Engineering, Vadoadara, 20th January 2013.
2. N. D. Shah(2011), "Reconstruction of 3D Medical Images by Neural Network", at Control, Microcomputer, Electronics and Communication by Institute of Electronics & Telecommunication Engineers, Vadodara, February 2011.

Awards Received

1. Awarded Second Prize for Paper in Research Category for, "A Novel Approach for Computed Tomography Reconstruction Algorithm Using Unsupervised Neural Network" at Target Technologies in Computing, Automation and Communication. TTCAC_2014, Organised by Institute of Electronics and Telecommunication Engineers and Institute of Engineering